RADAR SENSOR NETWORKS: WAVEFORM DESIGN, MIMO AND COMPRESSIVE SENSING

by

LEI XU

Presented to the Faculty of the Graduate School of

The University of Texas at Arlington in Partial Fulfillment

of the Requirements

for the Degree of

DOCTOR OF PHILOSOPHY

THE UNIVERSITY OF TEXAS AT ARLINGTON

December 2011

To my father Keqiang and mother Mingzhi

who always love me and support me

and who made me who I am

ACKNOWLEDGEMENTS

Though only my name appears on the cover of this dissertation, a great many people have contributed to its production. I owe my gratitude to all those people who help me to complete this dissertation and because of whom my graduate experience has been one that I will cherish forever.

My deepest gratitude goes to my supervising professor Dr. Qilian Liang, who is invaluable for constantly motivating me to explore my capability of doing research, encouraging me to provide innovative solutions and training me to possess instructing and cooperating skills. Dr. Liang patiently instructed me how to do the research from the very beginning, gave me the freedom to explore on my own and provided me valuable research guidance when my steps faltered. Without his mentorship and support, I could neither make this dissertation possible, nor have a well rounded experience consistent my long-term career goals in my Ph. D studies. Dr. Qilian Liang is such a self-disciplined, diligent and excellent researcher who was and will always lead my way through out my life.

I would like to thank Dr. Zheng Zhou and Dr. Ting Jiang, who are my M.S. advisors at Beijing University of Posts and Telecommunications, for encouraging and inspiring me to pursue my doctoral studies in United States..

I would also like to extend my appreciation to my committee members Dr. Jonathan Bredow, Dr. Jean Gao, Dr. Wei-Jen Lee and Dr. Saibun Tjuatja for their interest in my research, for their helpful discussions and invaluable comments and for taking time to serve in my dissertation committee.

I am indebted to the members of the Wireless Communications and Net- working Lab at UTA, including Dr. Xinsheng Xia, Dr. Jing Liang, Dr. Davis Kirachaiwanich, Qi Dong, Ji Wu, Steve Iverson, Ishirit Maherin, Junjiecheng, Zhuo Li and Xin Wang. I am also grateful to all of my friends who have helped me throughout my Phd career, including Eric Huang, Mario Di Francesco and so on. I have benefited enormously from their experience and help inside and outside the classroom.

Last but most importantly, I would like to express my sincere gratefulness to my parents who have unceasingly and unconditionally loved, encouraged and inspired me throughout not only in my Ph. D degree studies but also through out my whole career. I am extremely fortunate to be who I am now.

November 4, 2011

ABSTRACT

RADAR SENSOR NETWORKS: WAVEFORM DESIGN, MIMO AND COMPRESSIVE SENSING

Lei Xu, Ph.D.

The University of Texas at Arlington, 2011

Supervising Professor: Qilian Liang

In this dissertation, we have studied totally eight topics which are focused on but not limited to radar sensor networks (RSN) from a signal processing perspective. We propose the definitions of ZCZ/LCZ (Zero Correlation Zone/Low Correlation Zone) sequence-pair sets, provided three methods to construct optimized optimized punctured LCZ/ZCZ sequence-pair sets and study their properties in chapter 2 and 3. We further investigate the waveform design problem for radar system, radar sensor network, sonar sensor network and MIMO radar system from chapter 4 to chapter 7. In addition, we study radar sensor network from the view of information theory in chapter 8. We also study compressive sensing and apply it to RSN to further investigate the system performance in chapter 9 and chapter 10. In chapter 11, we briefly conclude our work in this dissertation. The main innovation works of this dissertation are as following.

We propose the LCZ/ZCZ Sequence-pair Sets that have ideal autocorrelation sidelobes and cross correlation values during LCZ/ZCZ. We also provide three methods to construct the Optimized Punctured LCZ/ZCZ Sequence-pair Sets which is a

specific case of the LCZ/ZCZ Sequence-pair Sets. We not only theoretically prove that the sequence-pair sets constructed by our methods satisfy the definitions of the Optimized Punctured LCZ/ZCZ Sequence-pair sets, but also provide examples for each method and analyze properties of the Optimized Punctured LCZ/ZCZ Sequence-pair sets to help further investigating our proposed codes.

The main purpose of pulse compression is to raise the signal to maximum sidelobe (signal-to-sidelobe) ratio to improve the target detection and range resolution abilities of the system. We apply the Optimized Punctured Binary Sequence-pair to the Radar system as the phase coded waveforms which is a kind of pulse compression codes. Comparing with the Barker and P4 codes of corresponding length, the Radar system within the Optimized Punctured Binary Sequence-pair could clearly improve the detection performances. Since multiple radar sensors can be combined to form a multi radar system to overcome performance degradation of single radar along with waveform optimization, we theoretically study RSN design using phase coded waveforms. We apply our newly proposed codes to RSN and analyze the detection performance of the system. We also apply the proposed ternary codes to the Sonar Sensor Network (SSN) as pulse compression codes for narrowband pulse signals and simulate the target detection performance of the system.

We provide two MIMO radar systems using our proposed codes as orthogonal pulse compression codes to study the direction finding performance of the MIMO radar systems. We theoretically analyze the two MIMO radar system models and simulate the direction finding performance of the system.

We also studied the RSN from the view of information theory. We investigate the use of information theory to design waveforms for the measurement of extended radar targets in RSN. We optimized the estimation waveforms that maximize the

mutual information between a target ensemble and the received signal within additive Gaussian noise so that characteristics of the target could be well recognized.

Finally, we provide and analyze a CS-SVD method to simplify the signal recovery algorithm and introduce CS to RSN using pulse compression technique. Our idea is to employ a set of Stepped-Frequency (SF) waveforms as pulse compression codes for transmit sensors, and to use the same SF waveforms as the sparse matrix to compress the signal in the receiving sensor. We obtain that the signal samples along the time domain could be largely compressed so that they could be perfectly recovered by a small number of measurements. We develop a Maximum Likelihood (ML) Algorithm for Radar Cross Section (RCS) parameter estimation and provide the Cramer-Rao lower bound (CRLB) to validate the theoretical result.

TABLE OF CONTENTS

LIST OF ILLUSTRATIONS

LIST OF TABLES

CHAPTER 1

INTRODUCTION

1.1 Introduction

1.1.1 Best Discrete Signals

The best discrete signals could improve the anti-jamming, anti-noise and anti-fading performances of the communication system, increase the confidentiality of the system data and fulfill the synchronization and tracking in CDMA communication system. Based on the signal elements, the best discrete signal could be divided into two (binary), ternary, quaternary, and multi-signal equivalents; Based on the periodic property, the best discrete signal could be divided into periodic signal and aperiodic signal. However, there is no strict mathematical definition for the best discrete signal in a variety of engineering fields, because of the different practical engineering applications. In some other words, there are different definitions of the best signal in different engineering applications. In general, the signals that meet the need of a particular system are known as the best signals for that engineering application. As a matter of fact, the best signals of one particular type of engineering standard might be the worst signals working with another standard. Therefore, it has been concluded that it is and will be impossible to find a class of best signals suitable for all the engineering applications.

Since the signal processing ability of the system is improving, the function of system becomes more and more intense and structure of the system becomes more and more complex. More strict signals are required in the system. Fortunately, as computer technology developed rapidly, computer digital signal processing has been

widely used and dominated in the electronic system. Consequently, it is possible for people to use more complex forms of signals other than binary signals to improve the system performance and to increase flexibility of the system.

1.1.2 Signals of Periodic Correlation

The signal processing in communication engineering often requires the set of signals to have at least one or both of the following two conditions:

(1) Each signal of the set could be easily distinguished from the signal with delay of itself;

(2) Each signal could be easily distinguished from the other signals of the set as well as the signal with delay of itself;

Conditions (1) is very important for the systems, such as telemetry systems, radar systems and spread spectrum communication system; and for multiple targets and the system of multiple terminals, the conditions (2) is even more important. LMS (least-mean-square) error is one of the most commonly used and most effective measures to distinguish signals, that is, when the MSE (mean square error) between the two signals is great, the two signals are easily distinguished from each other. It has been theoretically proved: When the signals have good periodic correlation properties, signal A could be distinguished from signal B, as well as the signal B with time delay. Thus, correlated receiver or matched filter could be used to extract the required signal or signal with time delay for navigation and radar systems. This is the reason why periodic correlation is profoundly investigated and periodic signal is required by engineering applications. Therefore, the challenging requirements of perfect discrete signals are the high autocorrelation peak, the low autocorrelation sidelobes and the low cross correlation properties which could meet the above two

conditions. It is necessary and significant for us to study the set of discrete signal of perfect periodic correlation.

1.1.3 Innovation Work Overview

Much time and effort was put in designing the perfect periodic correlation signals. These signals have abroad been applied in modern communication, radar, sonar, navigation, space ranging and controlling, and electronic antagonism systems. Therefore, it is one of the objects researching perfect periodic discrete signals which have ideal autocorrelation and cross correlation properties for engineering application, such as in modern communication, radar, sonar, navigation, space ranging and controlling, and electronic antagonism systems.

Since the length and number of perfect correlation signals are severely restricted, many methods have been accepted to extend the length of sequence and enlarge the number existent sequences. Considering the periodic codes, the m-sequences or Legendre sequences could achieve the lowest periodic autocorrelation function (ACF) of $|R_i(\tau \neq 0) = 1|$. For non-binary sequences, the Golomb codes [1] are a kind of two-valued (biphase) perfect codes which obtain zero periodic ACF but result in large mismatch power loss. The Ipatov code [2] shows a way of designing code pairs with perfect periodic autocorrelation (the cross correlation of the code pair) and minimal mismatch loss, but its reference code and construction method are complicated. Zero periodic autocorrelation function for all nonzero shifts could be obtained by polyphase codes, such as Frank and Zadoff codes, but the more complicated constructing methods and implementation cost are required. In addition to these well-known codes, by suffering a small S/N loss, the authors [3] present several binary pulse compression codes to greatly reduce sidelobes. In [4], pulse compression using a digital-analog hybrid technique is studied to achieve very low range sidelobes for potential appli-

cation to spaceborne rain radar. Tanner et al.[5] uses time-domain weighting of the transmitted pulse to achieve a range sidelobe level of -55 dB or better in flight tests. Nevertheless, all the above work have their own disadvantages, such as the large mismatch power loss for Golomb codes, the high energy of reference code and complicated construction method for Ipatov codes and so on. It is also known that for both binary and non-binary sequences in the periodic sequence field, the sequences can not obtain ideal impulsive autocorrelation function (ACF) and ideal zero cross-correlation functions (CCF) simultaneously although ideal CCFs could be achieved alone. Since the ACF and CCF have to be limited by certain bounds, such as Welch bound [6], Sidelnikov bound [7], Sarwate bound [8], Levenshtein bound [9], etc. As a reulst, the concept of Zero Correlation Zone (ZCZ) [10][11][12] during which ideal impulsive autocorrelation function and ideal zero cross-correlation functions could be achieved simultaneously is proposed to overcome the above problems. Here, the sequence-pair and ZCZ/LCZ (Zero Correlation Zone/ Low Correlation Zone) are introduced to help constructing the set of perfect correlation signals. Three constructing methods are provided and their properties are investigated.

In addition, waveform design is of great importance in the engineering field. Hence, it is necessary to study not only the theoretical analysis of the proposed codes' properties, but also the engineering application to the industrial world, such as pulse compression technique in radar system, radar sensor network, sonar sensor network and MIMO Radar.

1.2 Preliminaries to the Proposed Triphase Codes

The most popular biphase code widely used in radar system is the Barker code, which is only found at the maximum length of 13. It is also known that for most good binary sequences of length $N(N > 13)$, the attainable autocorrelation sidelobe levels

are approximately $\sqrt{N}$ [13] [14], and the mutual cross correlation peaks of sequences of the same length are larger and usually in the order of $2\sqrt{(}N)$ to $3\sqrt{(}N)$. Set of binary sequences of length N with autocorrelation sidelobes and cross-correlation peak values both of approximately $\sqrt{(}N)$ are only achieved in paper [15]. In addition to the binary sequences, the Polyphase code is another kind of code provided [16] [17] [18] to make up for the restriction of binary sequences and could have better Doppler tolerance and lower range sidelobes (such as the Frank and P1 codes, the Butler-matrix derived P2 code and the linear-frequency derived P3 and P4 codes). Nevertheless, the sidelobe's range of the polyphase codes can not be as low as zero either. The structure of polyphase codes is more complicated and is not easy to generate comparing with binary codes.

In this dissertation, we introduce the definitions of Optimized Punctured Binary Sequence-pair and ZCZ/LCZ (Zero Correlation Zone/Low Correlation Zone), based on which, we propose and construct a set of new kind of triphase codes–the Optimized Punctured ZCZ/LCZ Sequence-Pair Set which have the largely reduced autocorrelation sidelobes and cross correlation values. We also provide three methods to construct the above codes. Examples are given to study the codes' auto correlation and cross correlation properties.

1.3 Preliminaries to Pulse Compression Technique in Radar System

Pulse compression allows a radar to simultaneously achieve the energy of a long pulse and the resolution of a short pulse without the high peak power which is required by a high energy short duration pulse [19]. One of the waveform designs suitable for pulse compression is phase-coded waveform design, which is a long pulse of duration T divided into N subpulses each of width T_s. Each subpulse has a particular phase,

which is selected in accordance with a given code sequence. The pulse compression ratio equals the number of subpulses $N = T/T_s$. In general, a phase-coded waveform with longer code word, in other words, higher pulse compression ratio, can have lower sidelobe of autocorrelation, relative to the mainlobe peak, allowing its main peak to be better distinguished.

The lately proposed Optimized Punctured Binary Sequence-pair could achieve an ideal autocorrelation sidelobe as low as zero. Therefore, we apply the Optimized Punctured Binary Sequence-pair to the Radar system as the pulse compression codes and study the simulation results show that detection performance of the system using Optimized Punctured Binary Sequence-pair is superior to the one using traditional phase codes waveforms such as the Barker and P4 codes.

1.4 Preliminaries to Radar Sensor Network

With recent rapid development in information fusion technology, much time and effort have been put in radar waveform design for a single active radar [20][21]. However, multiple radar sensors can be combined to form a multi radar system to overcome performance degradation of single radar along with waveform optimization. In [22], Liang studied constant frequency (CF) pulse waveform design and proposed maximum-likelihood (ML) automatic target recognition (ATR) approach for both nonfluctuaing and fluctuating targets in a network of multiple radar sensors. In [23], RSN design based on linear frequency modulation (LFM) waveform was studied and LFM waveform design was applied to RSN with application to ATR with delay-Doppler uncertainty by Liang as well. J.Liang [24] provided an orthogonal waveform model for RSN, which eliminates interference when there is no Doppler shift.

Nevertheless, the radar sensor network using phase coded waveforms has not been well studied so far. As has been known, phase coded waveform design is one of

the widely used waveform design methods for pulse compression which could raise the signal to maximum sidelobe (signal-to-sidelobe) ratio to improve the target detection and range resolution abilities of the system.

In this dissertation, we would theoretically study RSN design based on phase coded waveforms: the conditions for waveforms co-existence. Then we apply our newly proposed triphase codes called optimized punctured ZCZ sequence-pair set (optimized punctured ZCZPS) to RSN. The detection performance of the system is improved because of the good orthogonal property of the proposed codes.

1.5 Preliminaries to Sonar Sensor Network

Much time and effort have been put in radar waveform design for radar sensor networks [22][23] [24], since multiple radar sensors could be combined to form a multiradar system to overcome performance degradation of sigle radar. Though underwater sonar system is more complicated than the radar system because of many unique channel characteristics such as fading, extended multipath and refractive properties of the sound, multiple sonar sensors could construct a underwater sonar sensor network so that the detection performance could be improved.

The long-range bistatic sound transmission through the ocean sound channel such as in ocean acoustic tomography [25] [26], in acoustic thermometry of ocean climate (ATOC) [27] used the signal that allows sufficient sound energy delivery into the ocean so that the signal received at long range, perhaps several megameters, has a sufficiently high signal-to-noise energy ratio but low signal-to-noise power ratio. Consequently, precision measurements of sound travel time could be made and good time resolution should be allowed after signal processing. m sequences, successfully used in previous experiments [25] [28] [29], satisfy the long-range transmission requirement and the same time resolution as a monopulse or periodic pulse system whose pulse

width is one digit duration achievable at high power. In other words, high signal energy is provided by transmitting over a long time (large T) and good time resolution is achieved by using a sequence of short pulse (large W), therefore having a large TW product [30]. It is called the phase coded waveform which is a widely used technique in radar system.

Therefore, family of m sequences could be applied to the SSN to achieve better targets detection performance than single sonar sensor. Nevertheless, the autocorrelation and cross correlation properties of family of m sequences or even Gold sequences are not optimized. As a result, the concept of ZCZ (Zero Correlation Zone) [31] is introduced.

In this dissertation, based on the definitions of optimized punctured ZCZPS and the method to construct optimized punctured ZCZPS proposed previously, we analyze the properties and ambiguity function of optimized punctured ZCZPS. We investigate the target detection performance of using the proposed codes as pulse compression codes in the sonar sensor network and draw some final conclusions on the proposed codes.

1.6 Preliminaries to MIMO Radar System

The previous work [32] [33] [34] showed that processing data from a radar network with spatially distributed nodes could offer significant performance improvement, as a result, there has been considerable interest in MIMO radars which employ multiple antennas both at the transmitter and at the receiver. The present important research of MIMO radar includes all kinds of techniques, such as waveform design [35] [36] [37], ambiguity function [38], patternform syntheses [39][40], detection and localization performance analysis [35]-[40], space-time adaptive signal processing, direction finding, etc. In [36], the authors design covariance matrix of the probing sig-

nal vector transmitted by the radar to achieve the desirable features of a MIMO radar system. The desirable features could be to choose freely the probing signals transmitted via its antennas to maximize the power around the locations of the targets of interest, more generally to approximate a given transmit beampattern, and also to minimize the cross-correlation of the signals reflected back to the radar by the targets of interest. In [37], they also propose a cyclic optimization algorithm for the synthesis of a given optimal covariance matrix R under various practical constraints to construct signals which also have good auto- and cross- correlation properties in time. In addition, based on investigating target detection and parameter estimation techniques for a multiple-input multiple-output (MIMO) radar system, the authors [41] propose an alternative estimation procedure, referred to as the combined Capon and approximate maximum likelihood (CAML) method which can provide excellent estimation accuracy of both target locations and target amplitudes.

Apart from the work mentioned above, direction finding [42] [43] is such a technology that a well known waveform is transmitted by an omnidirectional antenna, and a target reflects some of the transmitted energy toward an array of sensors that is used to estimate some unknown parameters, e.g. bearing, range, or speed. Also, beamforming [44] is another important process generally used in direction finding process that an array of receivers can steer a beam toward any direction in space. The advantages of using an array of closely spaced sensors at the receiver are the lack of any mechanical elements in the system, the ability to use advanced signal processing techniques for improving performance, and the ability to steer multiple beams at once.

In the dissertation, we would theoretically investigate the MIMO radar system using our proposed triphase orthogonal waveforms as pulse compression codes and study the direction finding performance of the MIMO radar system. To the best

of our knowledge, it is the first time to introduce pulse compression technique to MIMO radar system to improve the direction finding performance. We also study the ambiguity function of the MIMO radar system. The simulation results show that the MIMO radar systems using our models could obtain good direction finding performance.

1.6.1 Preliminaries to Radar Sensor Network From the View of Information Theory

Information theory has been applied to investigating radar system by Woodwar and Davies[45]-[46]. For these works, the information theory is particulary used in the area of radar detection. Considering the application of information theory in radar detection problem, it is summarized to gain information from a mixture of signal and unwanted noise by obtaining as large a signal-to-noise ratio as possible on the grounds in[47].

Meanwhile, much time and efforts has also been put into waveform design problem in the radar system. Wilcox[48] studied the problem of designing waveforms from the radar ambiguity function for narrowband signals. Naparst[49] considered the problem of wideband waveform design and processing to resolve targets in dense target environments. It is not until 1993 when Bell[50] first used mutual information in the design of single radar waveforms and processing to conclude that distributing energy is a good choice to better detect targets.

Recently, radar sensor network (RSN) is a newly studied topic that multiple radar sensors can be combined to form a multiradar system to overcome performance degradation of single radar along with waveform optimization. In [22] and [23], Liang has studied constant frequency (CF) pulse waveform design and LFM waveform design in a network of multiple radar sensors. Nevertheless, none of the works have considered the use of information theory in radar waveform design for RSN.

In this dissertation, we studied the problems of how to design a set of radar waveforms for optimal target information extraction in RSN. Here, the radar targets are modeled as extended radar targets of significant physical extent but not the simple point targets for the purpose of extracting information about a target. The problem is modeled to design of radar waveforms which maximize the mutual information between the extended target and the receiver output. Closed form expression has been derived for the waveform and an example has been illustrated to further study it.

1.7 Preliminaries to Compressive Sensing

Recent results in compressive sensing have shown that the information from a signal may be captured with a small set of nonadaptive, linear measurements as long as the signal is sparse in some basis or frame [51]-[52]. If the signal is properly chosen, the number of measurements to recover the signal can be much smaller than the number of Nyquist-rate samples. The application of compressive sensing to radar imaging has been investigated in [53], [54]. A CS-based data acquisition and imaging method was proposed to study a number of point-like targets for stepped-frequency continuous wave ground penetrating radars (SFCW-GPRs) in [55]. In [56], the authors proposed the step-frequency with compressive sampling (SFR-CS), that achieves high target range and speed resolution using significantly smaller bandwidth than transitional step-frequency radar. The application of CS to Multiple Input and Multiple Output (MIMO) radar has also attracted a lot of attention in recent research. The work of [57] studied angle-Dopper estimation of multiple targets for MIMO radar system. In addition, the authors in [58] also considered the range estimation performance of their proposed method for MIMO radar systems that employ CS. Based on adaptive radar design, the authors in [59] studied MIMO radar with widely separated anten-

nas in the context of sparse modeling for estimating the positions and velocities of multiple targets.

1.7.1 Preliminaries to Using Singular Value Decomposition in Compressive Sensing

Compressive sensing (CS) [60][61] is an emerging framework that a signal vector which is K-sparse in a specific domain can be completely characterized by M measurements ($M > K$) with $M << N$, where N is the traditional Nyquist based number of samples required.

The major algorithmic challenge in compressive sensing is to approximate a signal given a vector of noisy samples. There are three rough categories of signal recovery algorithms: convex relaxation, combinatorial algorithms and greedy pursuits. The convex relaxation algorithms leading to l_1-minimization–also called basis pursuit [62] succeed with a very small number of measurements, however, it tends to be computationally burdensome. Many of the combinatorial algorithms are extremely fast, but they require a large number of somewhat unusual samples that may not be easy to acquire. Greedy pursuits, such as various matching pursuits [63][64], are intermediate in their running time and sampling efficiency but has its own disadvantages.

In Chapter 8, we provide a new algorithm-the CS-SVD algorithm for signal recovery in compressive sensing by introducing the concept of SVD (Singular Value Decomposition). We use SVD to study the compressive sensing framework and develop two simple and straightforward methods to implement the CS-SVD algorithm in the presence of additive noise.

1.7.2 Preliminaries to Application of Compressive Sensing to Radar Sensor Network

Current requirements in warfighting functionality result in obtaining accurate and timely information about battlespace objects and events so that the warfighters

can make decision about reliable location, tracking, combat identification and targeting information. While massive amounts of data will be generated by a penetrating sensor, it is important for the warfighters to find technologies that not only integrate information from diverse sources but also provide indications of information significance in ways that help them to make tactical decision. The Radar Cross Section (RCS) is the property of a scattering object, or target, which represents the magnitude of the echo signal returned to the radar by the target. Hence, we could have different classes with different RCS values representing corresponding targets, such as bird, conventional unmanned winged missile, small single-engine aircraft and large flight aircraft. In this paper, we will study the target RCS in a Radar Sensor Network (RSN) by using compressive sensing techniques.

It is well known that Wireless Sensor Networks (WSN) are a fast growing class of systems. In [65], the authors presented a new method that makes use of the properties of data of multiple sensors to enable reliable data collection. In [66], the authors adopted a mutual-information-based sensor selection (MISS) algorithm to help sensing devices collaborate among themselves to improve the target localization and tracking accuracies. Alike WSN, RSN has been recently considered to overcome the performance degradation of a single radar. In [67], the authors design a network of distributed radar sensors that work in an ad hoc fashion and the simulation results showed that proposed RSN can provide much better detection performance than that of single radar sensor. However, RSN is quite different from WSN. The waveform of each radar sensor has to be properly designed, otherwise, these radar sensors are likely to badly interfere with each other in the RSN. As a result, the design of radar waveforms has been under the study with the goal of optimizing the performance of the RSN. In [68], binary coded pulses using simulated annealing in RSN are proposed. Liang [22] studied Constant Frequency (CF) pulse waveform de-

sign and proposed Maximum-Likelihood (ML) Automatic Target Recognition (ATR) approach for both nonfluctuating and fluctuating targets in a radar sensor network. Furthermore, Liang [23] studied the RSN design based on Linear Frequency Modulation (LFM) waveforms and also applied the LFM waveforms to RSN in the context of ATR with delay-Doppler uncertainty. In addition, it is known that the pulse compression technique allows a radar to achieve both the energy of a long pulse and the resolution of a short pulse, without the high peak power which is required by a high energy short duration pulse [69]. Pulse compression waveforms are obtained by adding frequency or phase modulation to a simple pulse. A Stepped-Frequency waveform is a frequency modulation waveform for obtaining a large bandwidth, and thus a fine range resolution without requiring intrapulse frequency modulation. The most common Stepped-Frequency waveform employs a linear frequency stepping pattern, where the RF frequency of each pulse is increased by ΔF. This representation motivates the applicability of the recently proposed Compressive Sensing (CS) theory [70], [53] that refers to such signals as 'sparse' or 'compressible'.

Due to the expansion of data introduced to RSN, the compression and reconstruction of the received data is a design challenge of future RSN. Unlike the above research, the work in this dissertation explores how to exploit compressive sensing in RSN composed of a number of transmit sensors but only one receiving sensor. It is known that the signal must be 'compressible' for compressive sensing to have benefit. Recognizing that the Stepped-Frequency train could act as the sparsity basis for the signal, we apply it as a pulse compression code to construct the 'compressible signal' for a transmit sensor. We choose the Gaussian matrix as the measurement matrix that satisfies the Restricted Isometry Property (RIP) with this basis. However, there are still a number of challenges in most CS theory applied to radar which specifically mentions that it eliminates the need for matched filter in the radar receiving sensor.

In [53], only the range parameter of the target was studied and the target reflectivity being probed must be compressible in some basis before their CS-based radar system could work. In [71], the transmitted signal must be sufficiently 'incoherent' and the targets have to be radially aligned with the transmitter and receiver. In this paper, we propose and investigate a totally different model of CS-based radar sensor network system. Hence, the matched filters are still used in the receiving sensor.

In addition to the proposed RSN model above, we investigate the application of compressive sensing to RSN to perform target RCS value estimation. We propose an Maximum Likelihood (ML) algorithm to estimate the target RCS parameter and use the Cramer-Rao lower bound (CRLB) to validate our theoretical result. In the simulation parts, the performance of signal recovery and the performance of target detection are studied as well as the performance of target RCS value estimation. The simulation results show that the the signal could be precisely recovered if the number of measurements is no less than the number of sensors in RSN. The target could be perfectly detected even if the signal could not be precisely recovered. As a result, much smaller measurement matrix could be used on the receive part for the purpose of target detection. Finally, the actual variance of the RCS parameter estimation $\widehat{\theta}$ satisfies the CRLB.

1.8 Organization of Dissertation

The remainder of this dissertation is organized as follows.

- **Chapter 2** presents and studies the Optimized Punctured Binary Sequence-pairs, the LCZ/ZCZ Sequence-pair Sets and the Optimized Punctured LCZ/ZCZ Sequence-pair Sets. These sequence-pair sets, which possess both the good cross correlation between different sequence-pairs of the set and the ideal autocorre-

lation property of each sequence-pair, could be potent candidates for set of best signals.

- **Chapter 3** provides three methods to construct the Optimized Punctured LCZ/ZCZ Sequence-pair sets and prove that the sequence-pair sets constructed by our methods satisfy the definitions of the Optimized Punctured LCZ/ZCZ Sequence-pair sets. Examples are illustrated for each method and properties of the Optimized Punctured LCZ/ZCZ Sequence-pair sets are also analyzed to help studying our proposed codes.
- **Chapter 4** applies Optimized Punctured Binary Sequence-pair to the radar system as the pulse compression code and simulate the detection performance of the system. The simulation results show that the new code can provide better performances than the Barker and P4 codes of corresponding length and be a good alternative for the current used pulse compression codes in radar system. **Chapter 5** studied the RSN using the Optimized Punctured ZCZ Sequence-pair set as the phase coded waveforms and simulated the detection performance of the system. The simulation results show that RSN based on a set of optimized punctured ZCZ sequence-pairs provides promising detection performance much better than that of single radar.
- **Chapter 6** applies our optimized punctured ZCZPS as a bank of phase coded waveforms to the SSN can effectively satisfy higher demands criterion for detection accuracy in modern military and security affairs.
- **Chapter 7** introduces our proposed codes as the orthogonal pulse compression codes to the MIMO radar system to improve the radar direction finding performance. antennas.
- **Chapter 8** studied the waveforms design for the measurement of extended radar targets in radar sensor networks (RSN) in the view of information theory.

- **Chapter 9** provides a new CS technique-the CS-SVD algorithm which requires less measurements than the standard state-of-art compressive sensing techniques and provide a simpler and more efficient recovery scheme.
- **Chapter 10** introduces CS to the Radar Sensor Network (RSN) exploiting the pulse compression technique to obtain better data compressing ratio. In addition, a ML algorithm is proposed to estimate the target RCS parameter and the CRLB is to successfully verify our theoretical result.
- **Chapter 11** provides the conclusion. It summarizes the main achievements of this dissertation and outlines future research directions.

CHAPTER 2

OPTIMIZED PUNCTURED SEQUENCE-PAIR SETS

2.1 Introduction

Based on the previous study, the perfect binary sequence is known to be the ideal signal in the industry field. However, only the perfect binary sequences of length 4 exist among the sequences of which length is less than 12100 [72]. As a result, people optimized binary sequences to construct the sequences of which the autocorrelation sidelobe is less than 1, such as m sequence, $GOLD$ sequence, $kasami$ sequence and M sequence.

In addition, the sequence-pair concept is another concept that is provided to enlarge the number of required sequences. It means that the transmitter and the receiver are using different sequences which have good correlation properties. The original best signal mentioned above is just a specific case of the best sequence-pair, where the transmitter and the receiver share the same sequence.

The definition and property of sequence-pair are as following.

Definition 2-1-1[73]: $X = (x_1, x_2, ..., x_N)$ and $Y = (y_1, y_2, ..., y_N)$ are two different sequences of length N, (X, Y) is called sequence-pair. If $x_i, y_i \in \pm 1$, the sequence-pair (X, Y) is N-length binary sequence pair.

Definition 2-1-2[73]: A sequence-pair $(\mathbf{x}, \mathbf{y})$ is made up of two N-length sequences $\mathbf{x} = (x_0, x_1, \cdots, x_{N-1})$ and $\mathbf{y} = (y_0, y_1, \cdots, y_{N-1})$,

$$R_{xy}(\tau) = R_{xy}(rT_s) = \sum_{j=0}^{N-1} x_j y^*_{(j+\tau) mod N}, \tag{2.1}$$
$$0 \le r \le N-1, 0 \le \tau \le (N-1)T_s$$

is called the periodic autocorrelation function of the sequence pair. $R_{xy}(0)$ is the autocorrelation peak of the sequence-pair, and $R_{xy}(\tau), \tau \neq 0$ is the autocorrelation sidelobe of the sequence-pair. While $x = y$, the sequence-pair $(\mathbf{x}, \mathbf{y})$ turns to be a one-sequence code.

Definition 2-1-3[73]: The cross correlations of two sequence-pairs (X, Y) and (U, V) could be expressed as

$$R_{(X,Y)(U,V)}(\tau) = \sum_{i=0}^{N-1} x_i v^*_{(i+\tau) mod N}, \tag{2.2}$$
$$R_{(U,V)(X,Y)}(\tau) = \sum_{i=0}^{N-1} u_i y^*_{(i+\tau) mod N}$$

Definition 2-1-4[73]: When the autocorrelation of the sequence-pair (X, Y) satisfies that

$$\tau = 0, R_{(X,Y)}(\tau) = F \neq 0, \tag{2.3}$$
$$\tau \neq 0, R_{(X,Y)}(\tau) = 0$$

, the sequence-pair (X, Y) is the Best Binary Sequence-pair.

Optimized Binary Sequence-pair is a kind of sequence which, to some extent, satisfies the requirement for the Best Signal that it has the high autocorrelation peak and zero autocorrelation sidelobe property. Based on the ideal autocorrelation property the Optimized Binary Sequence-pair, we would like to study whether there are a set of sequence-pairs which have good cross correlation between different sequence-pairs of the set while keeping the ideal autocorrelation property of the Optimized Binary Sequence-pair. Therefore, in this chapter, we will provide and investigate the Optimized Punctured Binary Sequence-pairs, the Zero/Low Cross Correlation Zone Sequence-pair Sets and the Optimized Punctured LCZ/ZCZ Sequence-pair Sets.

2.2 Optimized Punctured Binary Sequence-pairs

A CW sequence is made up of N bits of duration T_s. The complex envelope during one period is given by

$$x(t) = \sum_{i=1}^{N} x_i[t-(i-1)T_s], 0 \le t \le NT_s \tag{2.4}$$

Definition 2-2-1: The periodic autocorrelation values of such a signal, at delays which are multiple of T_s, are given by

$$R_{\mathbf{x}}(\tau) = R_{\mathbf{x}}(rT_s) = \frac{1}{N}\sum_{j=0}^{N-1} x_j y^*_{(j+r)modN}, \tag{2.5}$$
$$0 \le r \le N-1, 0 \le \tau \le (N-1)T_s.$$

Definition 2-2-2 [74]: Sequence $y = (y_0, y_1, \cdots, y_{N-1})$ is the punctured sequence for $x = (x_0, x_1, \cdots, x_{N-1})$,

$$y_j = \begin{cases} 0 & \text{if } y_j \text{ is punctured} \\ x_j & \text{if } y_j \text{ is Non-punctured} \end{cases} \tag{2.6}$$

Where p is the number of punctured bits in sequence x, suppose $x_j \in [-1, 1]$, y is p-punctured binary sequence, $y_j \in [-1, 0, 1]$, $(\mathbf{x}, \mathbf{y})$ is called a punctured binary sequence-pair. It is easy to see that there are only three possible choices for the phase state, corresponding to the $[-1, 0, 1]$ for the punctured binary sequence-pair. The punctured binary sequence-pair can be referred to as a new kind of triphase code.

Definition 2-2-3: The periodic autocorrelation of punctured sequence-pair $(\mathbf{x}, \mathbf{y})$ is defined

$$R_{\mathbf{xy}}(\tau) = R_{\mathbf{xy}}(rT_s) = \sum_{j=0}^{N-1} x_j y^*_{(j+r)modN}, 0 \le r \le N-1 \tag{2.7}$$

When punctured sequence-pair has the following autocorrelation property

$$R_{\mathbf{xy}}(\tau) = \begin{cases} E & \tau \equiv 0 \text{ mod N} \\ 0 & \text{otherwise} \end{cases} \tag{2.8}$$

$(\mathbf{x}, \mathbf{y})$ is called optimized punctured sequence-pair [74]. Here, $E = \sum_{j=0}^{N-1} x_i y_i = N - p$, is the energy of punctured sequence-pair. Then binary sequence-pair $(\mathbf{x}, \mathbf{y})$ is called a p-punctured sequence-pair. The energy efficiency of the sequence-pair is defined as

$$\eta = \frac{E}{N} = \frac{N\text{-}p}{N} \tag{2.9}$$

Definition 2-2-4: The balance of the sequence $\mathbf{x}$ is defined as $I = \sum_{j=0}^{N-1} x_j = n_p - n_n$, while n_p, n_n are the number of $'+1'$ and $'-1'$ in $\mathbf{x}$ separately.

We have also deduced several Theorems listed as below. Based on these Theorems, more optimized punctured sequence-pairs could be constructed easily.

Theorem 2-2-1: Mapping property, if $x_1(i) = x(-i), y_{1(i)} = y(-i)$,then sequence-pair $(\mathbf{x}_1, \mathbf{y}_1)$ is optimized punctured binary sequence-pair.

Theorem 2-2-2: Opposite to element symbol property, if $x_1(i) = -x(i), y_1(i) = -y(i)$,then sequence-pair $(\mathbf{x}_1, \mathbf{y}_1)$ is optimized punctured binary sequence-pair.

Theorem 2-2-3: Cyclic shift property, if $x_1(i) = -x(i+u), y_1(i) = -y(i+u)$,then sequence-pair $(\mathbf{x}_1, \mathbf{y}_1)$ is optimized punctured binary sequence-pair.

Theorem 2-2-4: Periodically sampling property, if $x_1(i) = -x(ki), y_1(i) = -y(ki), k$ and N are relatively prime, then sequence-pair $(\mathbf{x}_1, \mathbf{y}_1)$ is optimized punctured binary sequence-pair.

In [74], the properties, existing necessary conditions and some constructing methods have been well studied. The optimized punctured binary sequence-pairs of length from 3 to 31 are presented in the Table 1.

2.3 Zero/Low Cross Correlation Zone Sequence-pair Sets

In this section, we introduce several concepts of LCZ (Low Correlation Zone) and ZCZ (Zero Correlation Zone), and provide the the definition of LCZ/ZCZ sequence-pair sets.

Definition 2-3-1[75]: There is a set of spread spectrum codes $a_n^{(r)}$, where $r = 1, 2, ...M, n = 1, 2, ..N-1$, M is the number of the codes and N is the length of the code. When it is satisfied that

$$\begin{aligned} R_{\mathbf{rs}}(\tau) &= \sum_{n=0}^{N-1} a_n^{(r)} a_{n+\tau}^{(s)} \\ &= \begin{cases} N & \tau = 0, r = s \\ 0 & \tau = 0, r \neq s \\ 0 & 0 < |\tau| \leq Z_0 \end{cases} \end{aligned} \tag{2.10}$$

The set of codes is called Generalized Orthogonal Codes(GO)[76], or ZCZ codes[12]. $ZCZ(N, M, Z_0)$ is the abbreviation.

Definition 2-3-2[75]: There is a set of spread spectrum codes $a_n^{(r)}$, where $r = 1, 2, ...M, n = 1, 2, ..N-1$, M is the number of the codes and N is the length of the code. When it is satisfied that

$$\begin{aligned} R_{\mathbf{rs}}(\tau) &= \sum_{n=0}^{N-1} a_n^{(r)} a_{n+\tau}^{(s)} \\ &= \begin{cases} N & \tau = 0, r = s \\ \leq \epsilon & \tau = 0, r \neq s \\ \leq \epsilon & 0 < |\tau| \leq L_0 \end{cases} \end{aligned} \tag{2.11}$$

The set of codes is called Generalized Quasi-Orthogonal Codes(GO)[77], or LCZ codes[76]. $LCZ(N, M, L_0)$ is the abbreviation.

Based on the definitions mentioned above, the definition of LCZ/ZCZ sequence-pair sets is proposed.

Definition 2-3-3: There is a set of sequence-pairs $(c_n^{(r)}, d_n^{(r)})$, where $r = 1, 2, ...M, n = 1, 2, ..N-1$, M is the number of the sequence-pair and N is the length of the sequence. When it is satisfied that

$$\begin{aligned} R_{\mathbf{rs}}(\tau) &= \sum_{n=0}^{N-1} c_n^{(r)} d_{n+\tau}^{(s)} = \sum_{n=0}^{N-1} d_n^{(r)} c_{n+\tau}^{(s)} \\ &= \begin{cases} \lambda N & \tau = 0, r = s \\ 0 & \tau = 0, r \neq s \\ 0 & 0 < |\tau| \leq Z_0 \end{cases} \end{aligned} \tag{2.12}$$

Where $0 < \lambda \leq 1$. The set of sequence-pairs is the ZCZ sequence-pair set. $ZCZP(N, M, L_0)$ is the abbreviation.

Definition 2-3-4: There is a set of sequence-pairs $(c_n^{(r)}, d_n^{(r)})$, where $r = 1, 2, ...M, n = 1, 2, ..N-1$, M is the number of the sequence-pair and N is the length of the sequence. When it is satisfied that

$$\begin{aligned} R_{\mathbf{rs}}(\tau) &= \sum_{n=0}^{N-1} c_n^{(r)} d_{n+\tau}^{(s)} = \sum_{n=0}^{N-1} d_n^{(r)} c_{n+\tau}^{(s)} \\ &= \begin{cases} \lambda N & \tau = 0, r = s \\ \leq \epsilon & \tau = 0, r \neq s \\ \leq \epsilon & 0 < |\tau| \leq L_0 \end{cases} \end{aligned} \tag{2.13}$$

Where $0 < \lambda \leq 1$. The set of sequence-pairs is the LCZ sequence-pair set. $LCZP(N, M, L_0)$ is the abbreviation.

2.4 Optimized Punctured LCZ/ZCZ Sequence-pair Sets

We apply the Optimized Punctured Binary Sequence-pair to ZCZ/LCZ to construct the Optimized Punctured LCZ/ZCZ Sequence-pair sets.

Definition 2-4-1: If we use a pair of Optimized Punctured Binary Sequence-pair and a matrix, such as a Hadamard matrix or an orthogonal matrix, to construct

the sequence-pair sets $(c_n^{(r)}, d_n^{(r)})$ in Definition 2-3-3. The sequence-pairs set is called Optimized Punctured ZCZ Sequence-Pair Set.

Definition 2-4-2: If we use a pair of Optimized Punctured Binary Sequence-pair and a matrix, such as a Hadamard matrix or an orthogonal matrix, to construct the sequence-pair sets $(c_n^{(r)}, d_n^{(r)})$ in Definition 2-3-4. The sequence-pairs set is called Optimized Punctured LCZ Sequence-Pair Set.

2.5 Conclusions

We introduced the Optimized Binary Sequence-pair which has high autocorrelation peak and zero autocorrelation sidelobe. Based on the ideal autocorrelation property of the Optimized Binary Sequence-pair, we present and study the Optimized Punctured Binary Sequence-pairs, the LCZ/ZCZ Sequence-pair Sets and the Optimized Punctured LCZ/ZCZ Sequence-pair Sets. To sum up, these sequence-pair sets, which possess both the good cross correlation between different sequence-pairs of the set and the ideal autocorrelation property of each sequence-pair, could be potent candidates for set of best signals.

Table 2.1. Optimized Punctured Binary Sequence-pair

Length	Sequence (octet)	Punctured positions	Energy Efficiency(%)
3	6	3	66.67
5	32	3 4 5	40.00
5	34	2 4 5	40.00
7	162	4 5 7	57.14
7	164	4 6 7	57014
9	652	1 2 3 4 5 6 7	22.22
9	760	1 2 3 4 6 7 8	22.22
11	3426	4 5 6 8 11	54.54
11	3550	4 7 9 10 11	54.54
12	7426	1 6 7 12	66.67
12	7550	4 5 10 11	66.67
12	7624	3 6 9 12	66.67
13	16606	2 4 7 8 9 10 13	46.15
13	17124	5 6 8 9 10 12 13	46.15
15	74232	5 6 7 9 10 13 15	53.33
15	75310	6 7 10 11 13 14 15	53.33
17	351134	4 6 7 8 9 10 12 16 17	47.06
17	372142	3 6 8 9 10 13 14 15 17	47.06
19	1715412	5 6 9 12 13 14 15 17 19	52.63
19	1724154	5 7 9 10 11 12 15 18 19	52.63
20	3433330	2 5 6 7 8 9 12 15 16 17 18 19	40.00
20	3610556	1 6 7 8 9 10 11 16 17 18 19 20	40.00
21	7405316	2 5 6 7 8 9 11 13 14 16 17 20 21	38.10
21	7563240	3 5 6 9 10 12 13 15 17 18 19 20 21	38.10
23	37024632	6 7 8 9 11 13 14 17 18 21 23	52.17
23	37263120	6 8 11 12 15 16 18 20 21 22 23	52.17
28	1702164566	4 5 6 7 10 11 18 19 20 21 24 25	57.14
28	1734164226	4 5 8 9 10 11 18 19 22 23 24 25	57.14
28	1740465534	4 6 7 9 10 13 18 20 21 23 24 27	57.14
29	3556415302	4 7 11 13 14 15 16 19 20 21 24 25 26 27 29	48.28
29	3642213634	5 7 8 9 11 12 14 15 16 18 23 24 26 28 29	48.28
31	17053411166	5 6 7 9 11 15 16 17 18 20 21 23 24 28 31	51.61
31	17464412730	6 7 10 12 13 15 16 17 18 20 22 26 29 30 31	51.61

Note: The sequences in the table are presented by octets, '1' for '+1', '0' for '-1' and punctured positions begins from left to right.

CHAPTER 3

THREE METHODS TO CONSTRUCT THE OPTIMIZED PUNCTURED LCZ/ZCZ SEQUENCE-PAIR SETS

3.1 Introduction

We have provided the Optimized Punctured LCZ/ZCZ Sequence-pair sets in the last chapter. In this chapter, we would present three methods to construct the Optimized Punctured LCZ/ZCZ Sequence-pair sets and prove that the sequence-pair sets constructed by our methods satisfy the definitions of the Optimized Punctured LCZ/ZCZ Sequence-pair sets. In addition, examples are illustrated for each method and properties of the Optimized Punctured LCZ/ZCZ Sequence-pair sets are also analyzed to help studying our proposed codes.

Firstly, we apply the odd length Optimized Punctured Sequence-pair to ZCZ to construct an Optimized Punctured ZCZPS (ZCZ Sequence-pair Set). Then, we provide the method using even length Optimized Punctured Sequence-pair in LCZ to construct an approximately Optimized Punctured LCZPS (LCZ Sequence-pair Set). Since both of the above two construction methods are restricted by the specific length of the Optimized Punctured Sequence-pair, we present a method using any length Optimized Punctured Sequence-pair in ZCZ to construct an Optimized Punctured ZCZPS (ZCZ Sequence-pair Set).

3.2 Odd Length Optimized Punctured Sequence-pair in ZCZ

3.2.1 Constructing Method

Based on odd length optimized punctured binary sequence pairs and a Hadamard matrix, an optimized punctured ZCZPS (ZCZ Sequence-pair Set) can be constructed from the following steps:

Step 1: Considering an odd length optimized punctured binary sequence-pair (u, v), the length of each sequence is N_1

$$u = u_0, u_1, ..., u_{N_1-1}, u_i \in (-1, 1),$$
$$v = v_0, v_1, ..., v_{N_1-1}, v_i \in (-1, 0, 1),$$

Step 2: Considering Hadamard matrix B, the length of the sequence is N_2 which is equal to the number of the sequences. In other words, a Hadamard matrix of order N_2 is considered.

$$B = (b^0, b^1, ..., b^{N_2-1}),$$
$$b^i = (b^i_0, b^i_1, ..., b^i_{N_2-1}),$$

Step 3: Processing bit-multiplication on the optimized punctured binary sequence-pair and each row of Hadamard matrix B, then the sequence-pair set (X, Y) is obtained,

$$b^i = (b^i_0, b^i_1, ..., b^i_{N_2-1}), i = 0, 1, ..., N_2 - 1,$$
$$x^i_j = u_{jmodN_1} b^i_{jmodN_2}, 0 \le i \le N_2 - 1, 0 \le j \le N - 1,$$
$$X = (x^0, x^1, ..., x^{N_2-1}),$$
$$y^i_j = v_{jmodN_1} b^i_{jmodN_2}, 0 \le i \le N_2 - 1, 0 \le j \le N - 1,$$
$$Y = (y^0, y^1, ..., y^{N_2-1})$$

Where $GCD(N_1, N_2) = 1$, the common divisor of N_1 and N_2 is 1, $N = N_1 * N_2$. These three steps make the sequence-pair set (X, Y) an optimized punctured ZCZPS, where $N_1 - 1$ is the zero correlation zone Z_0. The length of each sequence in optimized punctured ZCZPS is $N = N_1 * N_2$ which depends on the product of length of optimized punctured sequence-pair and the length of each row in the Hadamard matrix. The number of sequence-pair in optimized punctured ZCZPS rests on the order of the Hadamard matrix. The sequence x^i in sequence set X and the corresponding sequence y^i in sequence set Y construct a sequence-pair (x^i, y^i) that can be used as a pulse compression code.

The correlation property of the sequence-pair in optimized punctured ZCZPS is:

$$\begin{aligned} R_{x^i y^j}(\tau) &= R_{x^j y^i}(\tau) = R_{uv}(\tau mod N_1) R_{b^i b^j}(\tau mod N_2) \\ &= R_{uv}(\tau mod N_1) R_{b^j b^i}(\tau mod N_2) \\ &= \begin{cases} EN_2, & \text{if } \tau = 0, i = j \\ 0, & \text{if } 0 < |\tau| \leq N_1 - 1, i = j \\ 0, & \text{if } i \neq j \end{cases} \end{aligned} \tag{3.1}$$

where $N_1 - 1$ is the zero correlation zone Z_0.

Proof:

1) When $i = j$,

$$\tau = 0, R_{uv}(0) = E, R_{b^i b^j}(0) = N_2,$$

$$R_{x^i y^j}(0) = R_{uv}(0) R_{b^i b^j}(0) = EN_2;$$

$$0 < |\tau| \leq N_1 - 1, R_{uv}(\tau) = 0,$$

$$R_{x^i y^j}(\tau) = R_{uv}(\tau mod N_1) R_{b^i b^j}(\tau mod N_2) = 0;$$

2) When $i \neq j$,

$$\tau = 0, R_{b^i b^j}(0) = 0,$$

$$R_{x^i y^j}(0) = R_{x^j y^i}(0) = R_{uv}(\tau mod N_1) R_{b^i b^j}(\tau mod N_2) = 0;$$

$$0 < |\tau| \leq N_1 - 1, R_{uv}(\tau) = 0,$$

$$R_{x^i y^j}(\tau) = R_{x^j y^i}(\tau) = R_{uv}(\tau mod N_1) R_{b^i b^j}(\tau mod N_2) = 0.$$

According to Definition 2-3-1, the sequence-pair set constructed by the above method is a ZCZPS.

3.2.2 Example and Property Analysis

Considering the optimized punctured ZCZPS that is constructed by the method mentioned in the last part, the autocorrelation and cross correlation properties can be simulated and analyzed with Matlab. For example, the optimized punctured ZCZPS (X, Y) is constructed by 31-length optimized punctured binary sequence-pair $(u, v), u = [+++-----+-+-+++----+--+--++++-++-], v = [++++000+0+0+++0000+00+00+++0++0]$ (using $'+'$ and $'-'$ symbols for $'1'$ and $'-1'$) and Hadamard matrix H of order 4. We follow the three steps presented in Section B to construct the 124-length optimized punctured ZCZPS. The number of sequence-pairs here is 4, and the length of each sequence is $31 * 4 = 124$. The first row of each matrix $X = [x_1; x_2; x_3; x_4]$ and $Y = [y_1; y_2; y_3; y_4]$ constitute a certain optimized punctured ZCZP (x_1, y_1). Similarly, the second row of each matrix

X and Y constitute another optimized punctured ZCZ sequence-pair (x_2, y_2) and so on.

$$
\begin{aligned}
\mathbf{x}_1 &= [+++{+}{-}{-}{-}{+}{-}{+}{-}{+}{+}{+}{-}{-}{-}{-}{+}{-}{-} \\
&\quad +{-}{-}{+}{+}{+}{-}{+}{+}{-}{+}{+}{+}{+}{-}{-}{-}{+}{-}{+}{-} \\
&\quad +{+}{+}{-}{-}{-}{-}{+}{-}{-}{+}{-}{-}{+}{+}{+}{-}{+}{+}{-}{+} \\
&\quad +{+}{+}{-}{-}{-}{+}{-}{+}{-}{+}{+}{+}{-}{-}{-}{-}{+}{-}{-}{+} \\
&\quad -{-}{+}{+}{+}{-}{+}{+}{-}{+}{+}{+}{+}{-}{-}{-}{+}{-}{+}{-}{+} \\
&\quad +{+}{-}{-}{-}{-}{+}{-}{-}{+}{-}{-}{+}{+}{+}{-}{+}{+}{-}], \\
\mathbf{y}_1 &= [+++{+}000{+}0{+}0{+}{+}{+}0000{+}00 \\
&\quad +00{+}{+}{+}0{+}{+}0{+}{+}{+}{+}000{+}0{+}0{+}{+}{+}00 \\
&\quad 00{+}00{+}00{+}{+}{+}0{+}{+}0{+}{+}{+}{+}000{+}0{+}0 \\
&\quad +{+}{+}0000{+}00{+}00{+}{+}{+}0{+}{+}0{+}{+}{+}{+}00 \\
&\quad 0{+}0{+}0{+}{+}{+}0000{+}00{+}00{+}{+}{+}0{+}{+}0], \\
\mathbf{x}_2 &= [+{-}{+}{-}{-}{+}{-}{-}{-}{-}{-}{-}{+}{-}{-}{+}{-}{+}{+}{+}{-} \\
&\quad -{-}{+}{+}{-}{+}{+}{+}{-}{-}{-}{+}{-}{+}{+}{-}{+}{+}{+}{+}{+} \\
&\quad +{-}{+}{+}{-}{+}{-}{-}{-}{+}{+}{+}{-}{-}{+}{-}{-}{-}{+}{+}{+} \\
&\quad -{+}{-}{-}{+}{-}{-}{-}{-}{-}{-}{+}{-}{-}{+}{-}{+}{+}{+}{-}{-} \\
&\quad -{+}{+}{-}{+}{+}{+}{-}{-}{-}{+}{-}{+}{+}{-}{+}{+}{+}{+}{+}{+} \\
&\quad -{+}{+}{-}{+}{-}{-}{-}{+}{+}{+}{-}{-}{+}{-}{-}{-}{+}{+}].
\end{aligned}
$$

$$
\begin{aligned}
\mathbf{y}_2 \;=\; & [+-+-000-0-0-+-0000+00 \\
& -00+-+0+-0-+-+000+0+0+-+00 \\
& 00-00+00-+-0-+0+-+-000-0-0 \\
& -+-0000+00-00+-+0+-0-+-+00 \\
& 0+0+0+-+0000-00+00-+-0-+0].
\end{aligned}
$$

3.2.2.1 Autocorrelation and Cross Correlation Properties

The autocorrelation property $R(x_1, y_1)$ and cross correlation property $R(x_1, y_2) = R(y_1, x_2)$ of 124-length optimized punctured ZCZPS (X, Y), are shown in Fig. 3.1.

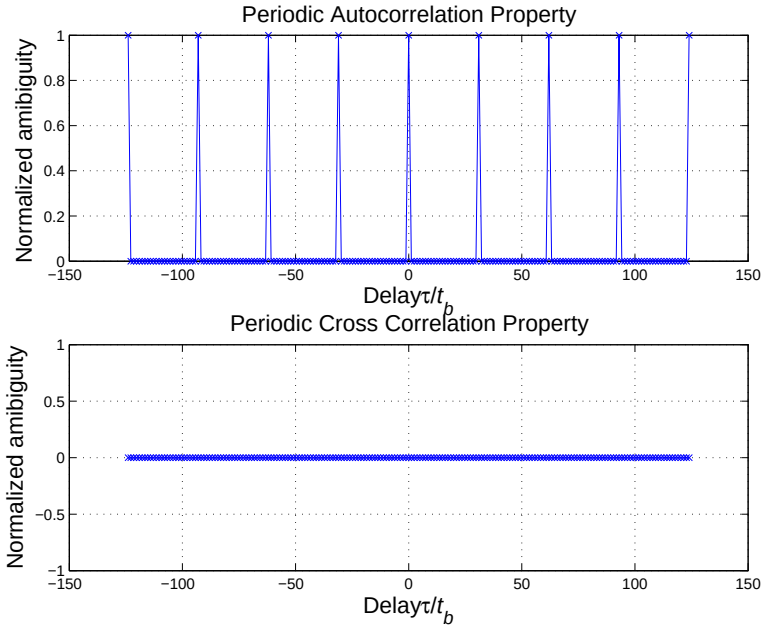

Figure 3.1. Periodic autocorrelation property of optimized punctured ZCZPS.

From the Fig. 3.1, the sidelobe of autocorrelation of ZCZPS can be as low as 0 when the time delay is kept within $Z_0 = N_1 = 31$ and the cross correlation value is 0 during the whole time domain.

It is known that a suitable criterion for evaluating code of length N is the ratio of the peak signal divided by the peak signal sidelobe (PSR) of their autocorrelation function, which can be bounded by [69]

$$[PSR]_{dB} \leq 20logN = [PSR_{max}]_{dB} \tag{3.2}$$

The only uniform phase codes that can reach the PSR_{max} are the Barker codes whose length is equal or less than 13. The sidelobe of the new code shown in Fig. 3.1 can be as low as 0, and the peak signal divided by the peak signal sidelobe can be as large as infinite. Besides, the length of the new code is various and much longer than the length of the Barker code.

3.2.2.2 Ambiguity function

When the transmitted impulse is reflected by a moving target, the reflected echo signal includes a linear phase shift, which comes from the Doppler shift f_d [69]. As a result of the Doppler shift f_d, the main peak of the autocorrelation function is reduced. At the same time, SNR degradation occurs as well.

The ambiguity function, which is commonly used to analyze the radar performance within Doppler shift can be found in [69] shown as following:

$$y(t, F_D) = \int_{-\infty}^{\infty} x(s)e^{j2\pi F_D s}x^*(s-t)ds \equiv \hat{A}(t, F_D) \tag{3.3}$$

where t is the time delay and F_D is the Doppler shift.

An equivalent definition can be given in terms of the signal spectrum by applying the basic Fourier transform properties

$$\hat{A}(t, F_D) = \int_{-\infty}^{\infty} X^*(F)X(F - F_D)e^{j2\pi Ft}dF \tag{3.4}$$

The *ambiguity function* is defined as the magnitude of $\hat{A}(t, F_D)$ [69] with the following:

$$A(t, F_D) \equiv |\hat{A}(t, F_D)| \tag{3.5}$$

However, we are focusing on the optimized punctured ZCZPS in the paper, so the transmitting code and the receiving code can be different. Assuming the ZCZPS are (X, Y), $x^{(p)} \in X$, $(x^{(p)} = \sum_{n=0}^{N-1} x_n^{(p)}(t - nT_s)$, $y^{(p)} \in Y$, $y^{(q)} = \sum_{n=0}^{N-1} y_n^{(p)}(t - nT_s))$, the periodic correlation is used instead of aperiodic correlation here. The $\hat{A}_{pair}(t, F_D)$ in one period of length NT_s can be expressed as:

$$\begin{aligned} & A_{pair}(t, F_D) \equiv |\hat{A}_{pair}(t, F_D)| \\ = \; & |\int_0^t x^{(p)}(s) y^{(q)*}(s + (NT_s - t)) e^{(j2\pi F_D s)} ds \\ & + \int_t^{(N-1)T_s} x^{(p)}(s) y^{(q)*}(s - t) e^{(j2\pi F_D s)} ds | p, q = 0, 1, 2..., K-1 \end{aligned} \tag{3.6}$$

At the same time, when $p = q$, equation (3.7) can be used to analyze the autocorrelation performance within the Doppler shift, and when $q \neq p$, equation (3.7) can be used to analyze the cross correlation performance within the Doppler shift. Equation (3.7) is plotted in Fig. 3.2 in a three-dimensional surface plot to analyze the radar performance of optimized punctured ZCZPS within the Doppler shift. Here, maximal time delay is 1 unit (normalized to length of the code, in units of NT_s) and the maximal doppler shift is 5 units for cross correlation and 3 units for autocorrelation (normalized to the inverse of the length of the code, in units of $1/NT_s$).

In Fig. 3.2(a), there is a relative uniform plateau suggesting low and uninform sidelobes. This low and uniform sidelobes minimizes target masking effect in ZCZ of time domain, where $Z_0 = 31$, $-31 < \tau < 31$. From Fig. 3.2(b), we can consider a cross correlation property between any two optimized punctured ZCZ sequence-pairs in the ZCZ sequence-pair set such as $R(x_1, y_2)$ or $R(y_1, x_2)$ where (x_1, y_1) and (x_2, y_2)

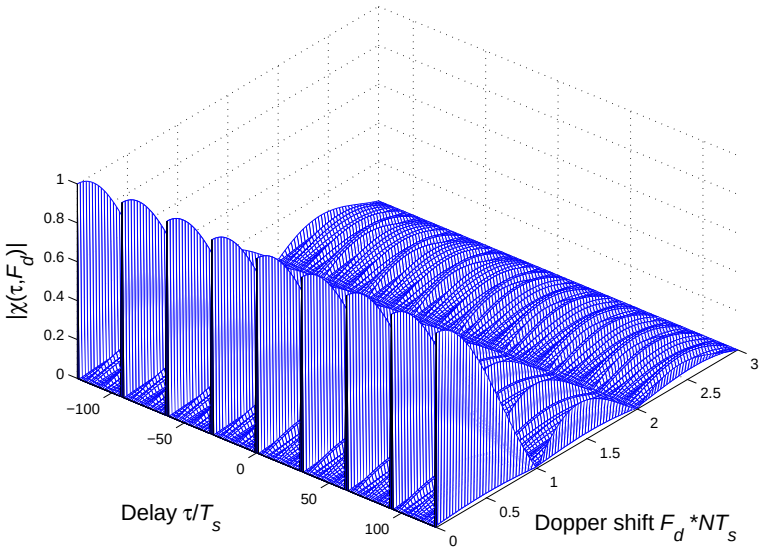

(a)

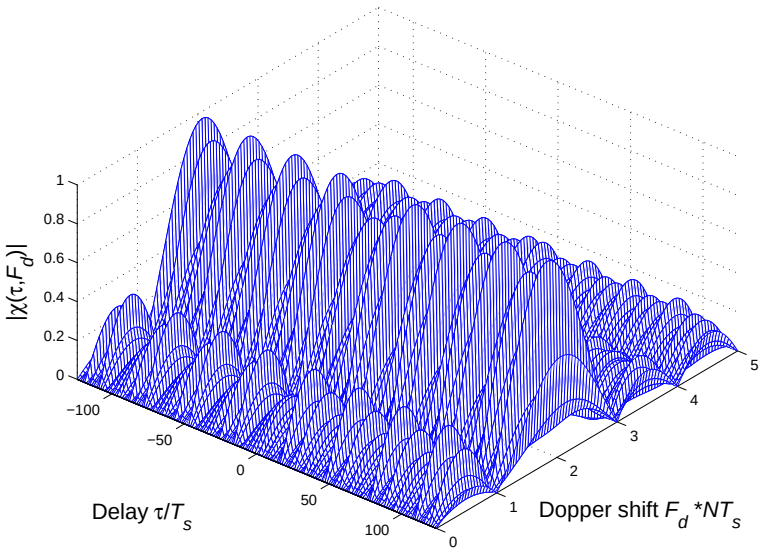

(b)

Figure 3.2. Ambiguity function of 124-length ZCZPS: (a) autocorrelation (b) cross correlation.

are two pairs of optimized punctured ZCZP. A 124-length optimized punctured ZCZP is tolerant of Doppler shift when the Doppler shift is not large. When the Doppler shift is zero, the range sidelobe of cross correlation of our proposed code is zero in the whole time domain.

As synchronization technology develops exponentially in the industrial world, time delay can, to some extent, be well controlled. Therefore, it is necessary to investigate the performance of our proposed code without time delay. When $t = 0$, the ambiguity function can be expressed as:

$$\hat{A}_{pair}(0, F_D) = \int_0^{(N-1)T_s} x^{(p)}(s) y^{(q)*}(s) e^{(j2\pi F_D s)} ds \tag{3.7}$$

And this kind of Doppler shift performance with no time delay is presented in the Fig. 3.3.

Fig. 3.3(a) illustrates that without a time delay and having the Doppler shift less than 1 unit, the autocorrelation value of optimized punctured ZCZPS falls sharply during one unit, and the trend of the amplitude over the whole frequency domain decreases as well. Fig. 3.3(b) shows that there are some convex surfaces in the cross correlation performance. One should observe Fig. 3.3(a) and Fig. 3.3(b), when Doppler frequencies equal to multiples of the pulse repetition frequency ($PRF = 1/PRI = 1/Ts$), all the ambiguity value turns to zero except when Doppler frequency is equal to 2 PRF for cross correlation. That is the same as many widely used pulse compression binary code such as the Barker code. Overall, the ambiguity function performances of optimized punctured ZCZP can be as efficient as conventional pulse compression binary code.

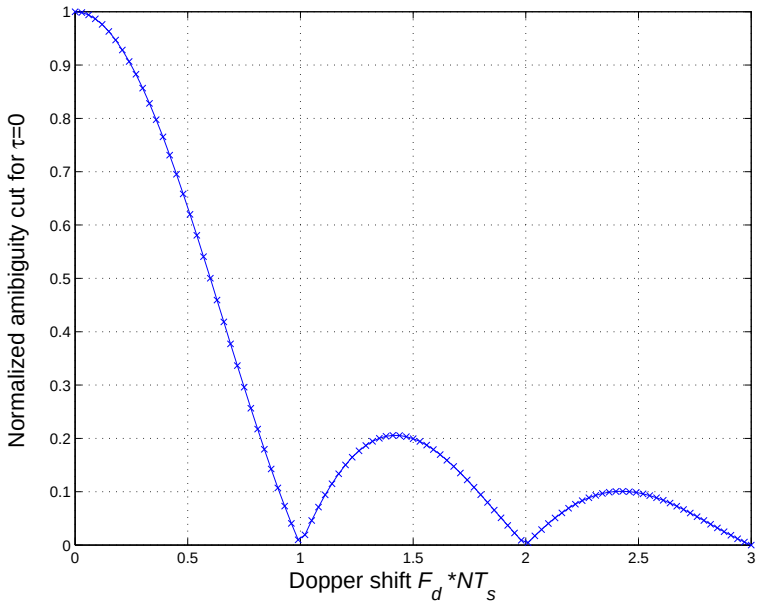

(a)

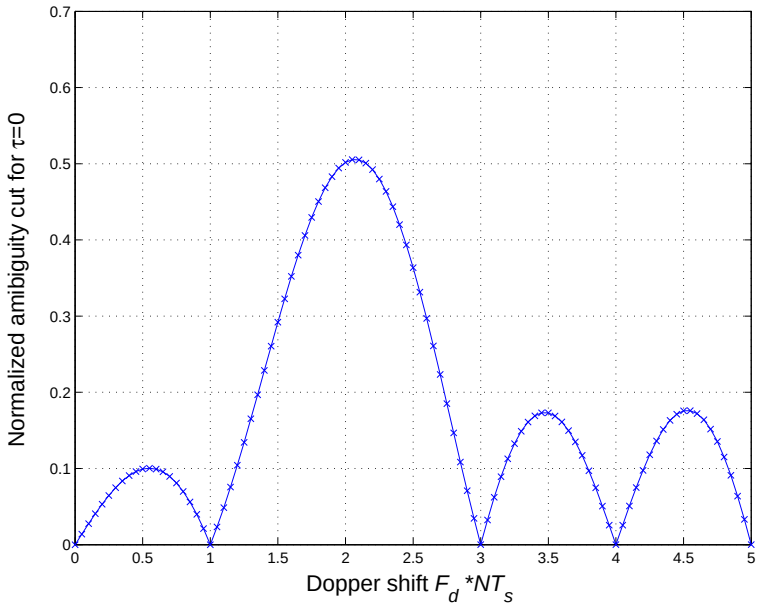

(b)

Figure 3.3. Doppler shift of 124-length ZCZPS(time delay=0): (a) autocorrelation (b) cross correlation.

3.3 Even Length Optimized Punctured Sequence-pair in LCZ

3.3.1 Constructing Method

The length of Optimized Punctured Sequence-pair is restricted to odd. As a result, we propose a method that depends on even length Optimized Punctured Sequence-pair and modified Hadamard matrix to construct the Approximately Optimized LCZ Sequence-pair Sets. The constructing steps are as following:

Step 1: Considering an even length optimized punctured binary sequence-pair (u, v), the length of each sequence is N_1

$$u = u_0, u_1, ..., u_{N_1-1}, u_i \in (-1, 1),$$

$$v = v_0, v_1, ..., v_{N_1-1}, v_i \in (-1, 0, 1),$$

where

$$R_{\mathbf{xy}}(\tau) = R_{\mathbf{xy}}(rT_s) = \sum_{j=0}^{N-1} x_j y^*_{(j+r)modN}, 0 \leq r \leq N-1$$

$E = \sum_{j=0}^{N_1-1} x_j y_j = N - p$, p is the number of punctured bits in the Optimized Punctured Sequence-pair.

Step 2: We modify the Hadamard matrix to construct a sequences set B. Any sequences $b^{(i)} \neq b^{(j)} \in B$ satisfy that $R_{bb'}(0) = \pm 1$. We delete a column in a Hadamard matrix of length 2^m to construct the sequences set B. The sequence length is $N_2 = 2^m - 1$, and the number of sequences is $M = 2^m$. The sequences set could be called modified Hadamard matrix.

Step 3: Processing bit-multiplication on the optimized punctured binary sequence-pair and each row of modified Hadamard matrix B, then the sequence-pair set (X, Y) is obtained,

$$
\begin{aligned}
&b^i = (b_0^i, b_1^i, ..., b_{N_2-1}^i), i = 0, 1, ..., N_2 - 1, \\
&x_j^i = u_{jmodN_1} b_{jmodN_2}^i, 0 \le i \le N_2 - 1, 0 \le j \le N - 1, \\
&X = (x^0, x^1, ..., x^{N_2-1}), \\
&y_j^i = v_{jmodN_1} b_{jmodN_2}^i, 0 \le i \le N_2 - 1, 0 \le j \le N - 1, \\
&Y = (y^0, y^1, ..., y^{N_2-1})
\end{aligned}
$$

Where $GCD(N_1, N_2) = 1$, the common divisor of N_1 and N_2 is 1, the length of the sequence is $N = N_1 * N_2$. The correlation functions of the sequence-pairs in the set (X, Y) satisfy that

$$
\begin{aligned}
R_{x^i y^j}(\tau) &= R_{x^j y^i}(\tau) = R_{uv}(\tau mod N_1) R_{b^i b^j}(\tau mod N_2) \\
&= R_{uv}(\tau mod N_1) R_{b^j b^i}(\tau mod N_2) \\
&= \begin{cases} EN_2, & \text{if } \tau = 0, i = j \\ \pm E, & \text{if } 0 < |\tau| \le N_1 - 1, i = j \\ 0, & \text{if } i \ne j \end{cases}
\end{aligned} \tag{3.8}
$$

.

These three steps make the sequence-pair set (X, Y) an optimized punctured LCZPS, where $N_1 - 1$ is the zero correlation zone L_0. The length of each sequence in optimized punctured LCZPS is $N = N_1 * N_2$ which depends on the product of length of optimized punctured sequence-pair and the length of each row in the modified Hadamard matrix. The number of sequence-pair in optimized punctured LCZPS rests on the order N_2 of the Hadamard matrix.

Proof:

It is known that $b^{(i)} \neq b^{(j)} \in B, R_{bb'}(0) = \pm 1$.

1) When $i = j$,

$$\tau = 0, R_{uv}(0) = E, R_{b^i b^j}(0) = N_2, R_{x^i y^j}(0) = R_{uv}(0) R_{b^i b^j}(0) = EN_2;$$

$$0 < |\tau| \leq N_1 - 1, R_{uv}(\tau) = 0, R_{x^i y^j}(\tau) = R_{uv}(\tau mod N_1) R_{b^i b^j}(\tau mod N_2) = 0;$$

2) When $i \neq j$,

$$\tau = 0, R_{b^i b^j}(0) = \pm 1, R_{x^i y^j}(0) = R_{x^j y^i}(0) = R_{uv}(\tau mod N_1) R_{b^i b^j}(\tau mod N_2) = \pm E;$$

$$0 < |\tau| \leq N_1 - 1, R_{uv}(\tau) = 0, R_{x^i y^j}(\tau) = R_{x^j y^i}(\tau)$$

$$= R_{uv}(\tau mod N_1) R_{b^i b^j}(\tau mod N_2) = 0.$$

According to Definition 2-4-2, the sequence-pair set constructed by the above method is a LCZPS.

3.3.2 Example and Property Analysis

In this section, we follow the method mentioned in the above section to an optimized punctured LCZPS. The autocorrelation and cross correlation properties can be simulated and analyzed with Matlab. For example, the optimized punctured LCZPS (X, Y) is constructed by 12-length optimized punctured binary sequence-pair $(u, v), u = [+++-----+-++-], v = [0+++-00+-++0]$ (using $'+'$ and $'-'$ symbols for $'1'$ and $'-1'$) and modified Hadamard matrix B which is a $8x7$ matrix. We follow the three steps presented in last section to construct the 84-length optimized punctured LCZPS. The number of sequence-pairs here is 8, and the length of each sequence is $12 * 7 = 84$. The first row of each matrix $X = [x_1; x_2; ...; x_8]$ and $Y = [y_1; y_2; ...; y_8]$ constitute a certain optimized punctured ZCZP (x_1, y_1). Similarly,

the second row of each matrix X and Y constitute another optimized punctured ZCZ sequence-pair (x_2, y_2) and so on.

$$
\begin{aligned}
\mathbf{x}_1 &= [+++-{-}{-}+-+{+}-+{+}{+}{+}{-}{-}{-}+-+{+}-{+}{+}{+}{-}{-}-\\
&\quad +-+{+}-+{+}{+}{+}-{-}{-}+-+{+}-+{+}{+}{+}{-}{-}{-}+-+{+}-{+}+\\
&\quad ++-{-}{-}+-+{+}-+{+}{+}{+}-{-}{-}+-+{-}],\\
\mathbf{y}_1 &= [0+++{-}00+-+{+}00+++{-}00+-+{+}00+++{-}00+-+{+}00+\\
&\quad ++{-}00+-+{+}00+++{-}00+-+{+}00+++{-}00+-+{+}00+++\\
&\quad {-}00+-+{+}0];\\
\mathbf{x}_2 &= [+-+-{-}+-+{+}+-{-}+{+}-{-}+-{-}{-}+-{-}{-}+-+-+-\\
&\quad {-}{-}{-}+-{-}+-+{+}-{-}{-}{-}{-}+{+}{+}{+}-+{+}-+{+}-{-}+{+}{+}-\\
&\quad ++{+}-+{+}{+}{+}{+}{+}{+}-+-{-}{-}+{+}{+}+{-}{-}],\\
\mathbf{y}_2 &= [0-+-{-}00+++{-}00++-{-}00--+{-}00+-+{-}00---{+}00+\\
&\quad -+{+}00---{+}00+-+{+}00+--{+}00-++{+}00+++{+}00-+-\\
&\quad {-}00+++{-}0].
\end{aligned}
$$

3.3.2.1 Autocorrelation and Cross Correlation Properties

The autocorrelation property $R(x_1, y_1)$ and cross correlation property $R(x_1, y_2) = R(y_1, x_2)$ of 84-length optimized punctured ZCZPS (X, Y), are shown in Fig. 3.4.

From the Fig. 3.4, the sidelobe of autocorrelation of LCZPS can be as low as 0 when the time delay is kept within $Z_0 = N_1 - 1 = 11$ and the cross correlation value is $E =$ during the whole time domain.

According to the simulation results, the auto correlation sidelobe of the new sequence-pair could be as low as 0, which is still better than the property of Barker codes. The cross correlation values of the two sequence-pairs do not reach zero nor

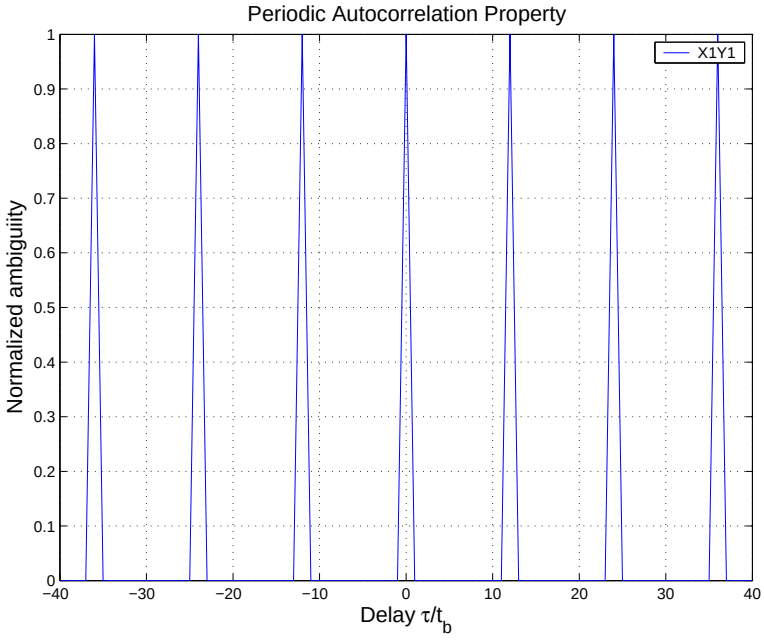

(a)

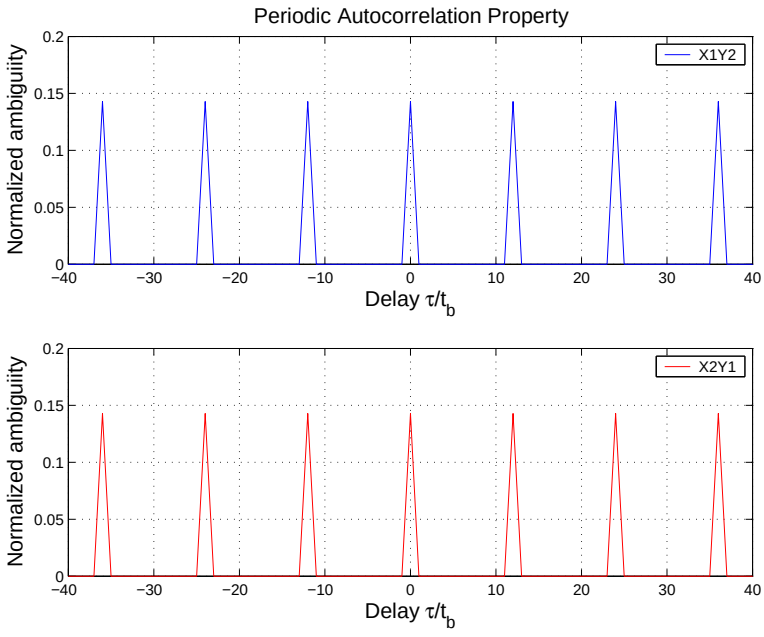

(b)

Figure 3.4. Periodic correlation property of optimized punctured LCZPS: (a) auto-correlation (b) cross correlation.

be equal. As a result, the correlation properties of LCZPS are not as good as the ZCZPS studied before. Nevertheless, LCZPS is proposed to effectively compensates for deficiency of ZCZPS that the length of optimized punctured binary sequence-pair.

3.3.2.2 Ambiguity function

Based on the deduction in Section 3.2.3, we use the equation (3.7) to analyze the autocorrelation performance of LCZPS within the Doppler shift when $p = q$. The equation (3.7) could be also used to analyze the cross correlation performance of LCZPS within the Doppler shift. A three-dimensional surface plot is illustrated in Fig. 3.5 to analyze the radar performance of optimized punctured ZCZPS within the Doppler shift. Here, maximal time delay is 1 unit (normalized to length of the code, in units of NT_s) and the maximal doppler shift is 5 units for cross correlation and 3 units for autocorrelation (normalized to the inverse of the length of the code, in units of $1/NT_s$).

In Fig. 3.5, there is a relative uniform plateau suggesting low and uninform sidelobes. This low and uniform sidelobes minimizes target masking effect in LCZ of time domain, where $L_0 = 11$, $-11 \leq \tau \leq 11$. Generally speaking, a 84-length optimized punctured LCZP is tolerant of Doppler shift when the Doppler shift is not large.

In addition, we study the Doppler shift performance of LCZP with no time delay.

Fig. 3.6 illustrates that without a time delay and having the Doppler shift less than 1 unit, the autocorrelation value of an optimized punctured LCZP falls sharply during one unit, and the trend of the amplitude over the whole frequency domain decreases as well. When Doppler frequencies equal to multiples of the pulse repetition frequency ($PRF = 1/PRI = 1/Ts$), all the ambiguity value turns to zero.

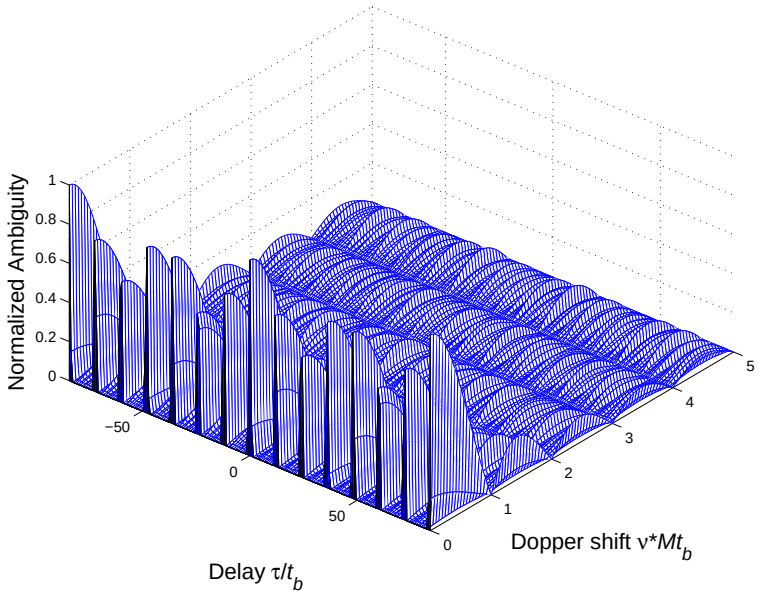

Figure 3.5. Ambiguity function of 84-length ZCZPS: autocorrelation.

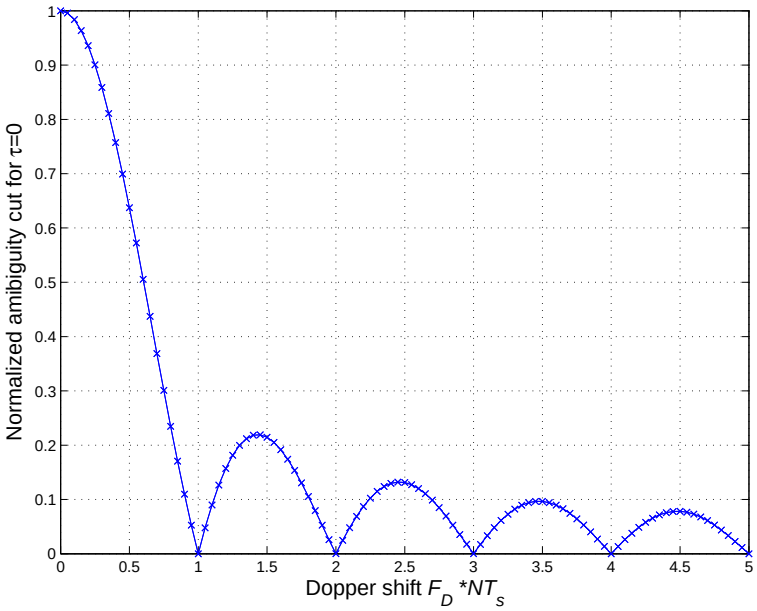

Figure 3.6. Doppler shift performance of 84-length LCZPS(time delay=0): autocorrelation.

It is easy to draw the conclusion that the property of the LCZP could be comparable to many widely used pulse compression binary code such as the Barker code.

3.4 Any Length Optimized Punctured Sequence-pair in ZCZ

3.4.1 Constructing Method

An optimized punctured ZCZ sequence-pair set can be constructed from the following steps:

Step 1: Given an optimized punctured binary sequence-pair (u, v), the length of each sequence is N_1

$$u = u_0, u_1, ..., u_{N_1-1}, u_i \in (-1, 1),$$

$$v = v_0, v_1, ..., v_{N_1-1}, v_i \in (-1, 0, 1),$$

Step 2: Given orthogonal matrix B, the length of the sequence is N_2 which is equal to the number of the sequences.

$$B = (b^0; b^1; ..., b^{N_2-1}), b^i = \frac{1}{\sqrt{N_2}}(b_0^i, b_1^i, ..., b_{N_2-1}^i)$$

Step 3: Process the optimized punctured binary sequence-pair with each row of the orthogonal matrix B,

$$x_j^i = u(((N_1/d) * j + \lfloor j/d \rfloor) mod N_1) b_{jmodN_2}^i,$$

$$X = (x^0; x^1; ...; x^{N_2-1}), x^i = (x_0^i, x_1^i, ..., x_{N-1}^i,)$$

$$0 \leq i \leq N_2 - 1, 0 \leq j \leq N - 1,$$

$$y_j^i = v(((N_1/d) * j + \lfloor j/d \rfloor) mod N_1) b_{jmodN_2}^i,$$

$$0 \leq i \leq N_2 - 1, 0 \leq j \leq N - 1,$$

$$Y = (y^0; y^1; ...; y^{N_2-1}), y^i = (y_0^i, y_1^i, ..., y_{N-1}^i,)$$

Where $d = GCD(N_1, N_2)$, $N = N_1 * N_2$ and $\lfloor j/d \rfloor$ means to get the integer of $\lfloor j/d \rfloor$. The three steps make the sequence-pair set (X, Y) an optimized punctured ZCZPS, where ZCZ $Z_0 = N_1 - 1$. The length of each sequence in optimized punctured ZCZPS is $N = N_1 * N_2$ that depends on the product of length of optimized punctured sequence-pair and the length of a row in Hadamard matrix. The number of sequence-pairs in optimized punctured ZCZPS rests on the order of the Hadamard matrix. The sequence x^i in X and the corresponding sequence y^i in Y construct an optimized punctured ZCZP (x^i, y^i) that can be used as a phase coded waveform, such as x^i for radar transmitter and y^i for radar receiver. The phase states for any sequence-pair among (x^i, y^i) are only of three options, so our newly provided optimized punctured ZCZPS is a new set of triphase codes.

Then we try to prove that the sequence-pair set constructed following the above steps are optimized punctured ZCZPS. Proof:

$$
\begin{aligned}
& R_{x^i y^j}(\tau) = \sum_{k=0}^{N_1 N_2 - 1} u_k^i v^j_{(k+\tau) mod N_1 N_2} \qquad (3.9) \\
= & \sum_{k=0}^{N_1 N_2 - 1} u((N_1/d)k + \lfloor k/d \rfloor) mod N_1 b_{i, k mod N_2} \cdot \\
& v^*((N_1/d)(k+\tau) + \lfloor (k+\tau)/d \rfloor) mod N_1 b^*_{j,(k+\tau) mod N_2} \\
= & \sum_{m=0}^{N_1 - 1} \sum_{r=0}^{N_2 - 1} b_{i,(mN_2 + r) mod N_2} b^*_{j,(mN_2 + r + \tau_0 d + \tau_1) mod N_2} \\
& u((N_1/d)(mN_2 + r) + \lfloor (mN_2 + r)/d) \rfloor) mod N_1 \\
& v^*((N_1/d)(mN_2 + r + \tau_0 d + \tau_1) \\
& + \lfloor (mN_2 + r + \tau_0 d + \tau_1/d) \rfloor) mod N_1 \\
= & \sum_{r=0}^{N_2 - 1} b_{i,r} b^*_{j,(r + \tau_0 d + \tau_1) mod N_2} \sum_{m=0}^{N_1 - 1} \\
& u((N_{1/d}/d)r + mN_2/d + \lfloor r/d \rfloor) mod N_1 \\
& v^*((N_1/d)(r + \tau_1) + mN_2/d + \tau_0 + \lfloor (r + \tau_1/d) \rfloor) mod N_1
\end{aligned}
$$

Here, $k = mN_2 + r, \tau = \tau_0 d + \tau_1, 0 \le m \le N_1 - 1, 0 \le r \le N_2 - 1, 0 \le \tau_1 \le d - 1$. If $T_{m,r} = ((N_1/d)r + mN_2/d + \lfloor r/d \rfloor) mod N_1)$, $T_{m,r+\tau} - T_{m,r}$ is unrelated to m. Then we can have that

$$\begin{aligned} t_{t,\tau} &= T_{m,r+\tau} - T_{m,r} \\ &= ((N_1/d) \cdot \tau_1 + \tau_0 + \lfloor (r + \tau_1)/d \rfloor) - \lfloor r/d \rfloor) mod N_1 \end{aligned} \tag{3.10}$$

So $R_{x^i y^j}$ could be abbreviated to

$$R_{x^i y^j} = \sum_{r=0}^{N_2-1} b_{i,r} b^*_{j,(r+\tau_0+\tau_1) mod N_2} R_{uv}(t_{r,\tau}) \tag{3.11}$$

(1) If $d = 1$, $\tau = \tau_0 d + \tau_1, 0 \le \tau_1 \le d - 1, \tau_1 = 0, t_{r,\tau} = \tau$. According to (3.11), we have $R_{x^i y^j}(\tau) = \sum_{r=0}^{N_2-1} b_{i,r} b^*_{j,(r+\tau_0 d+\tau_1) mod N_2} R_{uv}(\tau)$. Also (u, v) is the optimized punctured binary sequence-pair.

When $i = j$,

$$\begin{aligned} &\tau = 0, \\ &R_{x^i y^j}(0) = R_{x^j y^i}(0) = \sum_{r=0}^{N_2-1} b_{i,r} b^*_{i,r mod N_2} R_{uv}(0) = N_2 E; \\ &0 < |\tau| \le N_1 - 1, R_{uv}(\tau) = 0, \\ &R_{x^i y^j}(\tau) = \sum_{r=0}^{N_2-1} b_{i,r} b^*_{i,r mod N_2} R_{uv}(\tau) = 0; \end{aligned}$$

When $i \ne j$,

$$\begin{aligned} &\tau = 0, \\ &R_{x^i y^j}(0) = R_{xy}(0) \sum_{r=0}^{N_2-1} b_{i,r} b^*_{i,r mod N_2}, \\ &since \sum_{r=0}^{N_2-1} b_{i,r} b^*_{i,r mod N_2} = 0, R_{x^i y^j}(0) = 0; \\ &0 < |\tau| \le N_1 - 1, R_{uv}(\tau) = 0, \\ &R_{x^i y^j}(\tau) = \sum_{r=0}^{N_2-1} b_{i,r} b^*_{i,(r+\tau) mod N_2} R_{xy}(\tau) = 0; \end{aligned}$$

Similarly, $R_{x^jy^i}$ could be proved.

(2) If $d > 1$,

When $\tau_0 \leq N_1/d - 2$ and $0 \leq \tau_1 \leq d - 1$,

$$\begin{aligned} t_{r,\tau} &= ((N_1/d) \cdot \tau_1 + \tau_0 + \lfloor (r + \tau_1)/d \rfloor) mod N_1 \\ &\leq ((N_1/d)(d-1) + N_1/d - 2 + 1) mod N_1 \\ &= N_1 - 1 \end{aligned}$$

When $\tau_0 \leq N_1/d - 1, \tau_1 \leq d - 2$,

$$\begin{aligned} t_{r,\tau} &= (N_1/d)\tau_1 + \tau_0 + \lfloor (r + \tau_1)/d \rfloor + \lfloor r/d \rfloor) mod N_1 \\ &\leq ((N_1/d)(d-2) + N_1/d - 1 + 1) mod N_1 \\ &= N_1 - N_1/d \leq N_1 - 1 \end{aligned}$$

As a result, when $0 < \tau \leq N_1 - 2$, then $1 \leq t_{r,\tau} \leq N_1 - 1$. (u, v) is the optimized punctured binary sequence-pair, so we could get $R_{uv}(\tau) = 0$ and $R_{x^iy^j}(\tau) = 0$. Similarly, when $i \neq j, R_{x^iy^j}(0) = R_{uv}(0) \sum_{r=0}^{N_2-1} b_{i,r} b^*_{j,r mod N_2}$. Since $\sum_{r=0}^{N_2-1} b_{i,r} b^*_{j,r mod N_2} = 0$, $R_{x^iy^j}(-\tau) = R_{c^id^j}(\tau)$. It is also easy to prove that when $-(N_1 - 2) \leq \tau < 0$, $R_{x^iy^j}(\tau) = 0$. Similarly, $R_{x^jy^i} = 0$.

Theorem 3-4-1 The optimized punctured binary sequence-pair (u, v) and the N_2 order orthogonal matrix B constructed an optimized punctured ZCZPS (X, Y), $d = GCD(N_1, N_2)$, in some other words, N_1/d is relatively prime to N_2, then
(1) $d = 1$, the ZCZPS could be expressed as $ZCZPS(N_1N_2, N_2, N_1 - 1)$, and

$$R_{x^iy^j}(\tau) = \begin{cases} EN_2, & \text{if } \tau = 0, i = j \\ 0, & \text{if } 0 < |\tau| \leq N_1 - 1, i = j \\ 0, & \text{if } 0 < |\tau| \leq N_1 - 1, i \neq j \end{cases}$$

(2) $d > 1$, the ZCZPS could be expressed as $ZCZPS(N_1N_2, N_2, N_1 - 2)$, and

$$R_{x^iy^j}(\tau) = \begin{cases} \epsilon N_1 N_2, & \text{if } \tau = 0, i = j \\ 0, & \text{if } 0 < |\tau| \leq N_1 - 2, i = j \\ 0, & \text{if } 0 < |\tau| \leq N_1 - 2, i \neq j \end{cases}$$

If the punctured sequence-pair has the following autocorrelation property:

$$R_{uv}(\tau) = \begin{cases} E, & \text{if } \tau \equiv 0 \text{mod} N \\ 0, & \text{others} \end{cases} \tag{3.12}$$

the punctured sequence-pair is called optimized punctured sequence-pair [74]. Where, $E = \sum_{i=0}^{N-1} u_i v_{(i+\tau) mod N} = N - p$, is the energy of punctured sequence-pair.

The properties, existing necessary conditions and some construction methods of punctured binary sequence-pair have been well studied by Jiang [74]. Many optimized punctured sequence-pairs have been found of length from 7 to 31 so far.

3.4.2 Example and Property Analysis

An example is given to analyze the autocorrelation and cross correlation properties of the optimized punctured ZCZPS constructed by the method mentioned above. The 144-length optimized punctured ZCZPS (X, Y) is constructed by 12-length optimized punctured binary sequence-pair $(u, v), u = [+++-----+-++-], v = [0+++-00+-++0]$ (using $'+'$ and $'-'$ symbols for $'1'$ and $'-1'$) and orthogonal matrix B of order 12. Each row of matrix $X = [x_1; x_2; ...; x_{12}]$ and $Y = [y_1; y_2; ...; y_{12}]$ constitute a certain optimized punctured ZCZP (x_i, y_i).

3.4.2.1 Autocorrelation and Cross Correlation Properties

The autocorrelation property $R(x_1, y_1)$ and cross correlation property $R(x_1, y_2) = R(y_1, x_2)$ of 144-length optimized punctured ZCZPS (X, Y), are shown in Fig. 3.7.

According to Fig. 3.7(a), the sidelobe of autocorrelation of ZCZPS can be as low as 0 when the time delay is kept within $Z_0 = N_1 = 12$ and the cross correlation value is 0 during the whole time domain. The only uniform phase codes that can reach the maximum peak signal sidelobe ratio (PSR) [69] are the Barker codes whose length is equal or less than 13. The sidelobe of the new code shown in Fig. 3.7 can be as low as 0, and the PSR can be as large as infinite. Besides, the length of the new code is various and much longer than the length of the Barker code.

3.4.2.2 Ambiguity function

Because of the Doppler shift f_d [69], the main peak of the autocorrelation function is reduced and so as to the SNR degradation. Focusing on the sequence-pair (x, y) here, the receiving sequence in ambiguity function is different from the echo signal and the periodic correlation is used instead of aperiodic correlation here. The ambiguity function can be rewritten as

$$A(\tau, F_D) = \Big| \int_{-\frac{T}{2}}^{-\frac{T}{2}+\tau} x(t) exp(j2\pi F_D t) y^*(t + T - \tau)) dt + \int_{-\frac{T}{2}+\tau}^{\frac{T}{2}} x(t) exp(j2\pi F_D t) y^*(t - \tau) dt \Big| \tag{3.13}$$

In order to analyze the autocorrelation performance of an optimized punctured ZCZP with delay-Doppler shift, Equation (3.13) is plotted in Fig. 3.8 in a three-dimensional surface plot. In Fig. 3.8, there is relative uniform plateau suggesting

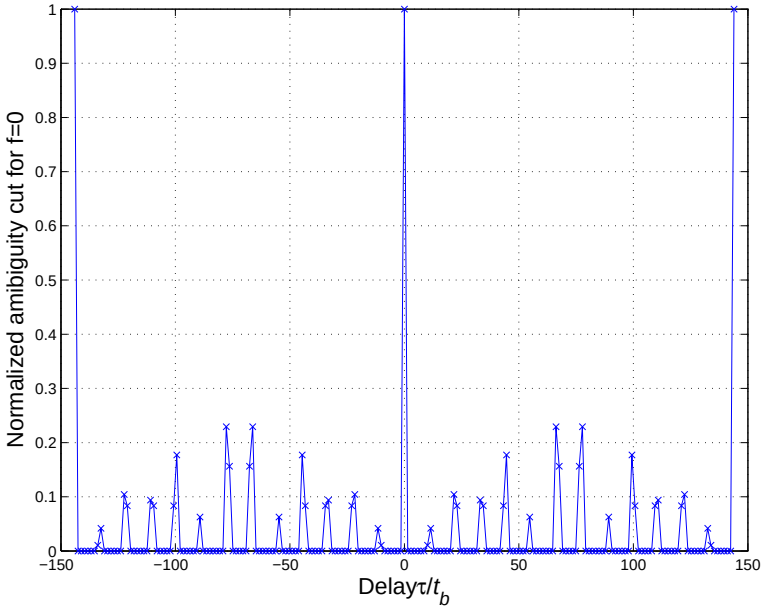

(a)

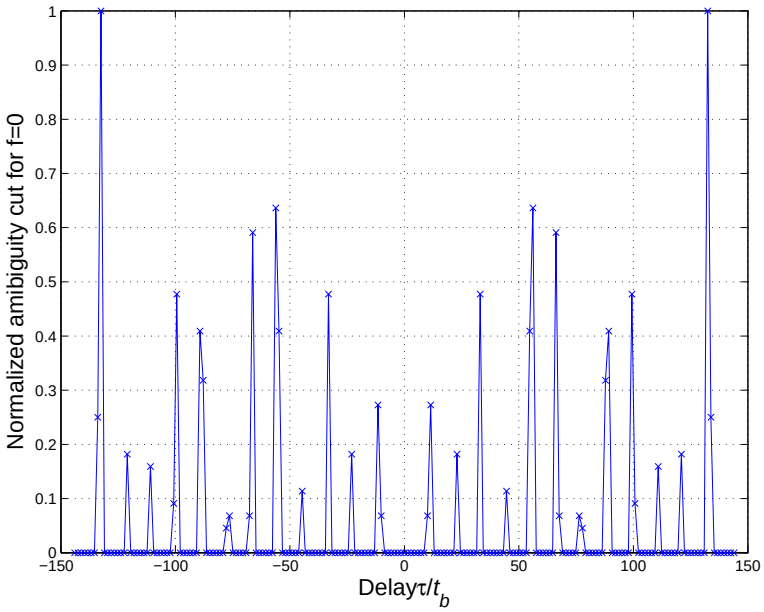

(b)

Figure 3.7. (a)Periodic autocorrelation property of 144-length optimized punctured ZCZ sequence-pair (x_1, y_1) (b)Periodic cross correlation property of 144-length optimized punctured ZCZ sequence-pair (x_1, y_2).

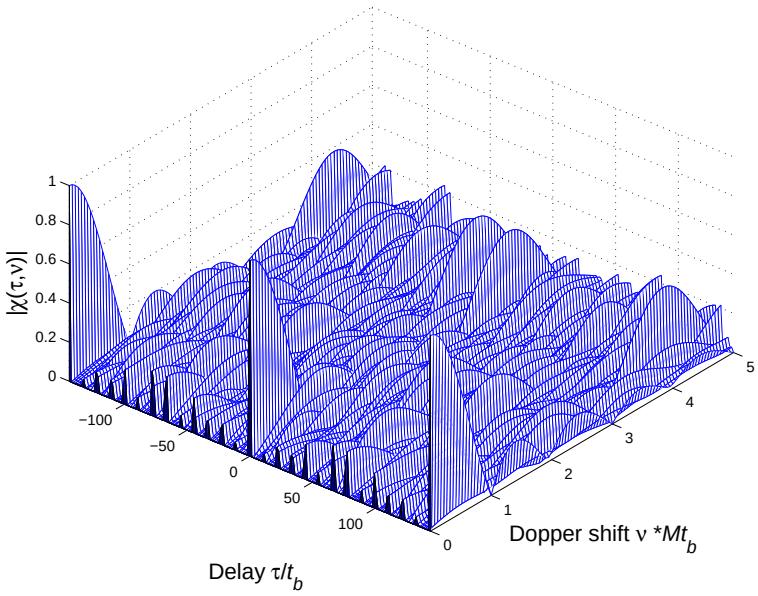

Figure 3.8. Ambiguity function of a 144-length ZCZ sequence-pair (x_i, y_i).

low and uninform sidelobes. This low and uniform sidelobes minimize target masking effect in ZCZ of time domain, where $Z_0 = 12$, $-12 < \tau < 12, \tau \neq 0$.

3.5 Conclusions

In this Chapter, we have presented three methods to construct the Optimized Punctured LCZ/ZCZ Sequence-pair sets: using the odd length Optimized Punctured Binary Sequence-pair together with Hadamard matrix to construct an Optimized Punctured ZCZ Sequence-pair set; using the even length Optimized Punctured Binary Sequence-pair together with modified Hadamard matrix to construct an approximately Optimized Punctured LCZ Sequence-pair set and using any length Optimized Punctured Binary Sequence-pair together with Orthogonal matrix to construct an Optimized Punctured ZCZ Sequence-pair set. According to the property analysis of sample sequence-pair sets constructed by each method, the Optimized Punctured

ZCZ Sequence-pair set constructed by the first method have zero autocorrelation sidelobes during the ZCZ but zero cross correlation values during the whole time domain, the approximately Optimized Punctured LCZ Sequence-pair set using the second method have zero autocorrelation sidelobes during the LCZ, a low cross correlation peak value and zero cross correlation sidelobe during the LCZ, and the Optimized Punctured ZCZ Sequence-pair set constructed by the last method have zero autocorrelation sidelobes and zero cross correlation values during the ZCZ. The ambiguity function is also used to study the sequence-pairs under the condition of time delay and Doppler shift.

CHAPTER 4

USING THE OPTIMIZED PUNCTURED SEQUENCE-PAIR AS PULSE COMPRESSION CODES

4.1 Introduction

Pulse compression, which allows a radar to simultaneously achieve the energy of a long pulse and the resolution of a short pulse without the high peak power required by a high energy short duration pulse [19], is generally used in modern radar system. The main purpose of this technique is to raise the signal to maximum sidelobe (signal-to-sidelobe) ratio to improve the target detection and range resolution abilities of the radar system. The lower the sidelobes, relative to the mainlobe peak, the better the main peak can be distinguished.

There are two kinds of basic waveform designs suitable for pulse compression: frequency-codes, such as linear frequency modulation (LFM) codes [78] [79] and non-linear frequency modulation codes (NLFM) [79] [80] [81]; phase-coded waveforms, such as binary phase codes and polyphase codes. For a phase-coded waveform, a long pulse of duration T is divided into N subpulses each of width T_s. Each subpulse has a particular phase, which is selected in accordance with a given code sequence. The pulse compression ratio equals to the number of subpulses $N = T/T_s$.

The criterion for selecting the subpulse phases is that all the time-sidelobe of the compressed pulse should be equal and as low as possible. One family of binary phase code widely used as a form of phase coding nowadays that can produce compressed waveforms with constant sidelobe levels equal to unity is the Barker code. It has special features with which its sidelobe structure contains the minimum energy which

is theoretically possible for binary codes, and the energy is uniformly distributed among the sidelobes (the sidelobe level of the Barker codes is $1/N^2$ that of the peak signal) [82]. Unfortunately, the length N of known binary and complex Barker codes is limited to 13 and 25, respectively [83], which may not be sufficient for the desired radar applications. In [16] [17] [18], polyphase codes, with better Doppler tolerance and lower range sidelobes such as the Frank and P1 codes, the Butler-matrix derived P2 code and the linear-frequency derived P3 and P4 codes were intensively analyzed. However, the low range sidelobe of the polyphase codes can not reach the level zero either, what is more, the structure of polyphase codes is more complicated and is not easy to generate comparing with binary codes.

A new triphase code–Punctured Binary Sequence-pair has been introduced in the Chapter 2. The sidelobe level of the sequence-pair is as low as zero and the longest length of them is found 31 so far, we would apply them to radar system as pulse compression waveform and simulate the detection performances in this chapter.

4.2 Properties of Optimized Punctured Sequence-pair

4.2.1 Autocorrelation Properties

The autocorrelation function is one of the most important properties that represents the compressed pulse in an ideal pulse compression system, since it is proportional to the matched filter response in the noise-free condition. The periodic autocorrelation function of the punctured binary sequence-pair is

$$R_{\mathbf{xy}}(\tau) = \sum_{j=0}^{N-1} x_j y^*_{(j+\tau) mod N} = \begin{cases} E & \tau \equiv 0 \text{ mod N} \\ 0 & \text{otherwise} \end{cases}$$

EXAMPLE 1

The autocorrelation property of 31-length punctured binary sequence-pair$(\mathbf{x}_{31}, \mathbf{y}_{31})$,

($\mathbf{x}_{31} = [+++++---+-+-+++---+--+--+++-++-]$ and $\mathbf{y}_{31} = [++++000+0+0+++0000+00+00+++0++0])$ $('+'for'1'and'-'for'-1')$is shown in the Fig. 4.1.

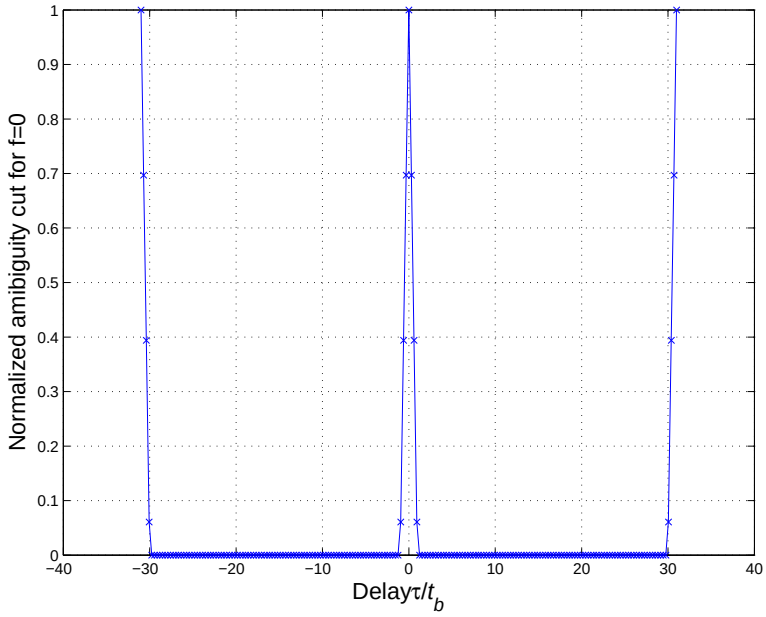

Figure 4.1. Periodic autocorrelation property of 31-length punctured binary sequence-pair.

As it is known that a suitable criterion for evaluating code of length N is the peak signal to peak signal sidelobe ratio (PSR) of their autocorrelation function, which can be bounded by [84]

$$[PSR]_{dB} \leq 20logN = [PSR_{max}]_{dB} \tag{4.1}$$

The only uniform phase codes that can reach the PSR_{max} are the Barker codes whose length is equal or less than 13. However, the sidelobe of the new code shown in Fig. 4.1 could be as low as 0. In some other words, the peak signal to peak signal sidelobe can be as large as infinite. In addition, it is also obvious that the length of the new code can expend to 31 that is much longer than the length of the Barker code.

4.2.2 Ambiguity Function

When the transmitted impulse is reflected by a moving target, the reflected echo signal includes a linear phase shift which corresponds to a Doppler shift F_D [69]. As a result of the Doppler shift F_D, the main peak of the autocorrelation function is reduced:

$$[d]_{dB} = 10log\frac{\int_0^T x(t)x^*(t)dt}{\int_0^T x(t)e^{j2\pi f_d T_c}x^*(t)dt} \tag{4.2}$$

The SNR degraded and the sidelobe structure is also changed thanks to the Doppler shift.

We focus on the sequence-pair in this paper, so the transmitting code and the receiving code are not the same. The ambiguity function of sequence-pair can be defined as:

$$A_{T-pair}(\tau, F_D) \cong |\frac{1}{T}\int_0^T x(t+\frac{\tau}{2})e^{j2\pi F_D t}y^*(t-\frac{\tau}{2})dt| \tag{4.3}$$

When the signal is of duration MT, the response of the correlation receiver is the PAF (periodic ambiguity function) for M periods. After normalization, it is defined as:

$$A_{MT-pair}(\tau, F_D) \cong |\frac{1}{MT}\int_0^{MT} x(t+\frac{\tau}{2})e^{j2\pi F_D s}y^*(t-\frac{\tau}{2})dt|$$

Splitting it into M sections

$$\begin{aligned} & A_{MT-pair}(\tau, F_D) \\ \cong\ & |\frac{1}{MT}\sum_{n=1}^{M}\int_{(n-1)T}^{nT} x(t+\frac{\tau}{2})e^{j2\pi F_D s}y^*(t-\frac{\tau}{2})dt| \\ =\ & A_{T-pair}(\tau, F_D)|\frac{sin(\pi F_D MT)}{Msin(\pi F_D T)}| \end{aligned} \tag{4.4}$$

EXAMPLE 2

Ambiguity functions of our triphase code within length of 13 used in the last section is simulated, where maximal time delay is 1 unit (normalized to length of the code, in units of NT_s) and maximal Doppler shift is 5 units (normalized to the inverse of the length of the code, in units of $1/NT_s$). The ambiguity functions of 13-length long Barker code is also presented in Fig. 4.2 in order to compare with our triphase code of the same length.

Fig. 4.2 shows that the sidelobe improvement of our triphase code is obvious comparing with those of Barker code when there is no Doppler shift. The sidelobe of our triphase code can reach as low as zero. Nevertheless, when there are Doppler shift and time delay, the ambiguity functions of punctured binary sequence-pair is not as flat as those of Barker code. In some other words, our triphase code is less tolerant of Doppler shifts than Barker code. One of the reasons why the proposed code is not tolerant of large Doppler shift is that periodic correlation property is used for our triphase code instead of the aperiodic correlation property which is used for the Barker code.

EXAMPLE 3

In order to improve the tolerance of Doppler shift, we repeat the sequence-pair M times to construct the signal of duration of MT. We study the performance of the sequence-pair of M periods in this section. Detailed results of the example are given in this part for the signals corresponding to the sequence-pairs of 7.

$$x_7 = [+++--+-], y_7 = [+++00+0];$$

Figs. 4.3 presents contour plots of the absolute amplitudes of the ambiguity function, for the three cases $M = 1, 4, 10$. The scales are normalized with respect to the bit duration of T_s. Namely, the delay axis is of τ/T_s, and the Doppler shift axis is of $F_D T_s$. Since the single period is $T = NT_s$, the ambiguity function repeats

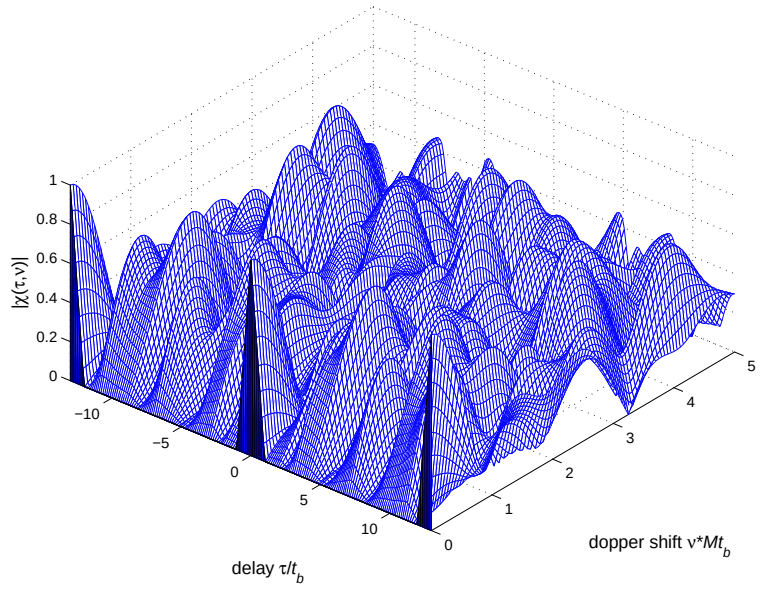

(a)

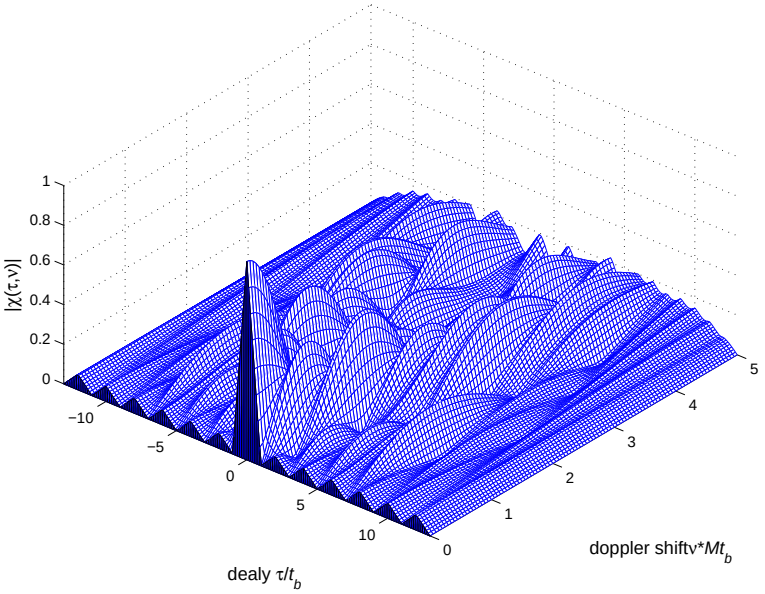

(b)

Figure 4.2. Ambiguity function of 13-length codes: (a) Punctured binary sequence-pair (b) Barker code.

itself every N normalization delay units. The cuts at $\tau/T_s = n/N$ repeat every N normalized delay units. The pronounced strips, parallel to the Doppler shift axis, appear at normalized delay.

The corresponding 3-D plots are given in Figs. 4.4. The prominent feature of the ambiguity function, when $M > 1$, the strips get narrower as M increases. The cuts of periodic ambiguity function at $\tau/T_s = nN$ are independent of the number of periods M.

4.2.3 Doppler Shift Performance Without Time Delay

According to the previous work [69], the cut along Doppler axis is obtained as, namely, when the time delay is zero,

$$A_T(0, F_D) = |\frac{sin(\pi F_D T)}{\pi F_D T}| \tag{4.5}$$

It is easy to see that $F_D = n/T$ for all but $n = 0, (n = \pm 1, \pm 2, ...)$, the amplitudes must get a zero. Namely, if $F_D T = \pm 1, \pm 2, ...$, then $A_T(0, F_D)$ becomes zero. It it known that Doppler frequency F_D is given by

$$F_D = 2\frac{v f_c}{c} \tag{4.6}$$

where v is the speed of moving target, f_c is the carrier frequency of radar and c is the speed of light. PRI (pulse repetition interval) is frequently used in time domain, while PRF (pulse repetition frequency) is commonly used in frequency domain, which is defined as $PRF = 1/PRI = 1/T$. This states that Doppler shifts which equal to multiples of the PRF will render the radar blind to the velocities of the targets. However, the optimized punctured sequence-pairs used here are in a quite different case which would be studied in this section.

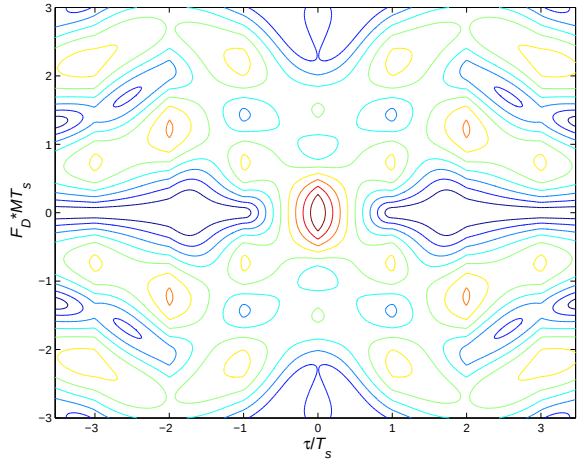

(a)

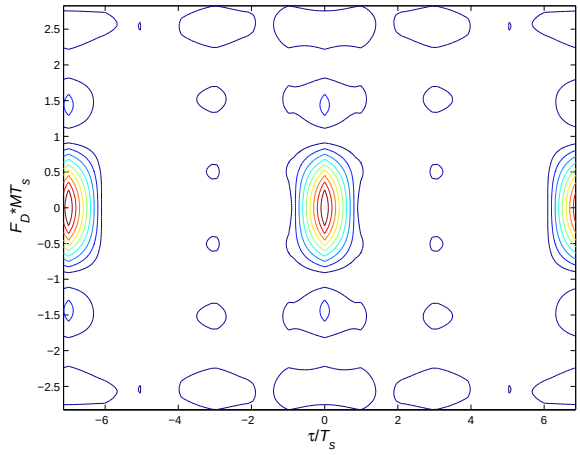

(b)

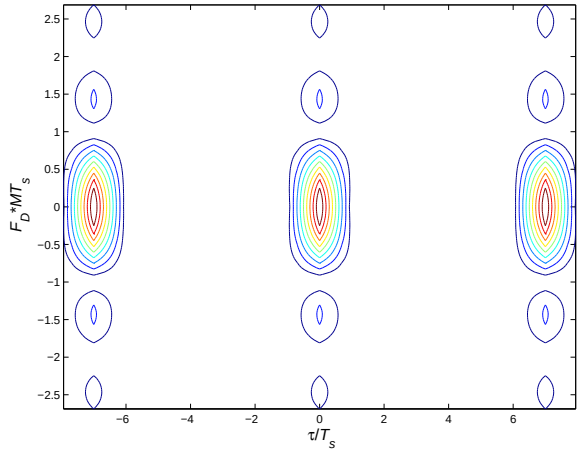

(c)

Figure 4.3. Contour plot of sequence-pair: (a) M=1 (b) M=4 (c) M=10 .

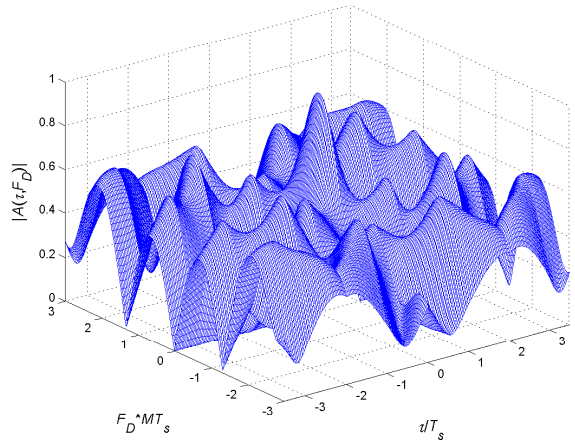

(a)

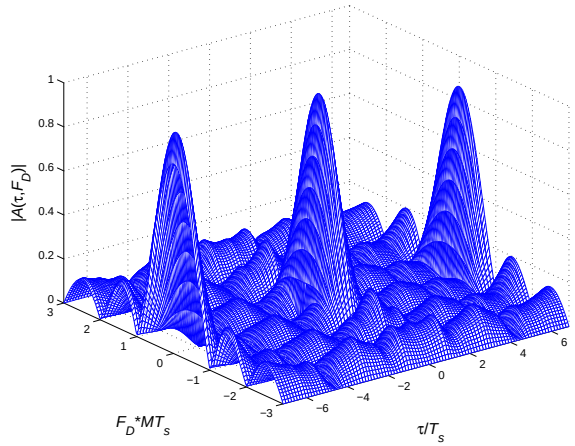

(b)

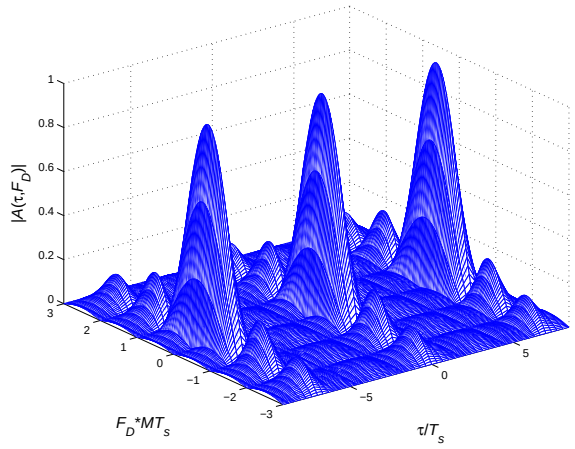

(c)

Figure 4.4. 3-D view of ambiguity function of sequence-pair: (a) M=1 (b) M=4 (c) M=10.

The ambiguity function of single period can be simplified when there is no time delay:

$$A_{T-pair}(0, F_D) = |\frac{1}{T}\int_0^T x(t)y^*(t)e^{(j2\pi F_D t)}dt| \tag{4.7}$$

According to the equation (4.5), the ambiguity function of duration of M periods could be expressed as:

$$A_{MT-pair}(0, F_D) = A_{T-pair}(0, F_D)|\frac{sin(\pi F_D MT)}{Msin(\pi F_D T)}| \tag{4.8}$$

Where M is the number of the periods.

The Doppler shift performance without time delay is presented in Fig. 4.5. Without time delay, while the Doppler shift is less than 1 unit (normalized to length of the code, in units of NT_s), the amplitude of our triphase code has a sharp downward trend and decreases more quickly than P4 code. However, when the Doppler shift is larger than 1 unit, the performances of these codes are distinguished. On one hand, the trend presented by our triphase code is not as regular as the other two codes when the Doppler shift is larger than 1. On the other hand, for P4 code, its multiples of the pulse repetition frequency will render the radar blind[19] to the velocities. Nevertheless, referring to punctured binary sequence-pair, ambiguity values do not go to zero when Doppler frequencies are equal to multiples of the PRF. According to Fig. 4.5(c), 7x5-length punctured binary sequence-pair generally resembles the 31-length P4 code. 7x5-length punctured binary sequence-pair is more tolerant of Doppler shift than single period of punctured binary sequence-pair, but it has more ambiguity values go to zero when Doppler shift equals to some multiples of the PRF. Therefore, using the our triphase code as the compression code could, to some extent, improve the blind speed problem in moving target detection system. Using several periods of punctured binary sequence-pair could improve the tolerance of Doppler shift when Doppler shift is larger than 1 unit.

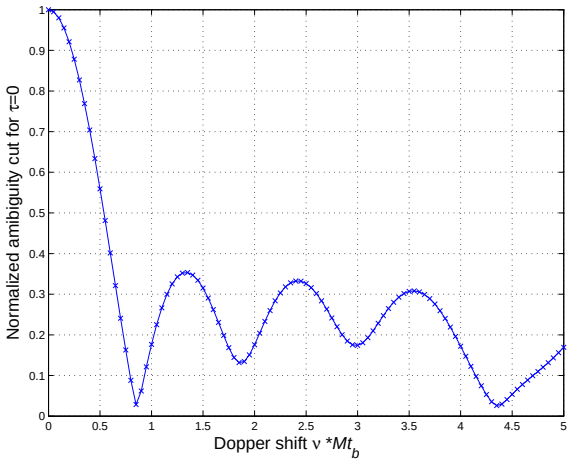

(a)

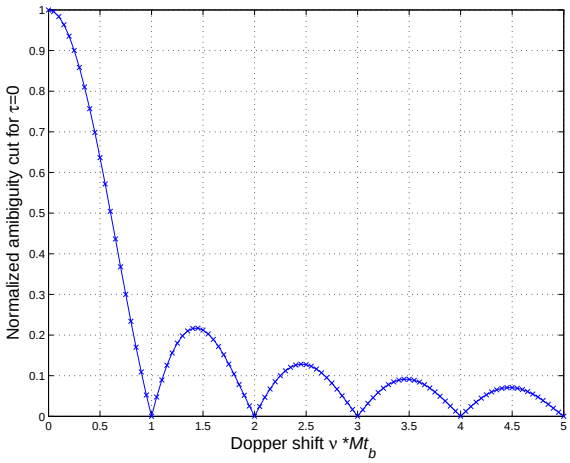

(b)

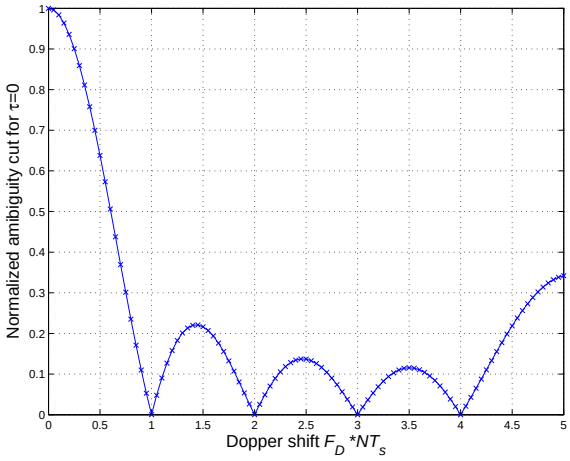

(c)

Figure 4.5. Doppler shift of codes(time delay=0): (a) 31-length Punctured binary sequence-pair (b) P4 code (c) 7x5-length Punctured binary sequence-pair.

4.3 Radar System Simulation Results

According to [69], P_D (Probability of Detection), P_{FA} (Probability of False Alarm) and P_M (Probability of Miss) suffice to specify all of the probabilities of interest in radar system.Therefore, the above three probabilities of our newly provided triphase code in radar system are simulated, as shown in Fig. 4.6 and Fig. 4.7. In addition, the performance of the our 13-length Barker code and 31-length P4 code are provided in order to compare with the performance of our triphase codes of corresponding lengths. In the simulation model, we ran Monte-Carlo simulation for 10^5 times at each SNR value, the Doppler shift frequency which is kept less than 1 unit (normalized to the inverse of the length of the code, in units of $1/NT_s$) is randomly given by Matlab, and the time delay is assumed to be zero. Threshold detection i used in coherent system and the threshold is adaptively determined in the simulation.

In Fig. 4.6(a), we plotted the miss detection probabilities P_M of 13-length punctured binary sequence-pair and the same length Baker code. Observe Fig. 4.6(a), the miss detection probability P_M of the system using 13-length punctured binary sequence-pair is lower than 13-length Barker code especially when the SNR is not large. It is in accordance with the result shown in Fig. 4.5 that when Doppler shift is kept less than 1 and the time delay is zero, the amplitude of punctured binary sequence-pair falls more sharply than Barker code.

In Fig. 4.6(b), we plotted the probabilities of miss targets detection of our 31-length triphase code and those of the same length P4 code. The probability of miss targets detection of the system using our 31-length triphase code is less than 31-length P4 code especially when the SNR is not large. When SNR is larger than 17 dB, both probabilities of miss targets detection of the system approach zero. However, the probability of miss targets of P4 code is a little lower than our triphase code.

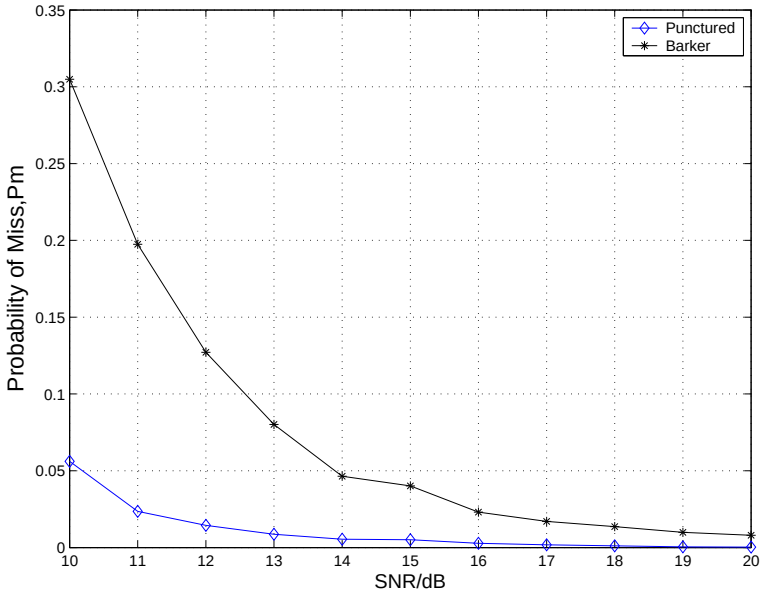

(a)

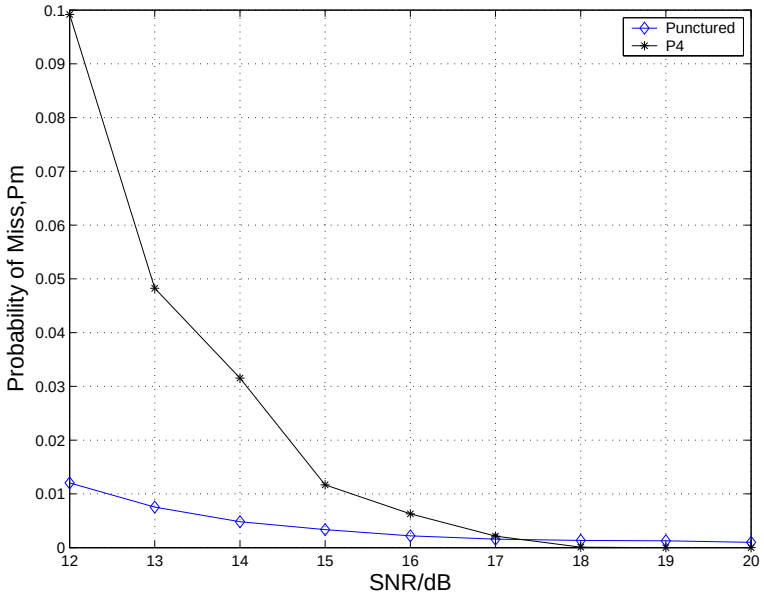

(b)

Figure 4.6. Probability of miss targets detection for 31-length Punctured binary sequence-pair VS. 31-length P4 code: (a) No time delay, Doppler shift is less than 1; (b) Time delay, Doppler shift is less than 1..

In addition, we also plotted the probability of detection versus probability of false alarm of the coherent receiver in Fig. 4.7.

Fig. 4.7(a) illustrates performance of 13-length punctured binary sequence-pair and the same length Baker code when the SNR is 10dB and 14dB. Having the same SNR value such as 10dB or 14dB in the figure, the P_D of 13-length punctured binary sequence-pair is larger than P_D of 13-length Barker code while the P_{FA} of the first code is also smaller than P_{FA} of the latter code. In some other words, 13-length punctured binary sequence-pair has much higher target detection probability while keeping a lower false alarm probability. Furthermore, observe Fig. 4.7(a), 13-length punctured binary sequence-pair even has much better performance at 10dB SNR value than 13-length Barker code at 14dB SNR value. Fig. 4.7(b) illustrates performance of our 31-length triphase codes and the same length P4 code when the SNR is 10dB and 14dB. Having the same SNR value such as 10dB or 14dB in the figure, the P_D of our 31-length triphase code is larger than P_D of our 31-length P4 code while the P_{FA} of the first code is also smaller than P_{FA} of the latter code. In some other words, our 31-length triphase code has much higher target detection probability while keeping a lower false alarm probability. Furthermore, observe Fig. 4.7(b), our 31-length triphase code even has much better performance at 10dB SNR than 31-length P4 code at 14dB SNR.

4.4 Conclusions

Optimized Punctured Binary Sequence-pair is a kind of triphase-code waveform known for its zero autocorrelation sidelobe. In this chapter, we successfully apply it to the radar system as the pulse compression code and simulate the detection performance of the system. According to the simulation results, the new code can provide better performances than the Barker and P4 codes of corresponding length

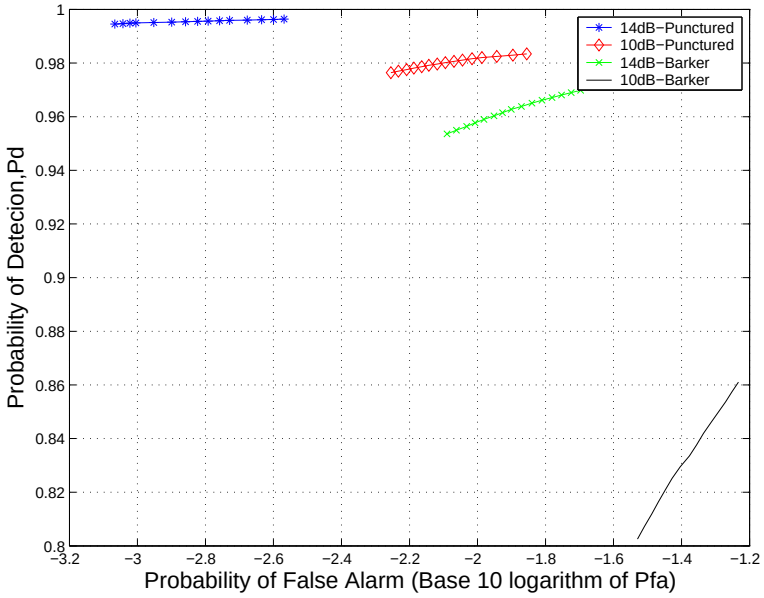

(a)

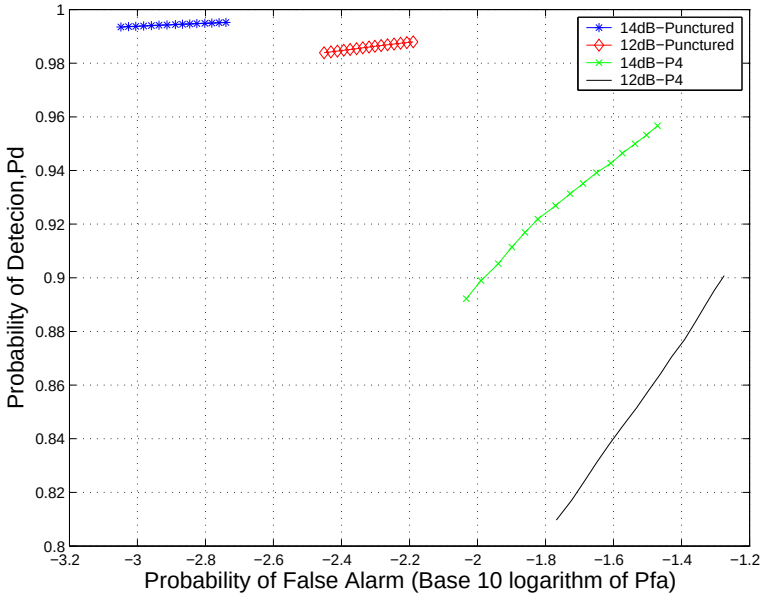

(b)

Figure 4.7. Probability of detection versus probability of false alarm of the coherent receiver for 31-length Punctured binary sequence-pair VS. 31-length P4 code: (a) No time delay, Doppler shift is less than 1; (b) Time delay, Doppler shift is less than 1..

and be a good alternative for the current used pulse compression codes in radar system.

CHAPTER 5

RADAR SENSOR NETWORK USING THE NEW TRIPHASE CODED WAVEFORMS

5.1 Introduction

A network of multiple radar sensors can be introduced to overcome performance degradation of single radar along with waveform optimization. This network of radar sensors should operate with multiple goals managed by an intelligent platform network that can combine waveform diversity to meet common goals of platform, rather than each radar to operate independently.

Much time and effort have been put in waveform design. Bell [20] who introduced information theory to radar waveform design, concluded that distributing energy is a good choice to better detect targets. Sowelam and Tewfik [21] applied a sequential experiment design procedure to select signal for radar target classification. In their work, each waveform selected maximizes the KullbackLeibler information number that measures the dissimilarity between the observed target and the alternative targets in order to minimize the decision time. However, all the above researches only focused on a single active radar. In [22], Liang studied constant frequency (CF) pulse waveform design and proposed maximum-likelihood (ML) automatic target recognition (ATR) approach for both nonfluctuaing and fluctuating targets in a network of multiple radar sensors. In [23], RSN design based on linear frequency modulation (LFM) waveform was studied and LFM waveform design was applied to RSN with application to ATR with delay-doppler uncertainty by Liang as well. J.Liang [24] provided an orthogonal waveform model for RSN, which eliminates inter-

ference when there is no doppler shift. They designed both coherent and noncoherent RSN detection systems which can apply equal gain combination technique performed by clusterhead to take the advantage of spatial diversity. In [68], binary coded pulses using simulated annealing in RSN are highlighted.

Nevertheless, the radar sensor network using phase coded waveforms has not been well studied. In this chapter, we firstly theoretically study RSN design based on phase coded waveforms: the conditions for waveforms co-existence. Then we apply our newly proposed triphase code–optimized punctured ZCZ sequence-pair set to RSN. We perform studies on the codes' properties, especially the cross correlation property and analyze the performance of optimized punctured ZCZ sequence-pairs in RSN system under the environment of doppler shift and time delay for each transmitting radar sensor. According to the Monte Carlo simulation results, RSN based on optimized punctured ZCZ sequence-pairs provides promising detection performance much better than that of single radar, in terms of probability of miss and false alarm detection.

5.2 Co-existence of Phase Coded Waveforms in RSN

We assume there are N radars networking together in a self-organizing fashion in our RSN. The radar i transmits a waveform as

$$x_i(t) = \sum_{n=0}^{N-1} x_i^{(n)}(t - n\tau_c) = \sum_{n=0}^{N-1} exp(j2\pi\beta_i^{(n)}(t - n\tau_c)) \tag{5.1}$$

Here, $0 < t <= \tau_c$.

When the phase coded waveforms are orthogonal to each other, the interference from one waveform to the another can be minimized or even removed. The cross correlation between $x_i(t)$ and $x_j(t)$ could be

$$\int_{-T/2}^{T/2} x_i(t)x_j^*(t)dt = \tau_c \sum_{n=0}^{N-1} exp[j2\pi(-\frac{N}{2}+\frac{1}{2})\tau_c(\beta_i^{(n)}-\beta_j^{(n)})]sinc[\tau_c(\beta_i^{(n)}-\beta_j^{(n)})] \quad (5.2)$$

The optimized cross correlation is that of orthogonal waveforms

$$\int_{-T/2}^{T/2} x_i(t)x_j^*(t)dt = \begin{cases} N\tau_c & i=j \\ 0 & i\neq j \end{cases} \quad (5.3)$$

It is easy to see that when $\pi\tau_c(\beta_i^{(n)}-\beta_j^{(n)}) = k\pi, k = 1, 2, 3...$, it satisfies the equation (5.3). In this way can phase coded waveforms be orthogonal to each other and work well simultaneously in Radar Sensor Network.

Nevertheless, there are time delay and Doppler shift ambiguity that will introduce interference to waveforms in RSN. Ambiguity function (AF) [69] is usually used to succinctly characterize the behavior of a waveform paired with its matched filter. In the RSN of M radars, the radar i not only receives its own back-scattered waveform, but also scattered signals generated by other $M-1$ radars which caused interference to radar i.

Assuming each radar transmits signal synchronously, $t_1 = t_2 = t_M = 0$. Considering time delay $\tau = m\tau_c$ for receiving radar i and interferences from all the other $M-1$ radars, the ambiguity function of radar i could be

$$\begin{aligned} & A_i(\tau, F_{D_1}, ..., F_{D_M}) \quad (5.4) \\ = \; & |\tau_c \sum_{j=1}^{M}\sum_{n=m}^{N-1} exp[j2\pi[\beta_i^{(n-m)}(\frac{N}{2}+m-1)\tau_c \\ & +\beta_j^{(n)}(-\frac{N}{2}+1)\tau_c + F_{D_j}(-\frac{N}{2}+n+1)\tau_c]] \\ & sinc[\tau_c(\beta_j^{(n)}-\beta_i^{(n-m)}+F_{D_j})]| \end{aligned}$$

Here, $0 < i <= M$. (5.5) consists of two parts: useful signal $j = i$ part in the (5.5); and interferences from other $M - 1$ radar waveforms, $j \neq i$ parts in (5.5). Since $\pi\tau_c(\beta^{(n)} - \beta^{(n-m)} + F_D) = k\pi, k = 1, 2...$, it satisfies that $A(\tau, F_D) = 0$, when $F_D = \frac{k}{\tau_c}, k = 0, 1, ...$

5.3 System Simulation in Radar Sensor Network

In RSN of M radars, the combined received signal for the radar i is

$$r_i(u,t) = \sum_{j=1}^{M} x_j(t - t_j)exp(j2\pi F_{D_j}t) + n(u,t) \tag{5.5}$$

F_{D_j} and t_j are Doppler shift of target and time delay relative to waveform j, and $n(u,t)$ is additive white Gaussian noise (AWGN). The structure can be constructed as Fig. 5.1.

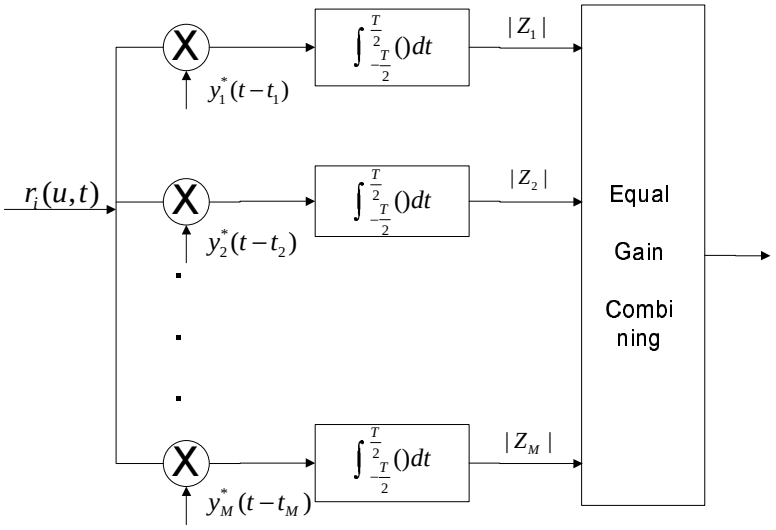

Figure 5.1. Waveform diversity combining in RSN.

According to this structure, the combined received signal $r_i(u,t)$ is processed by its corresponding matched filter i and the output of branch i is $Z_i(u,t)$. Each $Z_i(u,t)$ can be equal gain combined to construct the final output $Z(u,t)$.

The output $|Z_i(u)|$ of branch i is

$$|\int_{-\frac{T}{2}}^{\frac{T}{2}}[\sum_{j=1}^{M} x_j(t-t_j)exp(j2\pi F_{D_j}t)+n(u,t)]y_i^*(t-t_i)dt| \tag{5.6}$$

Where $n(u)=\int_{-\frac{T}{2}}^{-\frac{T}{2}} n(u,t)y_i^*(t-t_i)dt$ can be easily proved to be still an AWGN.

We can also have two special cases for $|Z_i(u)|$:

1) If there is Doppler shift but no time delay, all the radar sensors transmit signals synchronously, $|Z_i(u)|$ turns to be:

$$|\int_{-\frac{T}{2}}^{\frac{T}{2}}[\sum_{j\neq i}^{M} x_j(t)exp(j2\pi F_{D_j})+n(u,t)]y_i^*(t)dt| \tag{5.7}$$

Assuming that the Doppler shift can be well estimated in the receiving radar sensor, so the Doppler shift compensation factor $exp^*(j2\pi F_{D_j})$ is introduced here.

$$\begin{aligned}|Z_i(u)| &\leq |E|+|\int_{-\frac{T}{2}}^{\frac{T}{2}}[\sum_{j=1}^{M} x_j(t)exp(j2\pi(F_{D_j}-F_{D_i}))y_i^*(t)| \\ &+|\int_{-\frac{T}{2}}^{\frac{T}{2}} n(u,t)y_i^*(t)exp^*(j2\pi F_{D_i}t)dt|\end{aligned} \tag{5.8}$$

If $F_{D_1}=F_{D_2}=...=F_{D_j}=F_D$, further simplified as

$$|Z_i(u)| \leq |E|+0+|\int_{-\frac{T}{2}}^{\frac{T}{2}} n(u,t)y_i^*(t)exp^*(j2\pi F_{D_i}t)dt| \tag{5.9}$$

2) If both time delay and Doppler shift exist in the RSN, assuming $F_{D_1}=F_{D_2}=...=F_{D_j}=F_D$, considering the Doppler shift compensation factor in the receiving sensor,

$$\begin{aligned}|Z_i(u)| &\leq |E|+|\int_{-\frac{T}{2}}^{\frac{T}{2}}[\sum_{j\neq i}^{M} x_j(t-t_j)]y_i^*(t-t_i)dt| \\ &+|\int_{-\frac{T}{2}}^{\frac{T}{2}} n(u,t)y_i^*(t-t_j)exp^*(j2\pi F_{D_i}t)dt|\end{aligned} \tag{5.10}$$

Because of the good properties of our proposed codes, we modify the frame of receiving data before the matched filter on the receiver to improve the RSN performance. The data from $N+1$ to $max(t_j)+N$ are added to data from 1 to $max(t_j)$, bit

by bit, where N is the original data length and t_j is the time delay for jth transmitting radar sensor. In this way can we get the output of the matched filter

$$|Z_i(u)| \leq |E| + 0 + |\int_{-\frac{T}{2}}^{\frac{T}{2}} n(u,t) y_i^*(t) exp^*(j2\pi F_{D_i} t) dt| \tag{5.11}$$

According to (5.9) and (5.11), it is easy to see that using our provided codes and frame modification the RSN under the condition of time delay for each radar sensor can, to some extent, work as well as the RSN where all the radar sensors transmit signals synchronously.

We apply optimized punctured ZCZPS as a bank of phase coded waveforms together with equal gain combination technique in the simulation in order to study the performance versus different number of radars in RSN with Doppler shift. We respectively simulated P_M (Probability of Miss Detection) and P_{FA} (Probability of False Alarm) of different number of radars using different number of optimized punctured ZCZ sequence-pairs. Two special cases of performances have been simulated. They are performances under the condition of no time delay but Doppler shift, and under the condition of time delay for each radar sensor and having Doppler shift.

Fig. 5.2 illustrates that when $P_M = 10^{-3}$, SNR of 8-radars are $2.2dB$ smaller than that of single radar system using Barker code with Doppler shift. Considering time delay for each radar in Fig. 5.2, SNR of 8-radar RSN can gain $1.7dB$ smaller than 4-radar SNR to achieve the same $P_M = 10^{-3}$.

According to Fig. 5.3, the SNR of 8-radars can be nearly $3.8dB$ smaller than that of single radar system using Barker code in order to achieve the same $P_{FA} = 10^{-2}$. In addition, 4-radar system requires $1.7dB$ more than that of 8-radar RSN under the condition of both time delay and Doppler shift.

The above figures distinctly illustrate that performances of detection of multi-radars are superior to that of single radar. The performances of 4-radar and 8-radar

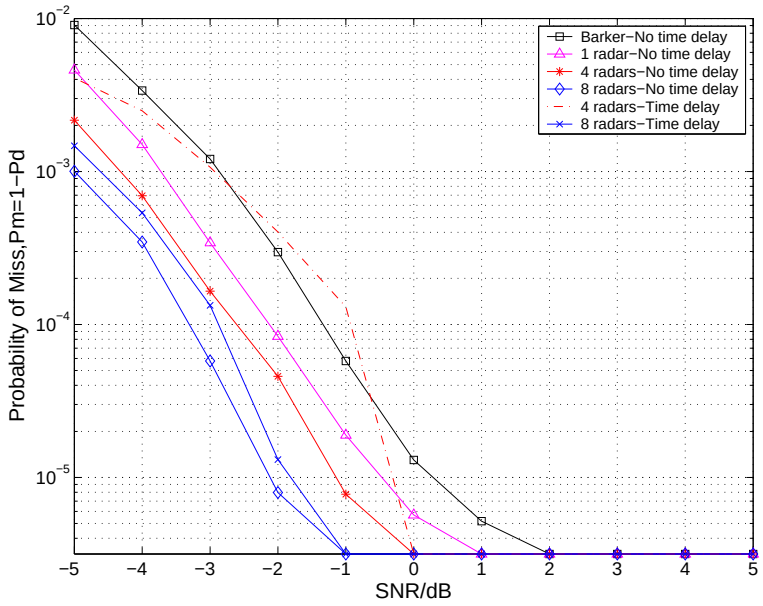

Figure 5.2. Probability of miss detection in RSN under the condition of no time delay but Doppler shift or time delay and Doppler shift.

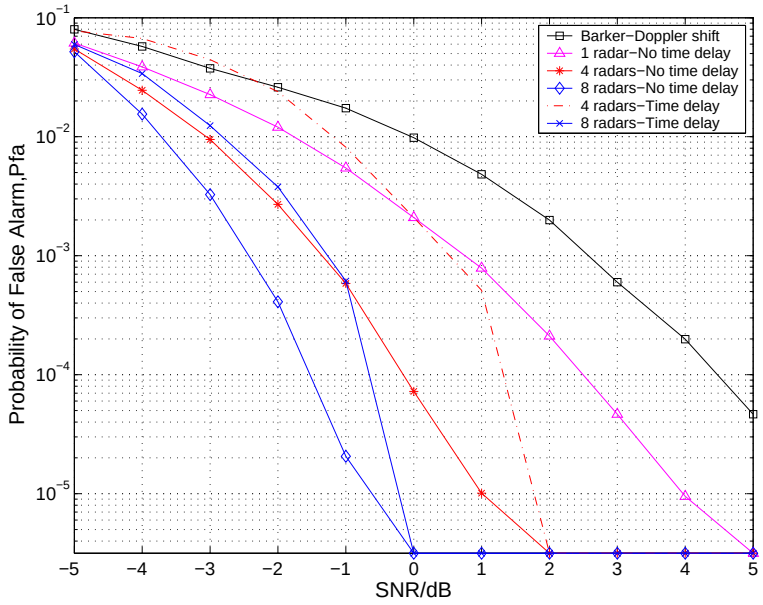

Figure 5.3. Probability of false alarm in RSN under the condition of no time delay but Doppler shift or time delay and Doppler shift .

RSN considering time delay for each radar transmitting sensor can be comparable to those under the condition of no time delay, when large amount of radars are used in the RSN.

5.4 Conclusions

The Optimized Punctured ZCZ Sequence-pair set (optimized punctured ZCZPS) is a set of sequence-pairs which have zero autocorrelation sidelobes during the ZCZ but zero cross correlation values during the whole time domain. Therefore, we studied the RSN using the Optimized Punctured ZCZ Sequence-pair set as the phase coded waveforms and simulated the detection performance of the system. The simulation results show that RSN based on a set of optimized punctured ZCZ sequence-pairs provides promising detection performance much better than that of single radar.

CHAPTER 6

SONAR SENSOR NETWORK USING THE NEW TRIPHASE CODED WAVEFORMS

6.1 Introduction

The narrowband pulse is most commonly used in underwater acoustics, in most sounders, sonars and positioning systems. The narrowband pulses are usually good enough for many applications because of the simplicity of transmission and processing, along with performances of the pulses. However, the major defect is the poor range resolution, which decreases interest in their use for advanced processing. The pulse compression is such a technique that high signal energy is provided by transmitting over a long time (large T) and good time resolution is achieved by using a sequence of short pulse (large W), therefore having a large TW product [30]. A phase coded waveform is one of the pulse compression waveforms that has a constant RF frequency, but an absolute phase that is switched between one of N fixed values at regular intervals within the pulse length. For an example, m sequences, successfully used in previous experiments [25][28], satisfy the long-range transmission through the ocean sound channel requirement and the same time resolution as a monopulse or periodic pulse system whose pulse width is one digit duration achievable at high power.

Family of m sequences could be applied to the SSN to achieve better targets detection performance than single sonar sensor. Nevertheless, the autocorrelation and cross correlation properties of family of m sequences or even Gold sequences are not optimized. As a result, the concept of ZCZ (Zero Correlation Zone) [31] is introduced.

A sequence set having the property whereby the autocorrelation sidelobes and cross-correlation functions are all equal to zero in a specified zone of phase shift is referred to as a Zero Correlation Zone sequence set (ZCZ sequence set) [85]. There are several constructions of a ZCZ sequence set using a perfect sequence [86][87][88][89]. However, existing ZCZ sequences sets are restricted by the length of the perfect sequences [10]. The width of the Zero Correlation Zone of an existing ZCZ sequence, which is generated from a perfect sequence, is shorter than the length of the perfect sequence.

In this chapter, we further analyze the properties and ambiguity function of optimized punctured ZCZPS, since the definitions optimized punctured ZCZPS and methods to construct optimized punctured ZCZPS are proposed previously. We investigate the target detection performance of using the proposed codes as pulse compression codes in the sonar sensor network. Some final conclusions on the proposed codes are drawn in the end of the chapter.

6.2 Properties of Optimized Punctured ZCZ Sequence-pair Set

The 144-length optimized punctured ZCZPS (X, Y) is constructed by 12-length optimized punctured binary sequence-pair $(u, v), u = [+++-\!-\!-+-++-], v = [0+ ++-00+-++0]$ (using $'+'$ and $'-'$ symbols for $'1'$ and $'-1'$) and orthogonal matrix B of order 12. Each row of matrix $X = [x^{(1)}; x^{(2)}; ...; x^{(12)}]$ and $Y = [y^{(1)}; y^{(2)}; ...; y^{(12)}]$ constitute a certain optimized punctured ZCZP $(x^{(p)}, y^{(p)}), p = 0, 1, ..., 11$.

6.2.1 Autocorrelation and Cross Correlation Properties

The autocorrelation property $R(x^{(1)}, y^{(1)})$ and cross correlation property $R(x^{(1)}, y^{(2)}) = R(y^{(1)}, x^{(2)})$ are shown in Fig. 6.1. According to Fig. 6.1, the sidelobe of autocorrelation and the cross correlation of ZCZPS can be as low as 0 when the time delay is kept

within $Z_0 = N_1 - 2 = 10$, here $d > 1$. The only uniform phase code that can reach the theoretical maximum peak signal sidelobe ratio (PSR) for autocorrelation [69] is the Barker code whose length is equal or less than 13. The PSR of the new code can be as large as infinite because of the zero sidelobe during ZCZ. The length of the new code is various and much longer than the length of the Barker code. Besides, a Gold code which is used in telecommunication (CDMA) and satellite navigation could also be compared with here. Though Gold codes have bounded small cross-correlations within a set, they could not obtain zero cross-correlation function and zero sidelobe of the autocorrelation function.

6.2.2 Ambiguity Function

When the transmitted signal is reflected by a moving target, the reflected echo signal includes a linear phase shift, which comes from the Doppler shift. Because of the Doppler shift F_D [69], the main peak of the autocorrelation function is reduced and so as to the SNR degradation. Focusing on the sequence-pair $(x^{(p)}, y^{(p)})$ here, we use the single-periodic ambiguity function expressed as:

$$A(\tau, F_D) = \frac{1}{T}\int_0^T x^{(p)}(s + \frac{\tau}{2})e^{j2\pi F_D s}y^{*(q)}(s - \frac{\tau}{2})ds \tag{6.1}$$

Equation (6.1) is plotted in Fig. 6.2 in a three-dimensional surface plot.

There is relative uniform plateau suggesting low and uninform sidelobes. This low and uniform sidelobes minimize target masking effect in ZCZ of time domain, where $Z_0 = 10$, $-10 \leq \tau \leq 10, \tau \neq 0$. When Doppler shift is not serious, there are small peaks on period of 12 but sharp peaks on period of 144 in time domain which could be used to detect the targets.

6.2.3 ZCZ Optimized Punctured Sequence-pair Waveform Coding in Sonar System

In this simulation part, we assume that it is the point target in the system. There are M sonar sensors using essentially different ZCZ optimized punctured sequence-pairs in the system. The receiver is pictured as M cross correlators; and each calculates the cross correlation function of the received signal $r(t)$ and the corresponding matched filter $(y_i^*(t), i = 1, 2, ..., M)$. In the sonar sensor network of M sensors, the combined received signal for the sensor i is

$$r(u,t) = \sum_{j=1}^{M} x_j(t - t_j)exp(j2\pi F_{D_j} t) + n(u,t) \tag{6.2}$$

F_{D_j} and t_j are Doppler shift and time delay relative to waveform j, and $n(u,t)$ is additive white Gaussian noise (AWGN). The combined received signal $r(u,t)$ is processed by the matched filter $y_i^*(t)$ and the output of branch i is $|Z_i(u)|$. Each $|Z_i(u)|$ can be equal gain combined to construct the final output $Z(u)$

$$\begin{aligned} Z(u) &= \sum_{i=1}^{M} |Z_i(u)| \\ &= \sum_{i=1}^{M} | \int_{-\frac{T}{2}}^{\frac{T}{2}} [\sum_{j=1}^{M} x_j(t - t_j)exp(j2\pi F_{D_j} t) + n(u,t)] y_i^*(t)dt| \end{aligned} \tag{6.3}$$

Where $n(u) = \int_{-\frac{T}{2}}^{\frac{T}{2}} n(u,t) y_i^*(t - t_i)dt$ can be easily proved to be still an AWGN.

We respectively simulated P_M(Probability of Miss) and P_{FA} (Probability of False Alarm) of sonar sensor network using our optimized punctured ZCZ sequence-pairs comparing with Gold codes of comparative length. Two special cases of performances have been simulated. One is under the condition of no time delay (all the transmitting sensors transmit simultaneously) but Doppler shift, and the another is of time delay (limited within the ZCZ) for each radar sensor and having Doppler shift. Fig. 6.3(a) illustrates that when $P_M = 10^{-3}$, SNR of 4-sensor SSN using Gold codes are $1dB$ greater than that of 4-sensor system using our proposed codes under

the condition of Doppler shift but no time delay. Observing the performance in Fig. 6.3(a), under the condition that all the sensors don't transmit simultaneously, SNR of 4-sensor SSN using our codes can gain $1.5dB$ less than 4-sensor system within Gold codes to achieve the same $P_M = 10^{-1.9}$.

According to Fig. 6.3(b), the SNR of 4-sensor sonar sensor network using our proposed codes can be nearly $0.8dB$ smaller than that using Gold codes in order to achieve the same $P_{FA} = 10^{-3}$. In addition, 4-sensor system requires $1.5dB$ more than that of 4-sensor system using Gold codes under the condition of both time delay and Doppler shift when $P_{FA} = 10^{-1.8}$.

The above figures distinctly illustrate that detection performances of SSN using our propose codes are superior to that using Gold codes. It is easy to conclude that the performance could be improved by increasing the number of sensors. In addition, considering time delay for each transmitting sensor, the performances of SSN are worse than those under the condition of no time delay because of the interference introduced by time shift of the transmitting signals, but still could be acceptable.

6.3 Conclusions

In this chapter, we investigate the definition and properties of optimized punctured ZCZPS constructed by a specific method proposed before. The significant advantage of the optimized punctured ZCZ sequence-pair set is a considerably reduced autocorrelation sidelobe as low as zero and zero mutual cross correlation value within ZCZ. The results show that applying our optimized punctured ZCZPS as a bank of phase coded waveforms to the SSN can effectively satisfy higher demands criterion for detection accuracy in modern military and security affairs.

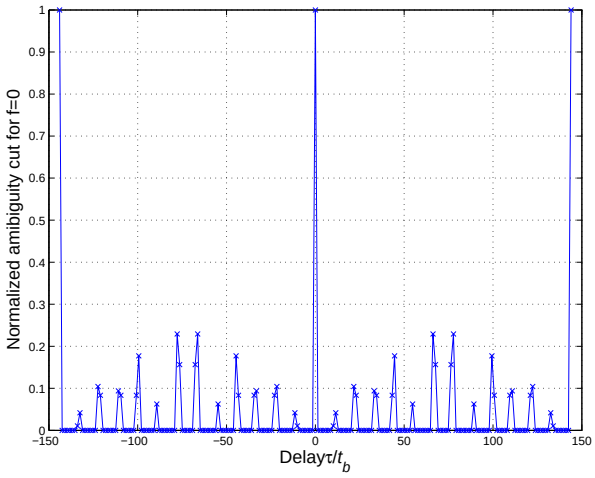

(a)

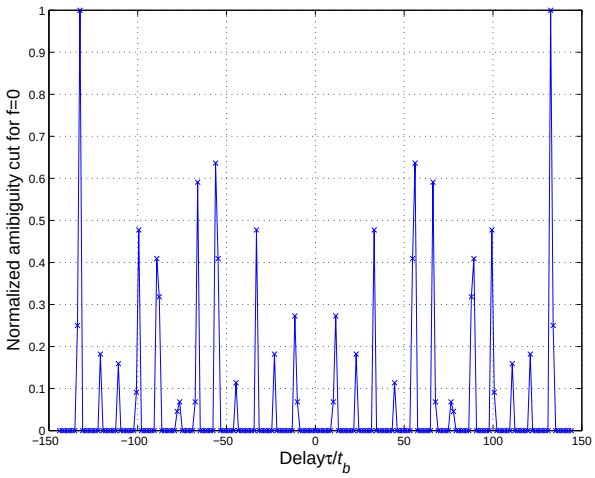

(b)

Figure 6.1. (a)Periodic autocorrelation property of 144-length optimized punctured ZCZ sequence-pair (x_1, y_1) (b)Periodic cross correlation property of 144-length optimized punctured ZCZ sequence-pair (x_1, y_2).

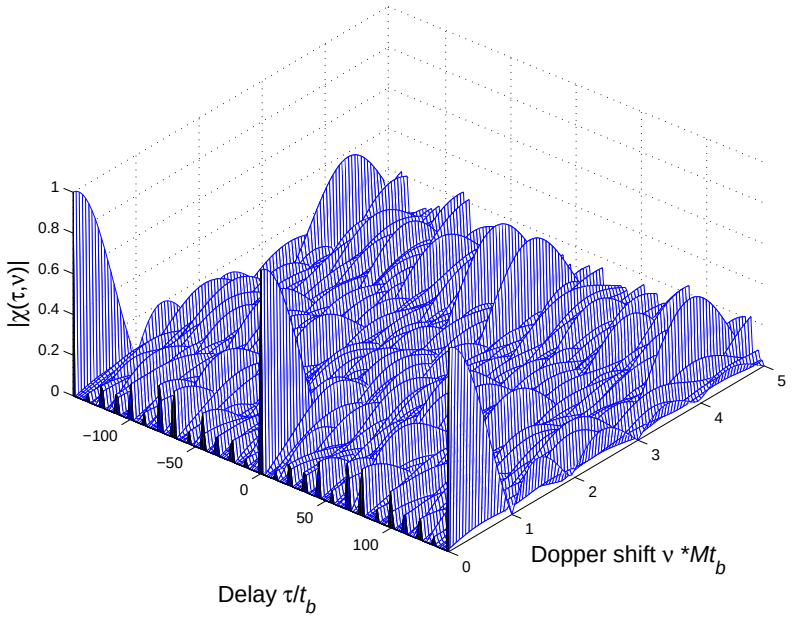

Figure 6.2. Ambiguity function of a 144-length ZCZ sequence-pair.

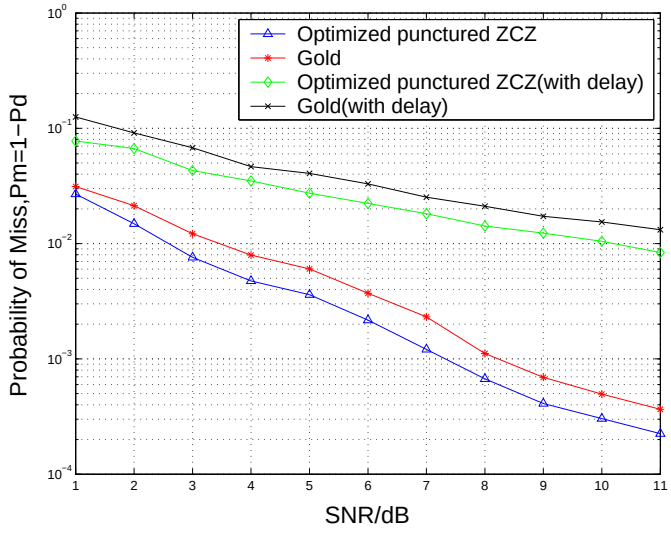

(a)

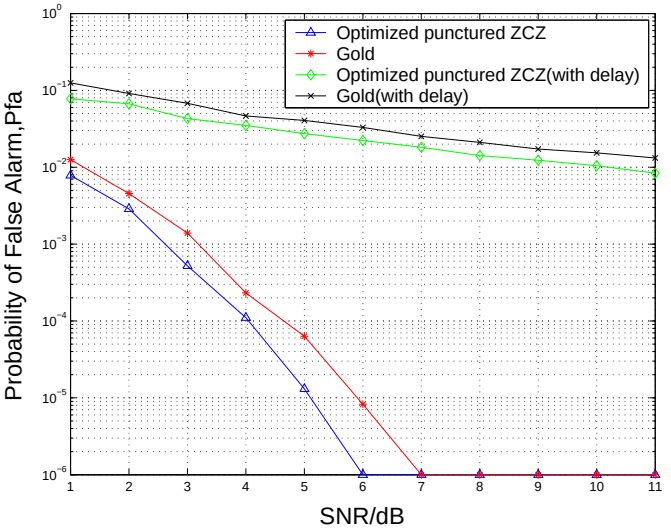

(b)

Figure 6.3. Detection performance: (a) P_m, (b) P_{fa}.

CHAPTER 7

ORTHOGONAL PULSE COMPRESSION CODES FOR MIMO RADAR SYSTEM

7.1 Introduction

MIMO radars, unlike phased array radars, transmit different waveforms on the different antennas of the transmitter, which makes it necessary to do the waveform design for the system. Some researchers have already done some work on the MIMO radar using orthogonal waveforms [90], partial correlation waveforms [40] or the more general non-orthogonal set of waveforms [91][92][93].

In this Chapter, we will focus on the direction finding performance of the MIMO radar systems. We would apply our proposed triphase orthogonal waveforms to the MIMO radar system as pulse compression codes. In addition, a generalized MIMO radar signal model using our triphase orthogonal pulse compression codes is analyzed and then simulated.

7.2 MIMO Radar Signal Model

There has been considerable interest in the use of multiple transmit and receive antennas to offer significant performance improvement in wireless communication. In particular, MIMO radar uses diversity techniques to improve the capacity and performance of the radar systems. In addition, pulse compression, which allows a radar to simultaneously achieve the energy of a long pulse and the resolution of a short pulse without the high peak power required by a high energy short duration pulse [19], is generally used in modern radar systems. In this section, we describe a signal model for the MIMO radar system using orthogonal pulse compression codes.

Shown in Fig. 7.1, we describe a signal model for the MIMO radar system using orthogonal pulse compression codes to improve the direction finding performance.

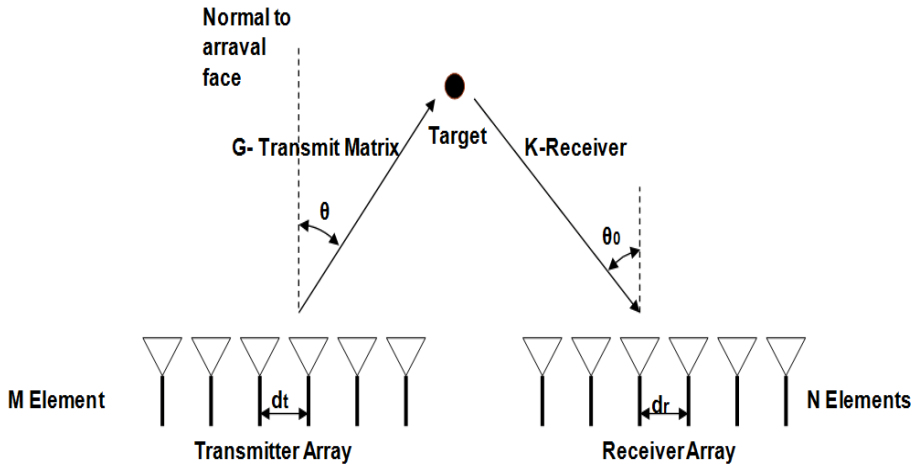

Figure 7.1. MIMO Radar Model.

Assume a radar system that utilizes an array with M antennas at the transmitter, and I antennas at the receiver. For simplicity, we assume that it is a point target, and the arrays at the transmitter and receiver are parallel. A transmitting linear array made up of M elements equally spaced a distance d_t apart. The elements are assumed to be isotropic radiators in that they have uniform response for signals from all directions. The first antenna will be taken as the reference with zero phase. The signal radiated by the transmit antenna impinges at angle θ which is the angle of arrival (AOA). From simple geometry, the difference in path length between

adjacent elements for signals transmitting at an angle θ with respect to the normal to the antenna, is $d_t sin\theta$. This gives a phase difference between adjacent elements of $\phi = 2\pi(d_t/\lambda)sin\theta$, where λ is wavelength of the transmit signal. And the phase difference for m-th transmit antenna is $\phi_m = 2\pi((m-1)d_t/\lambda)sin\theta$. For convenience, we take the amplitude of the signal at each element to be unity. A pulse compression code U_m of length N is applied to m-th transmit antenna, and the signal vector induced by the m-th transmit antenna is given by $\underline{g}_m$. Here,

$$U_m = [u_m^{(0)}, u_m^{(1)}, u_m^{(2)}, ..., u_m^{(N-1)}]; \tag{7.1}$$
$$\underline{g}_m = e^{-j\phi_m}[u_m^{(0)}, u_m^{(1)}, u_m^{(2)}, ..., u_m^{(N-1)}], 1 \leq m \leq M;$$

The signal vectors are organized in the $M \times N$ transmit matrix $\mathbf{G} = [\underline{g}_1; \underline{g}_2; ...; \underline{g}_M]$. The transmitted waveforms are listed as a $M \times 1$ vector $\mathbf{S} = [s_1, s_2, ..., s_M]^T$.

Similar to the transmitter, the model for the array at the receiver could be developed, resulting in an $I \times N$ channel matrix K. Similarly, the first antenna on the receive part will be taken as the reference with zero phase. The signal radiated by the n-th receive antenna impinges at angle θ_0. The phase difference for i-th receiver antenna is $\varphi_i = 2\pi((i-1)d_r/\lambda)sin\theta_0$. For phase-modulated pulse compression waveforms, the corresponding pulse compression code V_i has to be applied to each receive antenna to implement the matched filter. The matched filter for the i-th receive antenna could be given by

$$V_i = [v_i^{(0)}, v_i^{(1)}, v_i^{(2)}, ..., v_i^{(N-1)}]; \tag{7.2}$$
$$\underline{k}_i = e^{-j\varphi_i}[v_i^{(0)}, v_i^{(1)}, v_i^{(2)}, ..., v_i^{(N-1)}];$$
$$\mathbf{K} = [\underline{k}_1; \underline{k}_2; ...; \underline{k}_I]$$

Assume there is a near field point target and it is known that small changes in the aspect angle of the target can cause major changes in the radar cross section (RCS). Here, RCS for each transmit antenna is assumed to have isotropic reflectivity modeled by zero-mean, unit-variance, independent and identically distributed (i.i.d.) Gaussian random variable λ_m. The target RCS is then modeled by the diagonal matrix

$$\Sigma = \begin{bmatrix} \lambda_1 & 0 & \cdots & 0 \\ 0 & \lambda_2 & \ddots & \vdots \\ \vdots & \ddots & \ddots & 0 \\ 0 & ... & 0 & \lambda_M \end{bmatrix} \tag{7.3}$$

The nonfluctuating target modeled using non-zero constants for $\lambda_m = \lambda$ is identified as "$Swerling0$" or "$Swerling5$" model [94]. For the fluctuating target, if $|\lambda_m|$ is drawn from the Rayleigh pdf and vary independently from path to path, the target model represents a classical "$Swerling2$" model [94].

Processing the transmit RCS matrix, the target matrix and the receive matrix together, the received signal vector is shown in equation (7.2).

Here, the transmit signals which are organized in the vector $\mathbf{S} = [s_1, s_2, ..., s_M]^T$ and the additive white Gaussian noise vector $\underline{n}$ consists of i.i.d, zero-mean normal distributed random variables, $\underline{n} = [n_1, n_2, ..., n_N]^T$.

According to (7.2), it is easy to notice that each entry of the matrix could be expressed as

$$\mathbf{R} = \mathbf{K}\left[[\mathbf{G^H}\Sigma]S + \underline{n}\right] = \begin{bmatrix} \underline{k}_1 \\ \underline{k}_2 \\ \vdots \\ \underline{k}_I \end{bmatrix}$$

$$\begin{bmatrix} \left[\underline{g}_1^H, \underline{g}_2^H, \ldots, \underline{g}_M^H\right] \begin{bmatrix} \lambda_1 & 0 & \cdots & 0 \\ 0 & \lambda_2 & \ddots & \vdots \\ \vdots & \ddots & \ddots & 0 \\ 0 & \ldots & 0 & \lambda_M \end{bmatrix} \begin{bmatrix} s_1 \\ s_2 \\ \vdots \\ s_M \end{bmatrix} + \underline{n} \end{bmatrix} \tag{7.4}$$

$$= \begin{bmatrix} \underline{k}_1 \sum_{m=1}^{M} \lambda_m s_m \underline{g}_m^H + \underline{k}_1 \underline{n} \\ \underline{k}_2 \sum_{m=1}^{M} \lambda_m s_m \underline{g}_m^H + \underline{k}_2 \underline{n} \\ \vdots \\ \underline{k}_I \sum_{m=1}^{M} \lambda_m s_m \underline{g}_m^H + \underline{k}_I \underline{n} \end{bmatrix} \tag{7.5}$$

$$\underline{k}_i \sum_{m=1}^{M} \lambda_m s_m g_m^H + \underline{k}_i \underline{n} \tag{7.6}$$

$$= [e^{-j\varphi_i} V_i] \sum_{m=1}^{M} [e^{-j\phi_m} U_m]^H \lambda_m s_m + \underline{k}_i \underline{n} = V_i \sum_{m=1}^{M} U_m^H \lambda_m s_m e^{j(\phi_m - \varphi_i)} + \underline{k}_i \underline{n}$$

The receiver antenna uses a beamformer to steer towards direction $\theta_0^{'}$, $\varphi_i^{'} = 2\pi((i-1)d_r/\lambda)sin\theta_0^{'}$. The beamformer is modeled by a vector

$$\beta(\theta_0') = [e^{-j\varphi_1^{'}}, e^{-j\varphi_2^{'}}, \cdots, e^{-j\varphi_I^{'}}]^T \tag{7.7}$$

The following expression is evaluated:

$$\mathbf{y} = \beta^H(\theta_0^{'})R = [e^{j\varphi_1^{'}}, e^{j\varphi_2^{'}}, \cdots, e^{j\varphi_I^{'}}] \begin{bmatrix} V_1 \sum_{m=1}^{M} U_m^H \lambda_m s_m e^{j(\phi_m - \varphi_1)} + \underline{k}_1 \underline{n} \\ V_2 \sum_{m=1}^{M} U_m^H \lambda_m s_m e^{j(\phi_m - \varphi_2)} + \underline{k}_2 \underline{n} \\ \vdots \\ V_I \sum_{m=1}^{M} U_m^H \lambda_m s_m e^{j(\phi_m - \varphi_I)} + \underline{k}_I \underline{n} \end{bmatrix} \tag{7.8}$$

$$= \sum_{i=1}^{I} e^{j\varphi_i^{'}} (V_i \sum_{m=1}^{M} U_m^H \lambda_m s_m e^{j(\phi_m - \varphi_i)} + \underline{k}_i \underline{n})$$

For the sake of simplicity, but without loss of generality, we assume that $\lambda_m = \lambda_{const}$ is a constant for non-fluctuating model and each transmit signal has the same value $s_m = s$. In MIMO radar for direction finding (DF) purpose, the transmit antennas are separated sufficiently far [95], so the phase shifts at the transmitter are set to zero. It is easy to see that when $\theta = 0$, $\phi_m = 2\pi(d/\lambda)sin\theta = 0$.

Hence

$$\mathbf{y} = \sum_{i=1}^{I} e^{j(\varphi_i^{'}-\varphi_i)}\lambda_{const}s(V_i\sum_{m=1}^{M}U_m^H) + \sum_{i=1}^{I}\underline{k_i}\underline{n}e^{j\varphi_i^{'}} \tag{7.9}$$

If we select orthogonal pulse compression codes for transmit and receive antennas, it is satisfied that

$$V_iU_m^H = \sum_{n=1}^{N} v_i^{(n)}u_m^{(n)*} = \begin{cases} E_s, & i = m \\ 0, & i \neq m \end{cases} \tag{7.10}$$

We obtained that

$$\mathbf{y} = \lambda_{const}sE_s\sum_{i=1}^{L} e^{j(\varphi_i^{'}-\varphi_i)} + \sum_{i=1}^{I}\underline{k_i}\underline{n}e^{j\varphi_i^{'}} \tag{7.11}$$

where $L = \min(I, M)$.

The angle of arrival is estimated as the $\theta_0^{'}$ which maximizes $|\mathbf{y}|^2$,

$$\begin{aligned} |\mathbf{y}|^2 &= |\lambda_{const}sE_s\sum_{i=1}^{L} e^{j(\varphi_i^{'}-\varphi_i)} + \sum_{i=1}^{I}\underline{k_i}\underline{n}e^{j\varphi_i^{'}}|^2 \\ &\cong |\lambda_{const}sE_s\sum_{i=1}^{L} e^{j(\varphi_i^{'}-\varphi_i)} + \sum_{i=1}^{I} n_i^{'}|^2 \end{aligned} \tag{7.12}$$

where $n_i^{'} = \underline{k_i}\underline{n}e^{j\varphi_i^{'}}$.

It is obvious that if the beamformer can well estimate the direction θ_0 at the receiver antenna, $\theta_0^{'} \cong \theta_0$ and $\varphi_l^{'} = \varphi_l$, $\sum_{l=1}^{L} e^{j(\varphi_l^{'}-\varphi_l)}$ can be maximized as L.

$$|\mathbf{y}'|^2 = |\lambda_{const}sE_sL + \sum_{i=1}^{I} n_i^{'}|^2 \tag{7.13}$$

Since $L = \min(M, I)$, we investigate the three cases of different values of M and I.

If $M = I$, we obtain

$$|\mathbf{y}|^2 = |\lambda_{const} s E_s L + \sum_{i=1}^{L} n_i^{'}|^2 \tag{7.14}$$

If $M < I$, we have

$$|\mathbf{y}|^2 = |\lambda_{const} s E_s M + \sum_{i=1}^{I} n_i^{'}|^2 = |\sum_{i=1}^{M} (\lambda_{const} s E_s + n_i^{'}) + \sum_{i=M+1}^{I} n_i^{'}|^2 \tag{7.15}$$

It is seen that using more receive antennas than transmit antennas introduces more noise interference, shown as $|\sum_{i=M+1}^{I} n_i^{'}|^2$ on the second part of the right side of the equation above, which would ruin the system performance.

If $M > I$, we obtain

$$|\mathbf{y}|^2 = |\sum_{i=1}^{I} (\lambda_{const} s E_s + n_i^{'})|^2 = |\lambda_{const} s E_s I + \sum_{l=1}^{I} n_i^{'}|^2 \tag{7.16}$$

We find that equation (7.16) resembles equation (7.14). However, the performance in case $M > I$ is quite different from that in case $M = I$. In case $M > I$, using more transmit antennas than receive antennas introduces more paths within noise and the limit number of receive antennas wastes the signal transmitted by the extra transmit antennas because of the orthogonality of the system model.

The above conclusions are quite different from the previous results in MIMO radar system [96], since we used a different orthogonal model in this paper. However, we could also slightly modify the receive part of the system to construct another system model which can obtain results similar to the general results of MIMO system.

Slightly modified the equation (7.18), the matched filter for ith receive antenna could be

$$\begin{aligned} V_m &= [v_m^{(0)}, v_m^{(1)}, v_m^{(2)}, ..., v_m^{(N-1)}]; \\ \underline{k}_i &= e^{-j\varphi_i} \sum_{m=1}^{M} V_m; \\ \mathbf{K} &= [\underline{k}_1; \underline{k}_2; ...; \underline{k}_I] \end{aligned} \tag{7.17}$$

After the receive antenna uses a beamformer to steer towards a direction, we obtain the result that

$$\begin{aligned}
\mathbf{y} &= \beta^H(\theta_0^{'})R = [e^{j\varphi_1^{'}}, e^{j\varphi_2^{'}}, \cdots, e^{j\varphi_I^{'}}] \begin{bmatrix} \sum_{m'=1}^{M'} V_{m'} \sum_{m=1}^{M} U_m^H \lambda_m s_m e^{j(\phi_m - \varphi_1)} + \underline{k}_1 \underline{n} \\ \sum_{m'=1}^{M'} V_{m'} \sum_{m=1}^{M} U_m^H \lambda_m s_m e^{j(\phi_m - \varphi_2)} + \underline{k}_2 \underline{n} \\ \vdots \\ \sum_{m'=1}^{M'} V_{m'} \sum_{m=1}^{M} U_m^H \lambda_m s_m e^{j(\phi_m - \varphi_I)} + \underline{k}_I \underline{n} \end{bmatrix} \\
&= \sum_{i=1}^{I} e^{j\varphi_i^{'}} (\sum_{m'=1}^{M'} V_{m'} \sum_{m=1}^{M} U_m^H \lambda_m s_m e^{j(\phi_m - \varphi_i)} + \underline{k}_i \underline{n}) \qquad (7.18)
\end{aligned}$$

Suppose there are the same assumptions as above that when $\theta = 0$, $\phi_m = 2\pi(d/\lambda)sin\theta = 0$,

$$\mathbf{y} = \sum_{i=1}^{I} e^{j(\varphi_i^{'} - \varphi_i)} \lambda_{const} s (\sum_{m'=1}^{M'} V_{m'} \sum_{m=1}^{M} U_m^H) + \sum_{i=1}^{I} \underline{k}_i \underline{n} e^{j\varphi_i^{'}} \qquad (7.19)$$

Similarly, optimized orthogonal pulse compression codes are selected for transmit and receive antennas, we easily obtain that

$$\mathbf{y} = \lambda_{const} s M E_s \sum_{i=1}^{I} e^{j(\varphi_i^{'} - \varphi_i)} + \sum_{i=1}^{I} \underline{k}_i \underline{n} e^{j\varphi_i^{'}} \qquad (7.20)$$

If the beamformer can well estimate the direction, we could get $|y|^2$ maximized as

$$|\mathbf{y}'|^2 = |M \lambda_{const} s E_s I + \sum_{i=1}^{I} n_i^{'}|^2 \qquad (7.21)$$

where $n_i^{'} = \underline{k}_i \underline{n} e^{j\varphi_i^{'}}$. It is easy to see that direction finding performance could be improved by increasing either the number of transmit antennas M or the number of receive antennas I. Better performance could be obtained within this scheme, but the modified model is more complicated than the previous one. The equation (20) clearly shows the simple relation between the number of antennas and the system performance.

7.3 MIMO Radar Ambiguity Functions

In this section, we derive the MIMO radar ambiguity function for phase coded waveforms which is used to analyzed the proposed sequence-pair set in Section 5. Based on the result of the first model in Section 2, we will focus our attention on this model and assume that the number of transmit antennas is the same as the number of receive antennas.

We write the phase coded waveforms as following:

$$u(t) = \frac{1}{\sqrt{Nt_b}} \sum_{n=1}^{N} u^{(n)} rect[\frac{t-(n-1)t_b}{t_b}] \tag{7.22}$$

where $u^{(n)} = exp(j\phi^{(n)})$ and the set of N phases $\phi^{(1)}, \phi^{(2)}, ..., \phi^{(n)}$ is the phase code associated with $u(t)$. Nt_b is the duration of waveform $u(t)$.

Similarly, the matched filter for corresponding phase coded waveform is

$$v(t) = \frac{1}{\sqrt{Nt_b}} \sum_{n=1}^{N} v^{(n)} rect[\frac{t-(n-1)t_b}{t_b}] \tag{7.23}$$

As the **MIMO radar ambiguity function** is defined [97]

$$\chi(\tau, \nu, f, f') \cong \sum_{m=1}^{M} \sum_{m'=1}^{M} \chi_{m,m'}(\tau, \nu) e^{j2\pi(fm - f'm')r} \tag{7.24}$$

where

$$\chi_{m,m'}(\tau, \nu) \cong \int_{-\infty}^{\infty} u_m(t) v_{m'}^*(t+\tau) e^{j2\pi\nu t} dt \tag{7.25}$$

Here, the target spatial frequency f and the assumed spatial frequency f' represent the spatial mismatch. τ is the delay corresponding to the target range, and ν is the Doppler frequency of the target. $r \cong d_t/d_r$ where the spacing between the transmitting elements is d_t and the spacing between the receiving elements is d_r. M is the number of transmitting antennas and the function $\chi_{m,m'}(\tau, \nu)$ is called the **cross ambiguity function**. Taking equations (7.22) and (7.23) into (7.25), the cross ambiguity function of phase coded waveforms could be expressed as

$$
\begin{aligned}
& \chi_{m,m'}(\tau,\nu) && (7.26)\\
= & \int_0^{Nt_b} u_m(t) v_{m'}^*[(t+\tau) \mod Nt_b] e^{j2\pi\nu t} dt \\
= & \frac{1}{Nt_b} \int_0^{Nt_b} \\
& \sum_{n=1}^{N} u_m^{(n)} rect[\frac{t-(n-1)t_b}{t_b}] \sum_{n'=1}^{N} v_{m'}^{(n')*} rect([\frac{t+\tau-(n'-1)t_b}{t_b}] \mod N) e^{j2\pi\nu t} dt && (7.27)\\
= & \frac{1}{Nt_b} \sum_{n=1}^{N} u_m^{(n)} v_{m'}^{*(n+k)} \mod N \\
& \int_0^{Nt_b} rect[\frac{t-(n-1)t_b}{t_b}] rect([\frac{t+\tau-(n'-1)t_b}{t_b}] \mod N) e^{j2\pi\nu t} dt && (7.28)\\
= & \frac{1}{Nt_b} \sum_{n=1}^{N} u_m^{(n)} v_{m'}^{*(n+k)} \mod N \int_{(1-n)t_b}^{(N+1-n)t_b} rect(\frac{t}{t_b}) rect(\frac{t}{t_b}) e^{j2\pi\nu[t+(n-1)t_b]} dt \\
= & \frac{1}{Nt_b} \sum_{n=1}^{N} u_m^{(n)} v_{m'}^{*(n+k)} \mod N e^{j2\pi\nu(n-1)t_b} \int_0^{t_b} e^{j2\pi\nu t} dt \\
= & \frac{1}{N} \sum_{n=1}^{N} u_m^{(n)} v_{m'}^{*(n+k)} \mod N e^{j2\pi n\nu t_b} e^{-j\pi\nu t_b} sinc(\pi\nu t_b)
\end{aligned}
$$

where $\tau = kt_b$ is the time delay.

Using the definition of MIMO ambiguity function, we get

$$
\begin{aligned}
\chi(\tau,\nu,f,f') &= \frac{1}{N} \sum_{m=1}^{M} \sum_{m'=1}^{M} \sum_{n=1}^{N} u_m^{(n)} v_{m'}^{*(n+k)} \mod N e^{j2\pi n\nu t_b} e^{-j\pi\nu t_b} && (7.29)\\
& sinc(\pi\nu t_b) e^{j2\pi(fm-f'm')r} && (7.30)
\end{aligned}
$$

where $\tau = kt_b$.

The value $|\chi(0,0,f,f)|$ represents the matched filter output without mismatch. To obtain better system range resolution, the function $\chi(\tau,0,f,f')$ should be sharp around the line $\{(\tau,0,f,f')|\tau=0, f=f'\}$.

Here,

$$
\chi(\tau,0,f,f') = \frac{1}{N} \sum_{m=1}^{M} \sum_{m'=1}^{M} \sum_{n=1}^{N} u_m^{(n)} v_{m'}^{*(n+k)} \mod N e^{j2\pi(fm-f'm')r} \quad (7.31)
$$

where the Doppler shift is Zero or could be well estimated.

For $M = 1$ and $f = f'$, the equation (7.31) reduces to

$$\chi_0(\tau, 0, f, f) = \frac{1}{N} \sum_{n=1}^{N} u^{(n)} v^{*(n+k) \mod N} \tag{7.32}$$
$$\chi_0(0, 0, f, f) = \frac{E_s}{N}$$

where $\tau = kt_b$ and E_s is the energy of the sequence-pair $(\mathbf{u}, \mathbf{v})$.

It is easy to see that equation (7.33) is the correlation function of sequence $\mathbf{u} = (u^{(1)}, u^{(2)}, ..., u^{(N)})$ and its corresponding sequence $\mathbf{v} = (v^{(1)}, v^{(2)}, ..., v^{(N)})$ (if $u = v$, (7.33) is the autocorrelation of $\mathbf{u} = (u^{(1)}, u^{(2)}, ..., u^{(N)})$). For the MIMO radar case that $M > 1$, the cross correlation functions among different pulses also have to be taken into account in addition to the autocorrelation functions in order to have a sharp $\chi(\tau, 0, f, f')$.

Observing the equation (7.31), if the waveforms are orthogonal, the waveforms have high peak mainlobe, zero sidelobes of the autocorrelation function and have zero cross correlation values.

$$\sum_{n=1}^{N} u_m^{(n)} v_{m'}^{*(n+k) \mod N} = \begin{cases} E_s, & \text{for } m = m', k = 0 \\ 0, & \text{for } m = m', k \neq 0 \\ 0, & \text{for } m \neq m' \end{cases} \tag{7.33}$$

The equation (7.31) turns to be

$$\chi(\tau, \nu, f, f') = \begin{cases} \frac{E_s}{N} \sum_{m=1}^{M} e^{j2\pi(f-f')mr}, & \text{for } \tau = 0 \\ 0, & \text{for } \tau = kt_{b,k=1,2,...,N-1} \end{cases} \tag{7.34}$$

where $E_s = \sum_{n=1}^{N} u_m^{(n)} u_m^{(n)*}$ is the energy of the sequence u_m.

Assuming there exists no mismatch in range and Doppler domain and $f = f'$, the function becomes

$$\chi(0, 0, f, f) = \sum_{m=1}^{M} \frac{E_s}{N} = M \frac{E_s}{N} \tag{7.35}$$

It is obvious that the ambiguity function is a constant along the line $(0, 0, f, f)$ which is independent of the waveform design of the sequence set $\{u_m(t)\}$ and the matched sequence set $\{v_m(t)\}$. It implies that when there exists no mismatch in range and Doppler domain, the output of matched filter is independent of the waveform design but only relating to the length of waveform. However, if considering the mismatch, the waveforms design should be taken into account so that the range resolution could be improved. Besides, comparing equation (34) with (37), a diversity gain of M could be achieved here.

On the another hand, observing the right part of equation (7.30), Doppler resolution of the MIMO radar ambiguity function is affected by $e^{j2\pi n\nu t_b}e^{-j\pi\nu t_b}sinc(\pi\nu t_b)$. According to the property of $sinc(\pi\nu t_b)$, when Doppler frequencies equal to multiples of the pulse repetition frequency ($PRF = 1/PRI = 1/t_b$), all the ambiguity values turn to zero. That is the same as the single radar system widely using the pulse compression technology. Overall, the Doppler resolution of MIMO radar ambiguity function could keep the characteristics of the single radar system.

7.4 Properties of Optimized Punctured ZCZ Sequence-pair Set

Considering the optimized punctured ZCZPS that is constructed by the method mentioned in Section 3, the autocorrelation and cross correlation properties can be simulated and analyzed with MATLAB. For example, the optimized punctured ZCZPS $(\mathbf{U}, \mathbf{V})$ is constructed by 5-bit length optimized punctured binary sequence-pair $(\mathbf{x}, \mathbf{y}), \mathbf{x} = [+ + - + -], \mathbf{y} = [+ + 000]$ (using $'+'$ and $'-'$ symbols for $'1'$ and $' - 1'$) and Hadamard matrix $\mathbf{H}$ of order 4. We follow the three steps presented in Section 3 to construct the 20-bit length optimized punctured ZCZPS. The number of sequence-pairs here is 4, and the length of each sequence is $5 * 4 = 20$. Each row of the matrix $\mathbf{U} = [\mathbf{u}_1; \mathbf{u}_2; \mathbf{u}_3; \mathbf{u}_4]$ and the corresponding row of $\mathbf{V} = [\mathbf{v}_1; \mathbf{v}_2; \mathbf{v}_3; \mathbf{v}_4]$

constitute a certain optimized punctured ZCZP $(\mathbf{u}_m, \mathbf{v}_m), m = 1, 2, 3, 4$. Here, $\mathbf{u}_m$ can be used as the transmitting code at the transmit antenna and $\mathbf{v}_m$ is used as matched filter code at the receive antenna.

$$\mathbf{U} = \begin{bmatrix} ++-+-++-+-++-+-++-+- \\ +---+++++----++++ \\ +++--+-++---+++-+- \\ +-++---+-+--++++-- \end{bmatrix};$$

$$\mathbf{V} = \begin{bmatrix} ++000+000+000+000 \\ +-000-000+000-000 \\ ++000+000--000-000 \\ +-000--000-000+000 \end{bmatrix}.$$

The autocorrelation property and cross correlation property of 20-bit length optimized punctured ZCZ sequence pair set $(\mathbf{U}, \mathbf{V})$ are shown in Figs. 2 and 3.

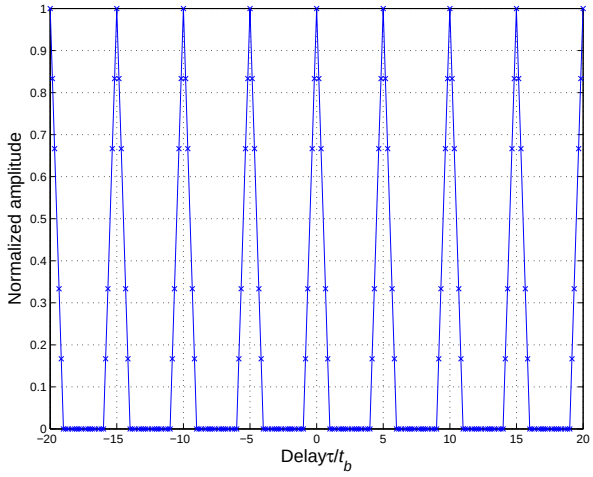

Figure 7.2. Periodic autocorrelation property of optimized punctured ZCZPS.

From the Figs. 7.2 and 7.3, the sidelobe of autocorrelation of ZCZPS can be as low as 0 when the time delay is kept within $Z_0 = N_1 = 5$ (zero correlation zone)

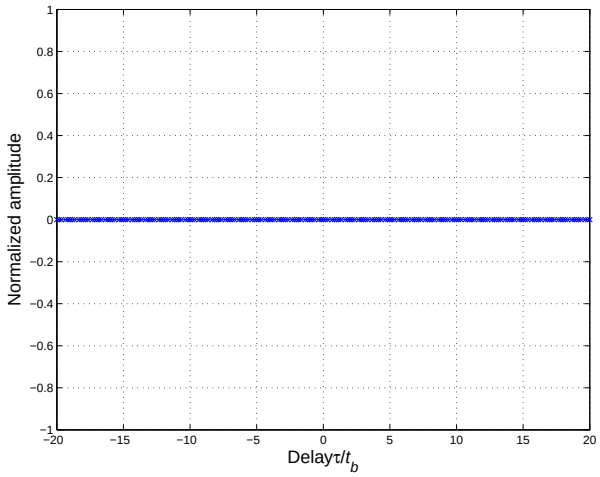

Figure 7.3. Periodic cross correlation property of optimized punctured ZCZPS.

and the cross correlation value is kept as low as 0. Some sequence sets with good periodic correlations have already been proposed and studied. However, the correlation functions of Gold sequences [98] take on the preferred three values. The Kasami sequences [99] can also have one of the preferred three values for the correlation functions. In [100], the authors propose a set of prime-phase sequences whose maximum cross-correlation function is smaller by a factor of $\sqrt{2}$ (3dB), comparing with the same family size of Gold codes. It is easy to see that the optimized punctured ZCZ sequence-pair set has better auto- and cross-correlation functions during ZCZ than most of the sequence sets mentioned above.

Referring to the MIMO ambiguity function of the previous section, the cut of MIMO ambiguity function parallel to the time axis at Doppler shift $\nu = 0$

$$\chi(\tau, 0, f, f') = \begin{cases} \frac{E_s}{N} \sum_{m=1}^{M} e^{j2\pi(f-f')mr}, & \text{for } \tau = 0 \\ 0, & \text{for } \tau = kt_b, k = 1, 2, ..., N_1 - 1 \end{cases} \tag{7.36}$$

Assuming that the estimated parameter equals to the normalized spatial frequency of the target, $f = f'$, we get the function

$$\chi(\tau, 0, f, f) = \begin{cases} \frac{ME_s}{N}, & \text{for } \tau = 0 \\ 0, & \text{for } \tau = kt_b, k = 1, 2, ..., N_1 - 1 \end{cases} \tag{7.37}$$

Consider the same example, where, $E_s = 8, M = 4$ and $N = 20$. We can easily get the range resolution shown as following

$$\chi(\tau, 0, f, f)) = \begin{cases} 1.6, & \text{for } \tau = 0 \\ 0, & \text{for } \tau = kt_b, k = 1, 2, ..., 4 \end{cases} \tag{7.38}$$

Accordingly, it is easy to draw the conclusion that the MIMO radar system using our proposed set of orthogonal codes could improve the range resolution to $\frac{1}{N}$ (N is the length of the corresponding sequence) of the original one. And the peak value is increased from 1 of single radar system without using pulse compression technique to 1.6 in the above case. However, the time delay should be limited to the value of ZCZ of the codes here.

Nevertheless, if there is no limit to the time delay, the range resolution would be interfered. We use the MATLAB to simulate the range resolution performance of three examples, such as 12x4 length ZCZ codes, 20x4 length ZCZ codes and 28x4 length ZCZ codes in Fig. 7.4.

The above figures show that the ambiguity function parallel along time domain at Doppler shift $\nu = 0$ has high peaks at the period of the ZCZ expect for a short sharp at zero time delay. However, there might be the concern that multiple peaks of the autocorrelation function would lead to ambiguity in ranging. Since the periodic correlation function is used in this paper, the peaks from other targets would not be high enough to mask the peak of the target under the study. In addition, we are studying the single target system in this research and well controlling the PRF (pulse

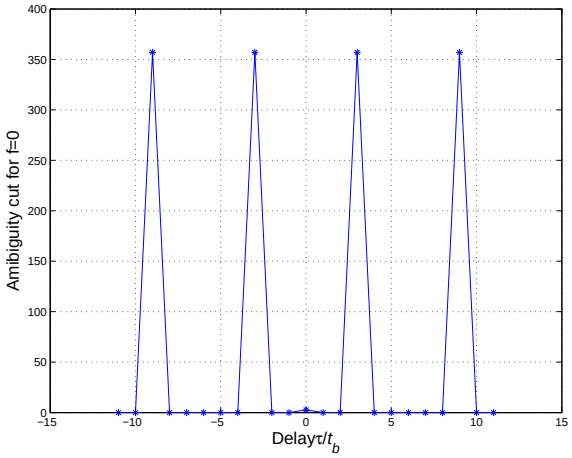

(a)

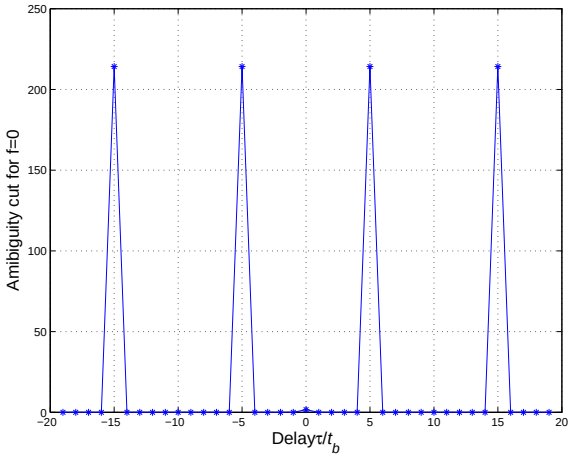

(b)

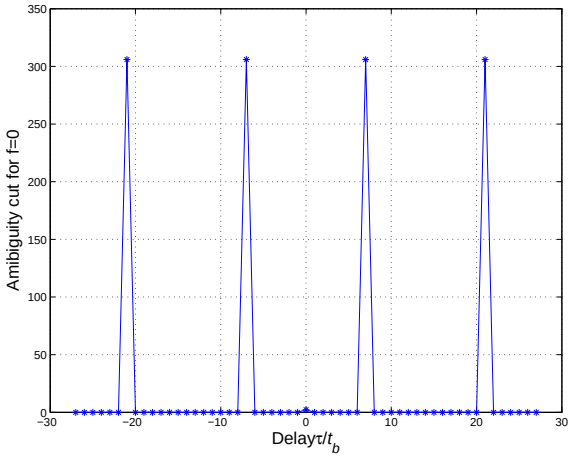

(c)

Figure 7.4. Range Resolution:(a) 12x4 ZCZ codes;(b) 20x4 ZCZ codes;(c) 28x4 ZCZ codes.

repetition frequency), the only concern is that multiple peaks of the transmitting signal reflected from one target may affect determining the main peak of ACF. As a matter of fact, the matched filter here could shift at the period of ZCZ length to track each peak instead of shifting bit by bit after the first peak is acquired, which could make the system work more efficiently. Alike the tracking technology in synchronization of CDMA system, checking several peaks instead of only one peak guarantee the precision of P_D and avoidance of P_{FA}. And the range could be determined by obtaining the the middle point of time range of the first and the last high peaks where we could achieve a short sharp.

7.5 Simulations and Analysis

In this section, we are running MATLAB simulations of the MIMO radar system using different number of transmit antennas and receive antennas to see the direction finding performance. The configurations of transmit and receive antennas are illustrated in Fig. 7.1. The transmit antennas are spaced sufficiently far to each other and the antenna array is used in the receive part. The target fluctuating model in which the channel fluctuated according to a Rayleigh distribution is considered besides the nonfluctuating model. The mean-squared errors (MSEs) of the angle-of-arrival (AOA) estimation is used as the common figure of merit for comparing the performance. Using nonfluctuating and fluctuating target model, the MIMO radar systems of different antennas are illustrated in Fig. 7.5.

According to Fig. 7.5, 8x8 MIMO radar system achieves better MSE of AOA estimation than the 4x4 MIMO radar system as is expected that more transmit and receive antennas can work better than less transmit and receive antennas. On one hand, if the number of receive antennas is increased from 4 to 8, the direction finding performance of 4x8 MIMO radar system becomes worse than that of 4x4 MIMO

radar system. This complies with the equation (7.15) that more receive antennas than transmit antennas introduces more noise interference to make the performance worse. On the another hand, by increasing the number of transmit antennas from 4 to 8, the 8x4 MIMO radar system could not obtain less MSE of AOA than 4x4 MIMO radar system which satisfies the analysis to equation (7.16) that using more transmit antennas than receive antennas brings more paths within noise to the system and the limit number of receive antennas wastes the signal transmitted by the extra transmit antennas. It is also easy to see that 4x8 MIMO radar system could perform better than 8x4 MIMO radar system when the value of SNR is small. However, 8x4 MIMO radar system obtains less MSE of AOA estimation than 4x8 MIMO radar system as the value of SNR increases. Since the noise interference brought by extra transmit antennas is not as sever as the noise introduced by extra receive antennas shown as the second part of equation (7.15) when the value of SNR is large. Comparing the Fig. 7.5(a) and 7.5(b), the performance for fluctuating model is degraded, since the the variable RCS value brought by Rayleigh fading may interfere with the orthogonality of the transmit waveforms and the receive waveforms. So we can see that the model using our proposed codes could work well both under fluctuating and nonfluctuating conditions. As a result, a general conclusion could be drawn that based on the same number of transmit antennas and receive antennas, the more antennas MIMO radar system utilized the better direction finding performance could be achieved.

In addition, we provide the MATLAB simulations of the MIMO radar system using the second model in Fig. 7.6. The results show that increasing the number of either transmit antennas or receive antennas could improve the direction finding performance of the system as expected. 4x2 MIMO radar system achieves better MSE of AOA estimation than the 2x4 MIMO radar system just as shown in equation 7.21 that more receive antennas introduce more noise to the receive part. Comparing

Fig. 7.5 and Fig. 7.6, it is also obvious that the system using second model could outperform the system within the first model. However, the second scheme is more complicated than the first one and may introduce more interference in the real world.

7.6 Conclusions

In this Chapter, we introduced the orthogonal pulse compression codes to the MIMO radar system to improve the radar direction finding performance. In addition, we presented and analyzed a generalized MIMO radar system model for our provided framework, in which Beamforming and estimate MSE are also used to find the direction of the target at receive part. Simulation results showed that significant diversity gain could be obtained in MIMO radar system using orthogonal pulse compression codes. The MIMO radar system using the same number of transmit antennas and receive antennas performs best in the first model.

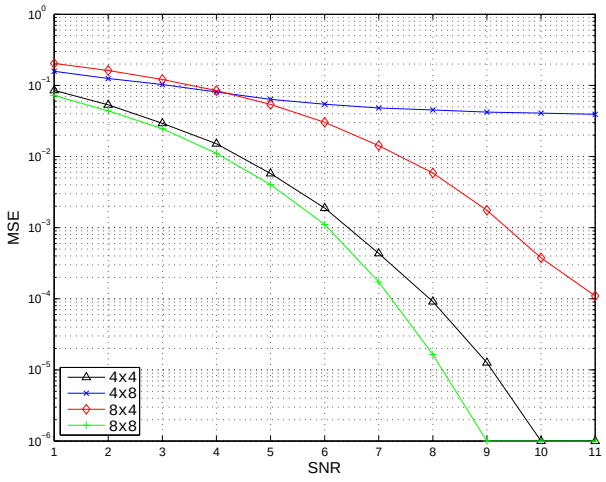

(a)

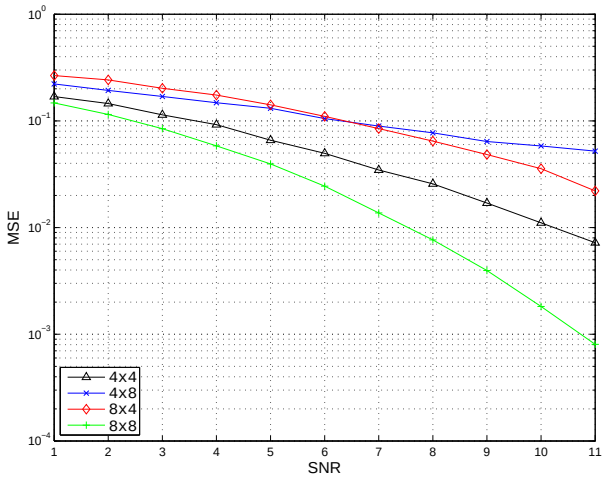

(b)

Figure 7.5. MSE of beamforming at the receiver within the first model: (a) Nonfluctuating model; (b) Fluctuating model .

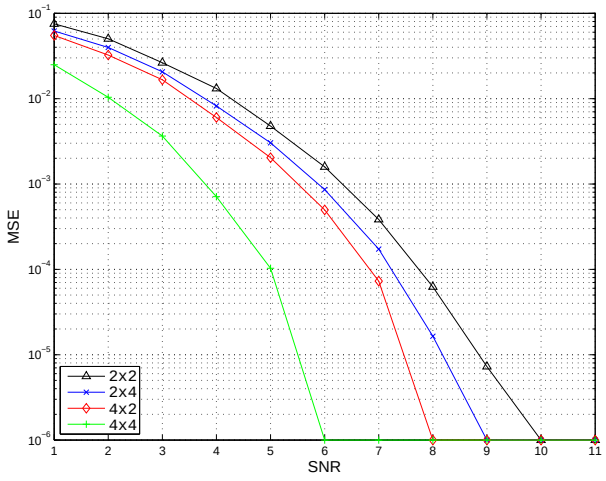

(a)

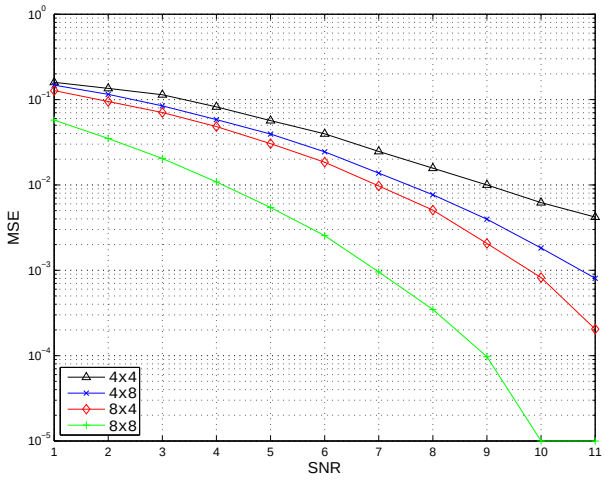

(b)

Figure 7.6. MSE of beamforming at the receiver within the second model: (a) Non-fluctuating model; (b) Fluctuating model .

CHAPTER 8

FROM VIEW OF INFORMATION THEORY FOR WAVEFORM DESIGN AND OPTIMIZATION IN RSN

8.1 Introduction

Information theory has been widely applied to investigating radar detection problem. It is summarized to gain information from a mixture of signal and unwanted noise by obtaining as large a signal-to-noise ratio as possible on the grounds[47]. In addition, Bell[50] firstly used mutual information in the design of single radar waveforms and processing to conclude that distributing energy is a good choice to better detect targets.

In this chapter, we analyze and formulate the problem of waveform design for target estimation in RSN. We further study the estimation waveform problem for target recognition in RSN and derive a close formula for the maximum mutual information between the extended target and the receiver output. We provide an example to show that the performance of waveforms for optimal target estimation problem in RSN. Finally, conclusions are drawn on waveform design by introducing of information theory to RSN

8.2 Problem Analysis

In a radar system, we make measurements of a target in order to determine unknown characteristics of it. In other words, we make measurements of a target in order to decrease *a priori* uncertainty about the target. From the view of information theory, it makes sense that if greater accuracy is required in the measurements, more

information must be provided about the object being measured. Thus, it is easy to understand that the greater the mutual information between the target and the received radar signal when the transmitting signal is given, the greater the quantity of information describing the object and the greater the reduction in the *a priori* uncertainty about the target. The waveforms solved for maximizing such mutual information is called information extraction waveforms or estimation waveform which is studied in this paper.

Considering the RSN, we still need to maximize the mutual information between the target and the received radar signal when transmitting signals are transmitted by several radar sensors. The radar sensor network channel model is shown in Fig. 8.1. Here, $x_1(t), ..., x_N(t)$ are a set of N finite-energy deterministic waveforms with the

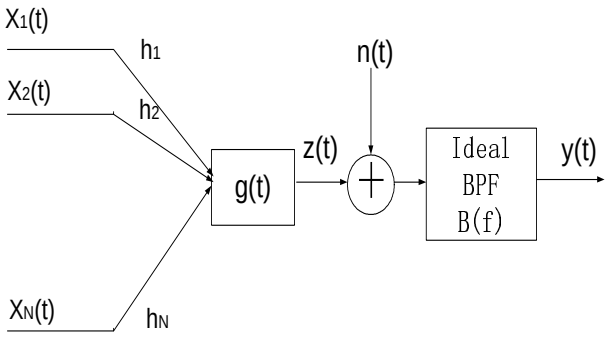

Figure 8.1. Radar sensor network channel model.

total energy E_x transmitted by all the transmitters in order to make a measurement of the radar target. Each waveform is assumed to be of the same duration T and confined to the symmetric time interval $[-T/2, T/2]$.

$$E_x = \sum_{i=1}^{N} \int_{-T/2}^{T/2} |x_i(t)|^2 dt \tag{8.1}$$

The average power P_x, which satisfies the relation $E_x = NP_xT$, is introduced, since most of the practical radar systems have the energy constraint on the average power of the waveform instead of the total energy. We also assume that each waveform is confined to a frequency interval $w = [f_0, f_0 + W]$ so that only negligible energy resides outside the frequency interval w.

The target has a scattering characteristic modeled by the random impulse response $g(t)$. The resulting scattered signal turns to be

$$z(t) = \sum_{i=1}^{N} \int_{-T/2}^{T/2} g(\tau) x_i(t - \tau) dt \tag{8.2}$$

The noise process at the receiver is the zero-mean additive Gaussian noise process $n(t)$ which is assumed to be stationary and ergodic, and to have one-sided power spectral density $P_{nn}(f) = 2S_{nn}(f)$ for $f > 0$. $n(t)$ is also statistically independent of both the transmitted waveforms and the target impulse response. The ideal linear time-invariant bandpass filter $B(f)$ is included so that the transmitted signal has no significant energy outside the frequency interval w, neither does $z(t)$ which is the summation of responses of a linear time-invariant system to the transmitted signal. According to the Fig. 8.1, the problem of Radar Sensor Network can be stated as following. Given a Gaussian target ensemble with random impulse response $g(t)$ having spectral variance $\sigma_G^2(f)$, find the set of waveforms $x_1(t), ..., x_N(t)$ each confined to the symmetric time interval $[-T/2, T/2]$ and having all but a negligible fraction of their energy confined in (one-sided) frequency to $w = [f_0, f_0 + W]$ that maximize the mutual information $I(y(t); g(t)|x_1(t), ..., x_N(t))$ within additive Gaussian noise and with one-sided power spectral density $P_{nn}(f)$.

8.3 Waveforms for Estimation in Radar Sensor Network

We are interested in finding the set of waveforms $x_1(t), ..., x_N(t)$ that maximize the mutual information $I(y(t); g(t)|x_1(t), ..., x_N(t))$ between the random target impulse response and the received radar waveform under the constraints of their energy and bandwidth. Since it could be shown that $I(y(t); g(t)|x_1(t), ..., x_N(t))$ could be maximized when $I(y(t); z(t)|x_1(t), ..., x_N(t))$ is maximized, we will find the functions $x_1(t), ..., x_N(t)$ that maximize $I(y(t); z(t)|x_1(t), ..., x_N(t))$. [50] could be referred to for the proof in detail.

According to the chain rule for mutual information in information theory,

$$\begin{aligned} & I(y(t); z(t)|x_1(t), x_2(t), ..., x_N(t)) \\ \overset{chain\ rule}{=} & \sum_{i=1}^{N} I(y(t); z(t)|x_i(t)) \end{aligned} \tag{8.3}$$

Then, we consider the small frequency interval $F_k = [f_k, f_k + \Delta f]$ of bandwidth Δf small enough so that for all $f \in F_k, X(f) \approx X(f_k), Z(f) \approx Z(f_k)$, and $Y(f) \approx Y(f_k)$. If $\hat{z_k}(t)$ correspond to the component of $z(t)$ with frequency components in F_k, and $\hat{y_k}(t)$ correspond to the component of $y(t)$ with frequency components in F_k, the mutual information between $\hat{z_k}(t)$ and $\hat{y_k}(t)$ could be expressed as [50], given that $x_i(t)$ is transmitted,

$$I(\hat{y_k}(t); \hat{z_k}(t)|x_i(t)) = \tilde{T}\Delta f \ln[1 + \frac{2|h_i X_i(f_k)|^2 \sigma_G^2(f_k)}{P_{nn}(f_k)\tilde{T}}] \tag{8.4}$$

Here, the observing time interval is $T = [t_0, t_0 + \tilde{T}]$.

We partition the frequency bandwidth into M disjoint frequency intervals F_k, with $\hat{y_k}(t), \hat{z_k}(t)$ and $\hat{n_k}(t)$ in the component in F_k. According to [101], when it is made up of Gaussian random processes with disjoint power spectral densities, such processes

corresponding to each F_k are known to be statistically independent. Therefore, the mutual information, given that $x_i(t)$ is transmitted, is equal to the sum of each mutual information between $\hat{y_k}(t)$ and $\hat{z_k}(t)$ given that $x_i(t)$ is transmitted:

$$I(y(t); z(t)|x_i(t)) = \sum_{k=1}^{M} I(\hat{y_k}(t); \hat{z_k}(t)|x_i(t)) \tag{8.5}$$

If we enlarge the number M of disjoint intervals of bandwidth Δf in the frequency bandwidth $w = [f_0, f_0+W]$, then $\Delta f \to 0$. In the limit, we achieve an integral for the mutual information $I(y(t); z(t)|x_i(t))$:

$$\begin{aligned} & I(y(t); z(t)|x_i(t)) \\ = \; & \tilde{T} \int_w \ln[1 + \frac{2|h_i X_i(f)|^2 \sigma_G^2(f)}{P_{nn}(f)\tilde{T}}]df \end{aligned} \tag{8.6}$$

Take equations (8.4) and (8.6) into consideration, we could easily get:

$$\begin{aligned} & I(y(t); z(t)|x_1(t), x_2(t), ..., x_N(t)) \\ = \; & \sum_{i=1}^{N} \tilde{T} \int_w \ln[1 + \frac{2|h_i X_i(f)|^2 \sigma_G^2(f)}{P_{nn}(f)\tilde{T}}]df \end{aligned} \tag{8.7}$$

We assume that

$$E_x = \sum_{i=1}^{N} \int_w |X_i(f)|^2 df, \tag{8.8}$$

and the resulting maximum value of $I(y(t); z(t)|x_1(t), ..., x_N(t))$ is

$$N\tilde{T} \int_w max[0, \ln(\frac{2\sigma_G^2(f)}{NP_{nn}(f)\lambda} \sum_{i=1}^{N} |h_i|^2)]df \tag{8.9}$$

Proof: According to Log sum Inequality[102]

$$\begin{aligned} & I(y(t); z(t)|x_1(t), x_2(t), ..., x_N(t)) \\ \leq \; & (\sum_{i=1}^{N} \tilde{T})[\int_w \ln(1 + \frac{2\sigma_G^2(f) \sum_{i=1}^{N} |h_i X_i(f)|^2}{\sum_{i=1}^{N} P_{nn}(f)\tilde{T}})df] \end{aligned} \tag{8.10}$$

with equality if and only if $\frac{\tilde{T}P_{nn}(f)}{\tilde{T}P_{nn}(f)+2|h_i X_i(f)|^2\sigma_G^2(f)} = \text{const.}$

Based equations (8.7) and (8.8), we use the Lagrange multiplier technique [103] to form a function

$$\begin{aligned}\Phi(|X_i(f)|^2) &= \sum_{i=1}^{N}\tilde{T}\int_w \ln[1+\frac{2|h_iX_i(f)|^2\sigma_G^2(f)}{P_{nn}(f)\tilde{T}}]df \\ &\quad -\lambda(\sum_{i=1}^{N}\int_w |X_i(f)|^2df - E_X) \end{aligned} \tag{8.11}$$

The equation (8.11) is equivalent to maximizing $\varphi(|X_i(f)|^2)$ with respect to $|X_i(f)|^2$, where

$$\begin{aligned}\varphi(|X_i(f)|^2) &= \sum_{i=1}^{N}\tilde{T}\ln[1+\frac{2|h_iX_i(f)|^2\sigma_G^2(f)}{P_{nn}(f)\tilde{T}}] \\ &\quad -\lambda\sum_{i=1}^{N}|X_i(f)|^2 \end{aligned} \tag{8.12}$$

Here, λ is the Lagrange multiplier which could be determined by the constraint of (8.8). Thus, maximizing $\Phi(|X_i(f)|^2)$, the $|X_i(f)|^2$ that maximizes $\varphi(|X_i(f)|^2)$ is

$$|X_i(f)|^2 = \tilde{T}/\lambda - \frac{P_{nn}(f)\tilde{T}}{2\sigma_G^2(f)|h_i|^2} \tag{8.13}$$

Since the magnitude-square spectrum should be no less than zero, we could further rewrite the equation (8.13) as

$$|X_i(f)|^2 = max[0, \tilde{T}/\lambda - \frac{P_{nn}(f)\tilde{T}}{2\sigma_G^2(f)|h_i|^2}] \tag{8.14}$$

We take (8.14) into (8.10), and the result could be easily proved.

In addition, substituting the (8.13) into the constraint of (8.8), we obtain

$$\begin{aligned}\sum_{i=1}^{N}\int_w |X_i(f)|^2df &= \sum_{i=1}^{N}\int_w (\tilde{T}/\lambda - \frac{P_{nn}(f)\tilde{T}}{2\sigma_G^2(f)|h_i|^2})df \\ &= E_x \end{aligned} \tag{8.15}$$

Solving it, we have

$$\lambda = \frac{\tilde{T}Nw}{E_x + \sum_{i=1}^{N} \int_w \frac{P_{nn}(f)\tilde{T}}{2\sigma_G^2(f)|h_i|^2} df} \tag{8.16}$$

As a result, $I(y(t); z(t)|x_1(t), ..., x_N(t))$ could be maximized by the $|X_i(f)|^2$ that

$$|X_i(f)|^2 = \frac{E_x + \sum_{i=1}^{N} \int_w \frac{P_{nn}(f)\tilde{T}}{2\sigma_G^2(f)|h_i|^2} df}{Nw} - \frac{P_{nn}(f)\tilde{T}}{2\sigma_G^2(f)|h_i|^2} \tag{8.17}$$

Observing the equation (8.14), we see that $|X_i(f)|^2$ is a function of several factors such as $\tilde{T}, \lambda, P_{nn}(f)$ and $|h_i|$. $|X_i(f)|^2$ gets larger as $P_{nn}(f)$ gets smaller if all the other factors are held constant for $f \in w$. Oppositely, $|X_i(f)|^2$ gets larger as the variance of $G(f)$, $\sigma_G^2(f)$ or the pulse duration $\tilde{T}$ get larger if all the other factors are held constant. Since we have different channels for different transmitting sensor in a RSN, the effect of different channel gain h_i for each transmitter should be of importance here. If all the other factors are held constant for $f \in w$, we show an interesting interpretation of the relationship between $|X_i(f)|^2$ and $|h_i|$ in Fig. 8.2.

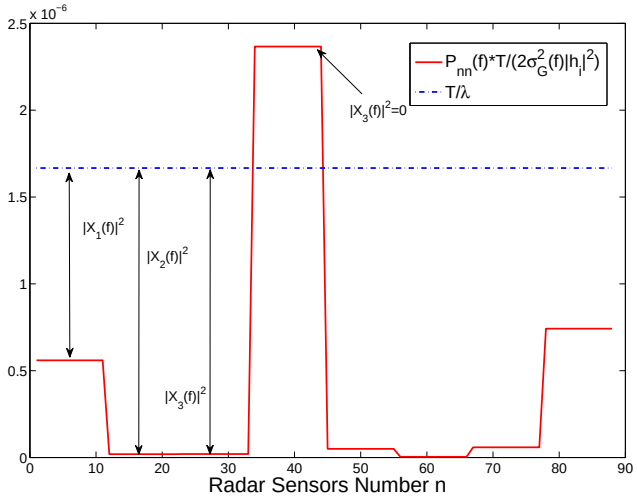

Figure 8.2. Waterfilling interpretation of magnitude-squared spectrum $|X_i(f)|^2$.

The Fig. 8.2 is a "waterfilling " strategy which is widely used in problems dealing with power or energy allocation in information theory [104]. As a result, Fig. 8.2 gives a pictorial view of optimal power allocation strategy for RNS if each channel gain could be properly estimated. The transmitter allocates more power to the stronger channel, taking advantage of the better channel conditions and less or even no power to the weaker ones.

8.4 Results and Comparison

In this section, we will illustrate an example to examine the optimal transmitted signals' spectrum characteristics and the amount of information obtained. From (8.9), the maximum mutual information is given

$$\begin{aligned} & I_{max}(y(t); z(t)|x_1(t), ..., x_N(t)) \\ = \; & N\tilde{T} \int_w max[0, \ln(\frac{2\sigma_G^2(f)}{NP_{nn}(f)\lambda} \sum_{i=1}^{N} |h_i|^2)]df \end{aligned} \tag{8.18}$$

The Fig. 8.3 displays the results of numerical solutions of (8.16) and (8.18) for the mutual information $I_{max}(y(t); z(t)|x_1(t), ..., x_N(t))$ as a function of both the pulse duration T (here, since we assume $T >> 1/w$, then $T = \tilde{T}$) and average power P_x. The value of T equals to $10\mu s, 100\mu s, 1ms, 10ms$ and $100ms$, while average power P_x varies over the range from $1W$ to $1000W$ for each T value. And the number of radar sensors in the RSN is 8.

Fig. 8.3 shows that the mutual information $I_{max}(y(t); z(t)|x_1(t), ..., x_N(t))$ is proportional to transmitted pulse duration T. In the practical RSN, the duration of the transmitted signal T is often referred to as the "time-on-target" in radar target-recognition problems. It makes sense that if all other factors are equal, the longer the "time-on-target", the better the target could be recognized. This point also well matches up to the expression in (8.18). In addition, it is easy to see and understand

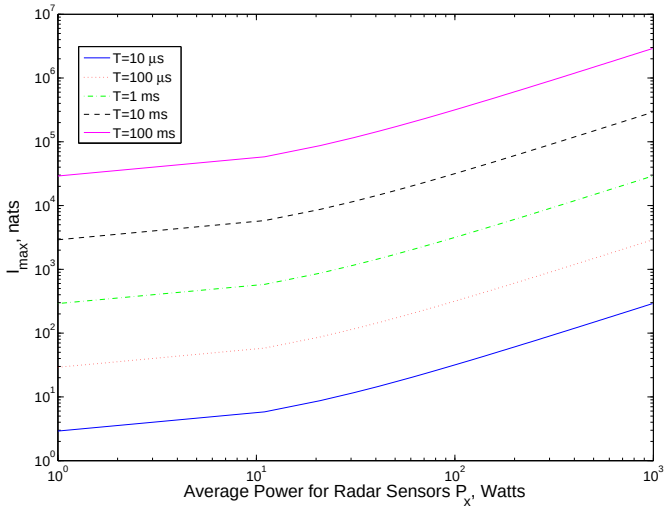

Figure 8.3. Maximum mutual information as a function of T and P_x.

that the more average power allocated on transmitting signals the more mutual information we get at the receiver, as well as the better performance of the target recognition system.

Since RSN is constructed by a number of radar sensors, it is necessary to study the maximum mutual information as a function of the number of radars N in RSN and average power P_x and a function of N and T. The resulting maximum values of $I(y(t); z(t)|x_1(t), ..., x_N(t))$ are plotted in Fig. 8.4(a). The solution is carried out for values of N equal to $1, 10, 20$ and 30, while P_x varies from $1W$ to $1000W$ and T varies over the range from $10\mu s$ to $100ms$.

Though the number of radar sensors are changing here, we assume the total power allocated on the transmitting sensors are equal in order to compare the target recognition performance. Observing Fig. 8.4(a), the maximum mutual information is proportional to the number of radars N in RSN. For larger number of radar sensors such as $N \geq 10$, the increase of the maximum mutual information is not as distinct as when the value of N is small. The same story happens to the the maximum mutual

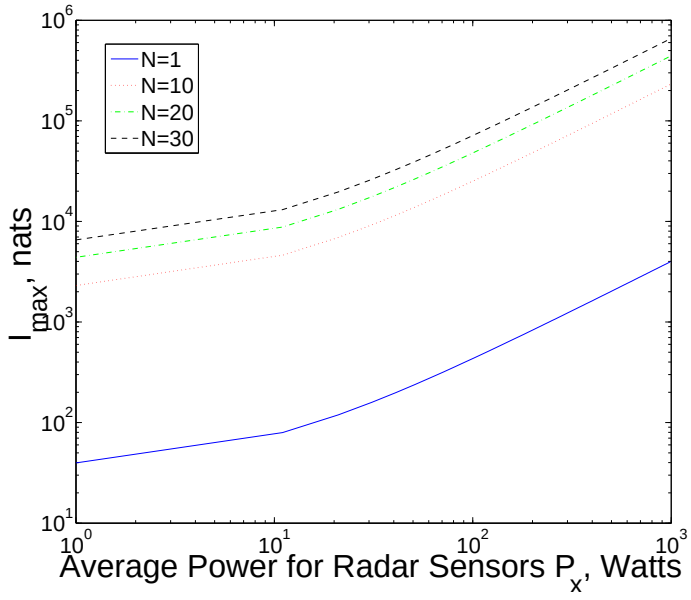

(a)

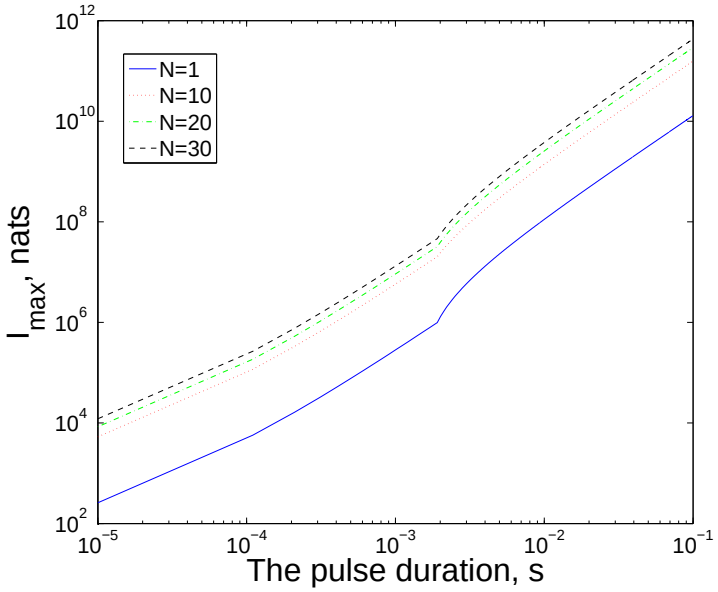

(b)

Figure 8.4. Maximum mutual information: (a) A function of N and P_x; (b) A function of N and T.

information as a function of N and T in Fig. 8.4(b). In a word, the more radar sensors, the better the target could be recognized. However, all three factors N, T and P_x should be carefully decided between the balance of optimizing recognizing performance and the industry implementation cost.

8.5 Conclusions

In this paper, we studied the waveforms design for the measurement of extended radar targets in radar sensor networks (RSN) in the view of information theory. Considering the effect of different channel gains, we investigated the estimation waveforms that maximize the mutual information between a target ensemble and the received signal within additive Gaussian noise when the transmitting signals are given in order to well recognize characteristics of the target. We also the study of the maximum mutual information under the constraints of the number of radar sensors, waveform energy and duration, which could be taken into consideration when waveforms are designed for RSN, and draw some useful conclusions for waveforms design in RSN. If the channel could be well estimated, the transmitter could allocate more power to the stronger channel to gain better performance.

CHAPTER 9

COMPRESSIVE SENSING WITH SIMPLIFIED RECOVERY

9.1 Introduction

Compressive sensing (CS) [60][61] is an emerging framework that a signal vector which is K-sparse in a specific domain can be completely characterized by M measurements ($M > K$) with $M << N$, where N is the traditional Nyquist based number of samples required.

The major algorithmic challenge in compressive sensing is to approximate a signal given a vector of noisy samples. There are three rough categories of signal recovery algorithms: convex relaxation, combinatorial algorithms and greedy pursuits. The convex relaxation algorithms leading to l_1-minimization–also called basis pursuit [62] succeed with a very small number of measurements, however, it tends to be computationally burdensome. Many of the combinatorial algorithms are extremely fast, but they require a large number of somewhat unusual samples that may not be easy to acquire. Greedy pursuits, such as various matching pursuits [63][64], are intermediate in their running time and sampling efficiency but has its own disadvantages.

In this chapter, we provide a new algorithm-the CS-SVD algorithm for signal recovery in compressive sensing by introducing the concept of SVD (Singular Value Decomposition). We use SVD to study the compressive sensing framework and develop two simple and straightforward methods to implement the CS-SVD algorithm in the presence of additive noise.

9.2 Preliminaries

9.2.1 Compressive Sensing

The recent results of compressive sensing have shown that the information from a signal may be captured with a small set of nonadaptive, linear measurements as long as the signal is sparse in some basis or frame [51][52]. We acquire a signal vector $\underline{x} \in \Re^N$ via linear measurements

$$\underline{y} = \Phi\underline{x} + \underline{e} = \Phi\Psi\theta + \underline{e} \tag{9.1}$$

where Φ is an $M \times N$ measurement matrix with $\phi_1, \phi_2, ..., \phi_M$ as rows modeling the sampling system, $\underline{y} \in \Re^M$ is the vector of samples observed, and $\underline{e}$ is an $M \times 1$ vector that represents measurement errors. If $\underline{x}$ is termed as $K-$sparse in the sparsity basis Ψ, i.e, $\underline{\theta} = \Psi^H\underline{x}$ containing no more than K nonzero elements, we need to acquire only $M = O(K\log(N/K))$ random measurements to recover the signal $\underline{x}$. It is convenient to express $\underline{x}$ as $\Psi\underline{\theta}$ where Ψ is the $n \times n$ matrix with $\psi_1, \psi_2, ..., \psi_N$ as columns.

Here, (Φ, Ψ) is a pair of orthobases which follow the incoherence restriction. In [70], the coherence between the measurement basis Φ and the sparsity basis Ψ is

$$\mu(\Phi, \Psi) = \sqrt{n} \cdot \max_{1 \le k,j \le n} | < \phi_k, \psi_j > | \tag{9.2}$$

the coherence measures the largest correlation between any two elements of Φ and Ψ. If Φ and Ψ contain correlated elements, the coherence is large. Otherwise, it is small. As for how large and how small, it follows from linear algebra that $\mu(\Phi, \Psi) \in [1, \sqrt{n}]$. And compressive sensing is mainly concerned with low coherence pairs.

In this chapter, we will take Fourier basis for Ψ. Φ is the random waveforms with independent identically distributed (i.i.d.) entries, e.g., Gaussian which exhibit a very low coherence with any fixed representation Ψ. According to equation (9.2), we assume that $\underline{y} = A\underline{\theta}$, then $H = \Phi\Psi$. It is easy to see that studying $\mu(\Phi, \Psi)/\sqrt{n}$ equals to find the maximum value of the entry in A.

The convex relaxation algorithm is a powerful method for CS signal recovery, so one can use l_1 minimization with relaxed constrains for reconstruction [105]:

$$\min||\widetilde{\theta}||_{l_1} \quad \text{subject to} \quad ||\Phi\Psi\widetilde{\theta} - \underline{y}||_{l_2} \leq \epsilon \tag{9.3}$$

where ϵ bounds the amount of noise in the data.

The convex relaxation algorithm could obtain a small number of measurements, but results in large computational complexity. In Section 4, the signal recovery performance of using the convex relaxation algorithm will be provided to compare with the performance of using the proposed algorithm.

9.2.2 Singular Value Decomposition

In this section, we introduce the concept of the extremely useful singular value decomposition.

Theorem 1 (Singular Value Decomposition (SVD))[106] If A is a real m-by-n matrix, then there exist orthogonal matrices

$$U = [u_1, ..., u_m] \in \Re^{m\times m} \text{ and } V = [v_1, ..., v_n] \in \Re^{n\times n}$$

such that

$$U^H AV = \text{diag}(\sigma_1, ..., \sigma p) \in \Re_{m\times n}, \quad p = \min(m, n)$$

where $\sigma_1 \geq \sigma_2 \geq ... \geq \sigma_p \geq 0$.

According to the above theorem, assuming that $\Sigma = U^H AV = \text{diag}(\sigma_1, ..., \sigma_p)$, then $A = U\Sigma V^H$, where $(\cdot)^H$ is the Hermitian symbol. We could also obtain the important properties of orthogonal matrices that $U^H U = \text{diag}(1, ..., 1) \in I^{m\times m}$ and $V^H V = \text{diag}(1, ..., 1) \in I^{n\times n}$.

9.3 The CS-SVD Algorithm

Based on the concept of SVD, we provide the CS-SVD algorithm for compressive sensing and propose two methods to implement the CS-SVD algorithm for signal recovery in this section.

9.3.1 The First Method

If the signal or the sparse representation scheme of signal is properly chosen, x is K-sparse in the basis ΨV (V would be mentioned in the latter part), i.e., $x = \Psi V \underline{\theta'}$ with $||\underline{\theta'}||_{l_0} = K$, the measurements M required to recover the original signal is only K, and the recover algorithm is easy and very straitforward.

9.3.1.1 Signal Model

We study the signal vector $\underline{x}$ which is obtained by linear measurements

$$\underline{y} = \Phi \underline{x} + \underline{e} = \Phi \Psi \underline{\theta} + \underline{e} \tag{9.4}$$

where Φ is an $M \times N$ measurement matrix modeling the sampling system, $\underline{x}$ is expanded in the sparsity basis Ψ, i.e,. $\underline{x} = \Psi \underline{\theta}$ and $\underline{y} \in \Re^M$ is the vector of samples obtained.

We assume that $A = \Phi\Psi$. Based on the definition and properties of SVD that $\Sigma = U^H A V = diag(\sigma_1, \sigma_2, ..., \sigma_p)$, we use SVD to decompose the matrix A so that $A = \Phi\Psi = U\Sigma V^H$. Without loss of generality, we let $\underline{\theta'} \triangleq V^H \underline{\theta}$, then $\underline{\theta} = V\underline{\theta'}$. Stating differently, $\underline{\theta'}$ is $K-$sparse when represented in the sparsity basis V. The equation (9.4) could be expressed as

$$\underline{y} = \Phi\Psi\underline{\theta} + e = U\Sigma V^H V \underline{\theta'} + \underline{e} = U\Sigma\underline{\theta'} + \underline{e} \tag{9.5}$$

9.3.1.2 Recovery Algorithm

Motivated by how SVD works in MIMO system, we multiply $\underline{y}$ by U^H and obtain that

$$U^H\underline{y} = U^H(\Phi\Psi\underline{\theta} + \underline{e}) = U^HU\Sigma V^HV\underline{\theta}' + U^H\underline{e} = \Sigma\underline{\theta}' + \underline{e}' \tag{9.6}$$

where $\underline{e}' = U^H\underline{e}$. As it is known that $\Sigma = \text{diag}(\sigma_1, \sigma_2, ..., \sigma_p) \in \Re^{M\times N}$, $p = \min(M, N)$, where $\sigma_1 \geq \sigma_2 \geq ... \geq \sigma_p \geq 0$. We observe that $p = \min(M, N)$ and M is usually less than N in CS, hence, we could obtain that $p = M$ here. We could express the equation (9.6) as the following vector

$$U^H\underline{y} = [y'_1, y'_2, ..., y'_M]^H = [\sigma_1\theta'_1, \sigma_2\theta'_2, ..., \sigma_M\theta'_M]^H + \underline{e}' \tag{9.7}$$

Without changing the property of sparsity basis, we could easily reorder the columns of sparsity basis corresponding to the non-zero value in $\underline{\theta}'$ so that all the non-zero values of $\underline{\theta}'$ are arranged in the beginning. Once Φ and Ψ are known, Σ is known and fixed. We could obtain θ'_i by

$$|\theta'_i - \frac{y'_i}{\sigma_i}|^2 \leq \epsilon, i = 1, 2, ..., M \tag{9.8}$$

According to equation (8), the values of $\theta'_i, i = 1, 2, ..., M$ are obtained and $\theta'_i = 0, i > M$ when $M \geq K$.

The original signal $\underline{x}$ could be recovered by

$$\underline{x} = \Psi\underline{\theta} = \Psi V\underline{\theta}' \tag{9.9}$$

Stating differently, the number of measurements M depends on the number and positions of nonzero values in $\underline{\theta}'$ where $\underline{x}$ is K-sparse when represented in the basis ΨV, i.e., $\underline{x} = \Psi V\underline{\theta}'$.

For the sake of simplicity, but without loss of generality, we assume that $\theta'_i = 0, i > K$, if the sparsity basis and measurements matrix are properly chosen, i.e., $\underline{x} =$

$\Psi V\underline{\theta}'$. Using the proposed scheme, we only have to capture $M(M \geq K)$ measurements to recover the signal vector $\underline{x}$. Recalling the standard state-of-art compressive sensing techniques, they usually require $M = O(K\log(N/K))$ measurements which is much larger than K to recover the original signal.

9.3.2 The Second Method

In the previous method, the original signal x has been represented by the basis ΨV. Stating differently, x is firstly mapped to basis Ψ, i.e., $x = \Psi\theta$ and secondly mapped to basis $\theta = V\theta'$. For the second method, we will map the original signal to the sparsity basis only once. Nevertheless, a new measurement matrix Φ' has to be produced here. If the signal or the sparse representation scheme of signal is properly chosen, x is K-sparse in the basis Ψ, i.e., $x = \Psi\theta$ with $||\theta||_{l_0} = K$ ($||\cdot||_{l_0}$ calculates the number of non-zero values among θ), the measurements M required to recover the original signal is only K, and the recover algorithm is demonstrated as following.

9.3.2.1 Signal Model

We study the signal vector $\underline{x}$ which is obtained by linear measurements

$$\underline{y} = \Phi\underline{x} + \underline{e} = \Phi\Psi\underline{\theta} + \underline{e} \tag{9.10}$$

where Φ is an $M \times N$ measurement matrix modeling the sampling system, $\underline{x}$ is $K-$sparse when expanded in the sparsity basis Ψ, i.e,. $\underline{x} = \Psi\underline{\theta}$ and $\underline{y} \in \Re^M$ is the vector of samples obtained.

We assume that $A = \Phi$. Based on the definition and properties of SVD that $\Sigma = U^H AV = diag(\sigma_1, \sigma_2, ..., \sigma_p)$, we use SVD to decompose the matrix A so that $A = \Phi = U\Sigma V^H$. It is known that the matrix V is the unitary matrix which satisfies $V^H V = I$, where I is the identity matrix. In addition, we usually take Fourier basis

f_b as the sparsity matrix Ψ which also satisfies $f_b^H f_b = I$. Without loss of generality, we use Fourier basis in place of the unitary matrix V to construct a new measurement matrix $\Phi' = U\Sigma f_b^H$. The equation (9.10) could be expressed as

$$\underline{y} = \Phi'\Psi\underline{\theta} + e = U\Sigma f_b^H f_b\underline{\theta} + \underline{e} = U\Sigma\underline{\theta} + \underline{e} \tag{9.11}$$

9.3.2.2 Recovery Algorithm

Motivated by how SVD works in MIMO system, we multiply $\underline{y}$ by U^H

$$U^H\underline{y} = U^H(\Phi\Psi\underline{\theta} + \underline{e}) = U^H U\Sigma f_b^H f_b\underline{\theta} + U^H\underline{e} = \Sigma\underline{\theta} + \underline{e}' \tag{9.12}$$

where $\underline{e}' = U^H\underline{e}$. As it is known that $\Sigma = \text{diag}(\sigma_1, \sigma_2, ..., \sigma_p) \in \Re^{M\times N}$. Similar to the first method, $p = \min(M, N) = M$, where $\sigma_1 \geq \sigma_2 \geq ... \geq \sigma_p \geq 0$. The equation (12) turns to be

$$U^H\underline{y} = [y_1', y_2', ..., y_M']^H = [\sigma_1\theta_1, \sigma_2\theta_2, ..., \sigma_M\theta_M]^H + \underline{e}' \tag{9.13}$$

Once Φ and Ψ are known, Σ is known and fixed.

As a result,

$$|\theta_i' - \frac{y_i'}{\sigma_i}|^2 \leq \epsilon, i = 1, 2, ..., M \tag{9.14}$$

Observing equation (9.14), we could obtain the values of $\theta_i, i = 1, 2, ..., M$ and $\theta_i = 0, i > M$ when $M \geq K$.

The original signal $\underline{x}$ could be recovered by

$$\underline{x} = \Psi\underline{\theta} = f_b\underline{\theta} \tag{9.15}$$

M depends on the number and positions of nonzero values in $\underline{\theta}$ where $\underline{x}$ is K-sparse when represented in the basis Ψ, i.e., $\underline{x} = \Psi\underline{\theta}$. We assume that $\theta_i = 0, i > K$, if the sparsity basis and measurements matrix are properly chosen, i.e., $\underline{x} = \Psi\underline{\theta}$. Using the proposed scheme, we only have to capture $M(M \geq K)$ measurements to recover the signal vector $\underline{x}$.

9.3.3 Comparison of the Above Two Methods

According to the results in second part of the chapter, the incoherence property depends on the maximum entry value of the matrix $U\Sigma$ which is determined by the measurement matrix Φ. In our research, the coherence becomes larger but is still acceptable.

For the first method, we firstly represent the original signal X into the basis Ψ and then represent $\underline{\theta}$ in the basis V. And for the second method, we reproduce the measurement matrix by $\Phi = U\Sigma f_b$. The second method is easy to implement when the original signal could be sparsely represented in the basis Ψ. However, when the original signal is not sparsely represented in the basis Ψ as $X = \Psi\underline{\theta}$, θ could be represented by $\underline{\theta} = V\underline{\theta}'$ to decrease the non-zero values in $\underline{\theta}'$, for which the first method could be considered.

9.4 Simulation Results

In this section, we firstly simulate the signal recovery from the data without the noise interference.

In Fig. 9.1(a), we use the first method to implement the CS-SVD algorithm and simulate the reconstructed signal comparing with the original signal. We set $N = 500$, $K = 40$ and $M = 40$, where N is the number of samples of the signal vector $\underline{x}$ and $\underline{x}$ has sparsity K in the properly chosen basis , i.e., $\underline{x} = (\Psi V)\underline{\theta}'$. The reconstructed signal is comparing with the original signal by applying the second method to implement the CS-SVD algorithm in Fig. 10.4(b), where $N = 500$, $K = 100$ and $M = 100$.

According to the above simulation results, it is easy to see that the reconstructed signal could perfectly comply with the original signal by using both of the two methods when there is no noise with the data.

In addition, we compare the mean-squared error (MSE) for the proposed algorithm with the MSE for the convex relaxation algorithm as we increase the number of measurements M for fixed $SNR = 20dB$. Here, SNR is the power ratio of useful signal to noise among the original signal. According to the two different methods mentioned above, we study two different cases here.

Considering the first method, where $x = \Psi V \underline{\theta'}$, we assume that $\underline{\theta'}$ contains only K non-zero values in the beginning of vector $\underline{\theta'}$ and set $N = 500$ and $K = 40$, where N is the number of samples of the signal vector $\underline{x}$. We use different values of M to reconstruct the compressed signal.

According to the Fig. 9.2(a), it is easy to see that the lower values of M results in higher error. Increasing the value of M, we see the expected decay in MSE. Observing Fig. 9.2(a), the first method for implementing CS-SVD algorithm could provide stable and best recovery performance in this case. Because the original signal used here could be termed as K-sparse as $\underline{x} = \Psi V \underline{\theta'}$.

Taken the second method into account, we assume that $\underline{\theta}$ is K-sparse in the beginning of vector $\underline{\theta}$. Setting $N = 500$ and $K = 100$, we use different value of M to reconstruct the compressed signal.

Similar to Fig. 9.2(a), it is obvious that the lower values of M results in higher error in Fig. 9.2(b). Increasing the value of M, we see the expected decay in MSE. The second method for implementing CS-SVD algorithm could provide stable and best recovery performance in this case, since the original signal used here could be termed as K-sparse as $\underline{x} = \Psi \underline{\theta}$. In addition, we also find that when the number of measurements M is larger than the number of non-zero values $K = 100$, the MSE

decreases sharply which comply with the theoretical result. Based on the above simulation results, two different methods could be chosen to implement the CS-SVD algorithm according to the different sparsity representation of the original signal.

9.5 Conclusion

Motivated by the concept of SVD, we provide a new CS technique-the CS-SVD algorithm in this dissertation. We propose two methods to implement the CS-SVD algorithm. The theoretical results show that the CS-SVD algorithm requires less measurements than the standard state-of-art compressive sensing techniques and provide a simpler and more efficient recovery scheme. The simulation results demonstrate that both of our two methods provide considerable gains over convex relaxation algorithm in terms of number of measurements required for stable recovery. And each of them could work well in different cases in which different original signal could be sparsely represented in different sparse basis.

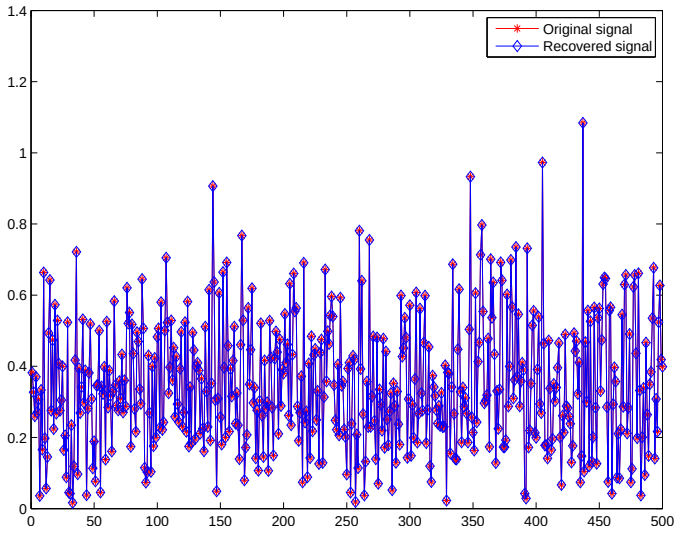

(a)

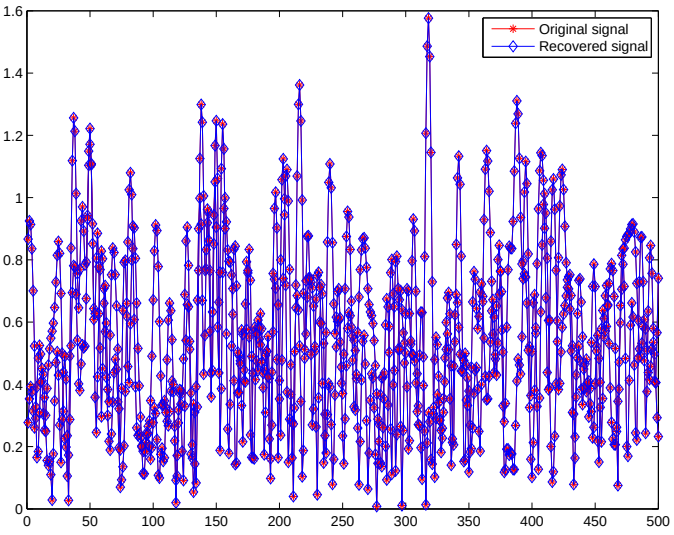

(b)

Figure 9.1. Reconstructed signal VS. original signal: (a) Using the first method for $K = 40$ and $M = 40$; (b) Using the second method for $K = 100$ and $M = 100$.

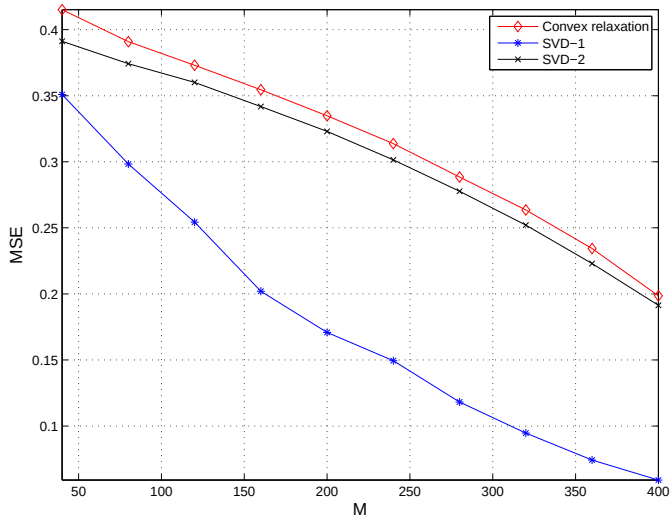

(a)

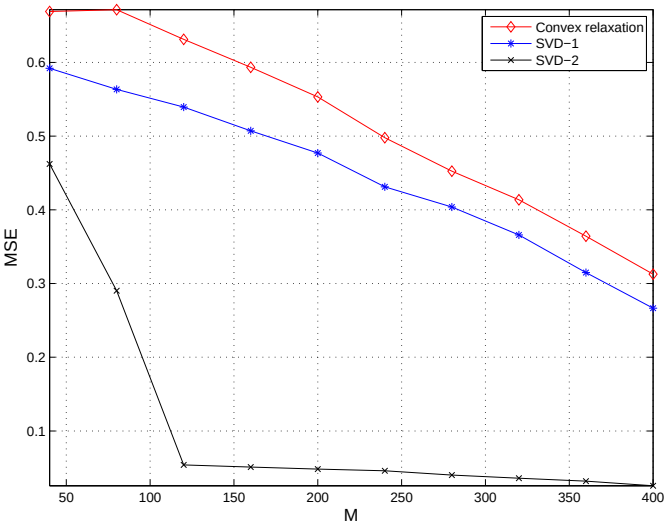

(b)

Figure 9.2. MSE versus M for fixed $N = 500$ and $SNR = 20dB$: (a)$K = 40$; (b)$K = 100$.

CHAPTER 10

COMPRESSIVE SENSING IN DISTRIBUTED RSN USING PULSE COMPRESSION WAVEFORMS

10.1 Introduction

RSN has been recently considered to overcome the performance degradation of a single radar. Due to the expansion of data introduced to RSN, the compression and reconstruction of the received data is a design challenge of future RSN. In this chapter, we investigate how to employ compressive sensing in Radar Sensor Network (RSN), in which we have a number of transmit sensors but only one sensor on the receiving part. It is known that the scene must be 'compressible' for compressive sensing to have benefit. Recognizing that the Stepped-Frequency train could act as the sparsity basis for the signal, we apply Stepped-Frequency train as the pulse compressions codes to construct the 'compressible signal' at each transmit sensor. We choose the Gaussian matrix as the measurement matrix that satisfies the restricted isometry property (RIP) with this basis. In addition, we propose an Maximum Likelihood (ML) algorithm to estimate the target RCS parameter and use the Cramer-Rao lower bound (CRLB) to validate our theoretical result. In the simulation parts, the performance of signal recovery is studied as well as the performance of target RCS value estimation. The simulation results show that the the signal could be precisely recovered if the number of measurements is no less than the number of sensors in RSN and the actual variance of the RCS parameter estimation $\widehat{\theta}$ satisfies the CRLB.

10.2 The Basic Model

10.2.1 The Produced Signal for Compressed Sensing

The Stepped-Frequency pulse train is a pulse burst waveform which obtains large overall bandwidth while maintaining narrow instantaneous bandwidth. Each pulse in the burst is a simple, constant-frequency pulse; however, the RF frequency is added by a frequency step ΔF between consecutive pulses. The most common Stepped-Frequency waveform employs a linear frequency stepping pattern, where the RF frequency of each pulse is increased by ΔF Herts from the preceding pulse. In addition, the frequency steps can be added to a train of unmodulated pulses, as well as to a train of modulated pulses. The Stepped-Frequency waveform we study in this chapter is expressed as follows:

$$s(t) = \sum_{i=0}^{I-1} s_i(t - iT_p) e^{j2\pi i \Delta F(t - iT_p)} \tag{10.1}$$

where T_p is the length of each pulse and I is the number of pulses in a burst (train) of pulses. Observing the right side of equation (10.1), we see that $e^{j2\pi i \Delta F(t-iT_p)}$ can be expressed into the orthogonal Fourier basis $e^{j2\pi \frac{ni}{I}(t-iT_p)}$, where $\Delta F = \frac{n}{I}$ and n is the index of a transmit sensor in a radar sensor network. Here, we let the frequency step ΔF among each pulse burst waveform corresponding to each specific transmit sensor be different and related to the index n. The goal of CS is to perform good reconstruction of the signal by using a few sparse samples. Here, we collect the data in such a way that is compressed already. We establish a RSN which uses the Stepped-Frequency waveforms as pulse compression codes. The radar sensor network consists of N transmit sensors indexed by n and only one receiving sensor. Then $s_n(t) = \sum_{i=0}^{I-1} x_n(t - iT_p) e^{j2\pi \frac{ni}{I}(t-iT_p)}$ denotes the transmit signal for the transmit sensor n. Let $x_n(t) = \sum_{i=0}^{I-1} x_n(t - iT_p)$ and $\psi_n(t) = \sum_{i=0}^{I-1} e^{j2\pi \frac{ni}{I}(t-iT_p)}$ denote the information signal and the pulse compression waveforms, where N is the number

of transmit sensors and I is still the number of pulses in a burst or the number of time samples. In order for the later use, we express the preceeding equations in vector format that $\bar{x}_n = [x_n(t_1), x_n(t_2), ..., x_n(t_I)]^T$ and $\bar{\psi}_n = [e^{j2\pi\frac{n}{I}t_1}, e^{j2\pi\frac{2n}{I}t_2}, ..., e^{j2\pi\frac{nI}{I}t_I}]^T = [\psi_{1n}, \psi_{2n}, ..., \psi_{In}]^T$. Then, $S = \Psi X^T$ is the transmit matrix, where $X = [\bar{x}_1, \bar{x}_2, ..., \bar{x}_N]$ and $\Psi = [\bar{\psi}_1; \bar{\psi}_2; ...; \bar{\psi}_N]$.

The RCS is the property of a scattering target that is included in the radar equation to represent the magnitude of the echo signal returned to the radar by the target. As a result, the RCS returned to the receiving sensor by the target is assumed to have isotropic reflectivity modeled by zero-mean, unit-variance, independent and identically distributed (i.i.d.) Gaussian complex random variables λ_n. Assuming that it is the slow fading system, where the amplitude and phase change imposed by the channel can be considered roughly constant over the period of use, we suppose that the Rayleigh distortion does not fluctuate during the whole pulse burst. The RCS can be modeled by the diagonal matrix

$$\Sigma = \frac{1}{\sqrt{2N}} \begin{bmatrix} \lambda_1 & 0 & \cdots & 0 \\ 0 & \lambda_3 & \ddots & \vdots \\ \vdots & \ddots & \ddots & 0 \\ 0 & ... & 0 & \lambda_N \end{bmatrix} \tag{10.2}$$

where the normalization factor makes the target average RCS= $\frac{\sum_{n=1}^{N}|\lambda_n|^2}{2N} = 1$ independent of the number of transmit sensors in the model. A popular method for representing the fluctuations of targets are the four statistical models described by Swerling in [107]. The nonfluctuating target modeled using non-zero constants for $\lambda_n = \lambda$ is identified as $'Swerling\ 0'$ or $'Swerling\ 5'$ model. For the fluctuating target, if $|\lambda_n|$ is drawn from the Rayleigh P.D.F. and varies independently from path to path, the target model represents a classical $'Swerling\ 2'$ model.

Taken all the above parameters into account, we use the following block diagram illustrating as Fig. 10.1 to show our basic model.

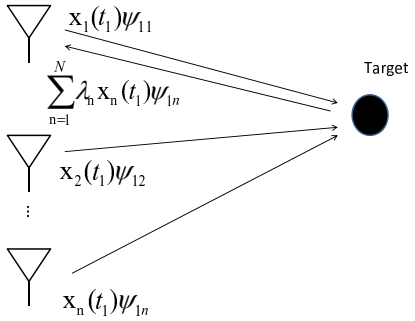

Figure 10.1. The block diagram of the model.

A vector form of the received signal including the useful signal and the system noise is $\bar{r}$ and we will process with this $\bar{r}$ in the following section

$$
\begin{aligned}
\bar{r} &= \mathrm{diag}(\Psi\Sigma X^T) + \overline{n} \qquad (10.3)\\
&= \frac{1}{\sqrt{2N}}\mathrm{diag}(\begin{bmatrix} \psi_{1,1} & \psi_{1,2} & \cdots & \psi_{1,N} \\ \psi_{2,1} & \psi_{2,2} & \cdots & \psi_{2,N} \\ \vdots & \vdots & \ddots & \vdots \\ \psi_{I,1} & \psi_{I,2} & ... & \psi_{I,N} \end{bmatrix} \cdot \begin{bmatrix} \lambda_1 & 0 & \cdots & 0 \\ 0 & \lambda_2 & \ddots & \vdots \\ \vdots & \ddots & \ddots & 0 \\ 0 & ... & 0 & \lambda_N \end{bmatrix} \cdot \\
&\quad \begin{bmatrix} x_1(t_1) & x_1(t_2) & \cdots & x_1(t_I) \\ x_2(t_1) & x_2(y_2) & \cdots & x_2(t_I) \\ \vdots & \vdots & \ddots & \vdots \\ x_N(t_1) & x_N(t_2) & \cdots & x_N(t_I) \end{bmatrix}) \\
&\quad +\overline{n} \\
&= \frac{1}{\sqrt{2N}} \left[\sum_{n=1}^{N} \lambda_n x_n(t_1)\psi_{1,n}, \sum_{n=1}^{N} \lambda_n x_n(t_2)\psi_{2,n}, ..., \sum_{n=1}^{N} \lambda_n x_n(t_I)\psi_{I,n} \right]^T + \overline{n} \\
&= \frac{1}{\sqrt{2N}} \left[\sum_{n=1}^{N} \lambda_n x_n\psi_{1,n}, \sum_{n=1}^{N} \lambda_n x_n\psi_{2,n}, ..., \sum_{n=1}^{N} \lambda_n x_n\psi_{I,n} \right]^T + \overline{n}
\end{aligned}
$$

where $\overline{n}$ is the noise vector. Here, the transmitted information bits are always known and the pulse compression technique is used, it is assumed that $x_n(t_1 = x_n(t_2 = ... = x_n(t_I = x_n$.

10.2.2 Decomposition and Recovery of the Signal

In order to obtain some benefit form CS, we choose the same orthogonal basis $\bar{\psi}_n$ as the sparse matrix Ψ to study the received signal $\bar{r}$ including the useful signal and the noise, where

$$\bar{r} = \sum_{n=1}^{N} \theta_n \bar{\psi}_n = \Psi\bar{\theta} \qquad (10.4)$$

with $\bar{\theta} = [\theta_1, ..., \theta_N]^T = [< \bar{r}, \bar{\psi}_1 >, ..., < \bar{r}, \bar{\psi}_N >]^T$. The CS can only work when there are K non-zero coefficients in the vector $\bar{\theta}$, where $K < I$. There should be only a few large coefficients and many small ones in $\bar{\theta}$.

The CS approach uses a set of measurement probes $\{\bar{\varphi}_m = [\varphi_{1,m}, \varphi_{2,m}, ..., \varphi_{I,m}]^T\}_{m=1}^{M}$ where M is significantly less than the dimensionality I of each individual probe (I is just the size of receive signal $\bar{r}$ in our case). In a different way, we would like to recover all the I coefficients of $\bar{r}$ by observing or measuring a subset M of these

$$y_m =< \bar{r}, \bar{\varphi}_m >, \forall m \in M \tag{10.5}$$

where $\mathbf{Y} = [y_1, y_2, ..., y_M]^T$, $M \subset 1, ..., I$. Since random matrix Φ with independent identically distributed (i.i.d.) entries, e.g., Gaussian or binary entries, exhibit a very low coherence with any fixed sparse matrix Ψ [53], we take the Gaussian matrix as the measurement matrix.

The recovery of $\bar{r}$ is done by solving a constrained l_1-norm minimization problem and the reconstructed $\bar{r}^*$ is given by $\bar{r}^* = \Psi\bar{\theta}^*$ where $\bar{\theta}^*$ is the solution to the convex optimization program

$$\min_{\bar{\theta}^* \in R^I} ||\bar{\theta}^*||_{l_1} \quad \text{subject to} \quad y_m =< \bar{\varphi}_m, \Psi\bar{\theta}^* >, \forall m \in M \tag{10.6}$$

We choose the solution whose coefficient sequence has the minimal l_1 norm.

We describe how our model recovers a particular $\bar{r}^*$ in Table 10.1. We first produce the transmit signal and receive it as $\overline{r}$. Then, we compute $\mathbf{Y}$ by compressing the received signal $\overline{r}$. Finally, we use the l_1 minimization with relaxed constraints to reconstruct the original signal $\bar{r}^*$.

Table 10.1. The Basic Model

Input: Φ, Ψ, Σ, X
$\bar{r} \leftarrow \bar{r} = \text{diag}(\Psi \Sigma X^T)$
$\mathbf{Y} \leftarrow y_m =< \bar{\varphi}_m, \Psi\bar{\theta} >$, for all $m \in M$
$\bar{\theta}^* \leftarrow \min_{\bar{\theta}^* \in R^I} \|\|\bar{\theta}^*\|\|_{l_1}$, subject to $\|\|\Phi^T \Psi \bar{\theta}^* - y_m\|\|_{l_2} \leq \epsilon$
Output:$\bar{r}^* = \Psi\bar{\theta}^*$

We explicitly tie together the parameters for the decompressive process, i.e.,

$$\mathbf{Y} = \Phi^T \bar{r}^* = \Phi^T \Psi \bar{\theta}^* = A\bar{\theta}^* \tag{10.7}$$

One of the important properties that $A = \Phi^T \Psi$ should satisfy is the Restricted Isometry Property (RIP) [60]. A sufficient condition for the RIP is that the measurement vectors and the sparsity basis must be incoherent with each other. The coherence between the measurement matrix Φ and the sparsity basis Ψ here is defined as

$$\mu(\Phi, \Psi) = \max_{1 \leq m \leq M, 1 \leq n \leq N} | < \varphi_m, \psi_n > | \tag{10.8}$$

If Φ and Ψ contain uncorrelated elements, the coherence is large. So the 'incoherency' here means that the inner products between the probes and the sparsity basis vectors are small, or, in other words, μ is small.

In this dissertation, we express the SF coefficients in the method of Fourier basis as the sparse matrix

$$\bar{\psi}_n = [e^{j2\pi \frac{n}{I} t_1}, e^{j2\pi \frac{2n}{I} t_2}, ..., e^{j2\pi \frac{nI}{I} t_I}]^T = [\psi_{1n}, \psi_{2n}, ..., \psi_{In}]^T \tag{10.9}$$

Here, the sparse matrix can be non-squared, i.e., the number of rows can be different from the number of columns in the sparse matrix. The number of rows is based on the number of transmit sensors N and the number of columns depends on the number of time samples I. The reason why we can use such a non-squared matrix is that we use the same sparse matrix to produce the 'compressible' transmit signal. In addition, the random waveforms $\varphi_m(t)$ with independent identically distributed (i.i.d) vectors are largely incoherent with the fixed basis Ψ. Hence, we choose the complex Gaussian random vectors as the measurement matrix in our work.

10.2.3 The Output of the Matched Filter

Different from previous CS-based radar system, we proposed a totally new model for CS-based RSN. Since we use the matched filters in the receiving sensor, let us assume that the received signal could be well recovered as $\bar{r}^*$

$$\bar{r}^* = \bar{r} \;=\; \frac{1}{\sqrt{2N}}\left[\sum_{n=1}^{N}\lambda_n x_n(t_1)\psi_{1,n}, \sum_{n=1}^{N}\lambda_n x_n(t_2)\psi_{2,n}, ..., \sum_{n=1}^{N}\lambda_n x_n(t_I)\psi_{I,n}\right]^T + \overline{n}'$$

where $\overline{n}' = [n'_1, n'_2, ..., n'_I]^T$ is the noise vector. Actually, the noise $\overline{n}'$ in the recoverd signal is less than the system noise in the received signal in equation (10.4). Since the $\overline{n}$ may not have good sparsity property in the basis Φ, some information of $\overline{n}$ could not be exactly recovered by $\overline{n}'$ Here, we choose the matched filters corresponding to the transmit signal $S = \Psi X^T$. Processing by a bank of matched filters, we express the output of the matched filter as the following matrix operations

$$\begin{aligned}
\bar{Z} \;=\; & \begin{bmatrix} x_1^*(t_1)\psi_{1,1}^* & x_1^*(t_2)\psi_{2,1}^* & \cdots & x_1^*(t_I)\psi_{I,1}^* \\ x_2^*(t_1)\psi_{1,2}^* & x_2^*(t_2)\psi_{2,2}^* & \cdots & x_2^*(t_I)\psi_{I,2}^* \\ \vdots & \vdots & \ddots & \vdots \\ x_N^*(t_1)\psi_{1,N}^* & x_N^*(t_2)\psi_{2,N}^* & ... & x_2^*(t_I)\psi_{I,N}^* \end{bmatrix} \\
& \cdot\frac{1}{\sqrt{2N}}\begin{bmatrix} \sum_{n=1}^{N}\lambda_n x_n(t_1)\psi_{1,n} + \sqrt{2N}n_1 \\ \sum_{n=1}^{N}\lambda_n x_n(t_2)\psi_{2,n} + \sqrt{2N}n_2 \\ \vdots \\ \sum_{n=1}^{N}\lambda_n x_n(t_I)\psi_{I,n} + \sqrt{2N}n_I \end{bmatrix} \\
=\; & \frac{1}{\sqrt{2N}}\left[\sum_{n=1}^{N}\lambda_n\left[\sum_{i}^{I}x_n(t_i)\psi_{i,n}x_1^*(t_i)\psi_{i,1}^*\right] + n'_1\right., \\
& \sum_{n=1}^{N}\lambda_n\left[\sum_{i}^{I}x_n(t_i)\psi_{i,n}x_2^*(t_i)\psi_{i,2}^*\right] + n'_2, ..., \\
& \left.\sum_{n=1}^{N}\lambda_n\left[\sum_{i}^{I}x_n(t_i)\psi_{i,n}x_N^*(t_i)\psi_{i,N}^*\right] + n'_N\right]^T
\end{aligned} \tag{10.10}$$

Since Ψ is the Fourier basis in this dissertation, and X is information bits expressed as pulsed signals, it is easy to obtain that

$$\sum_{i}^{I} x_n(t_i)\psi_{i,n}x_k^*(t_i)\psi_{i,k}^* = \begin{cases} E, & n = k \\ 0, & \text{Otherwise} \end{cases} \tag{10.11}$$

Where E is the energy of the burst of pulses. Therefore,

$$\bar{Z} = \frac{1}{\sqrt{2N}}[\lambda_1 E + n_1', \lambda_2 E + n_2', ..., \lambda_N E + n_N']^T \tag{10.12}$$

Where λ_n is the radar cross section for n-th transmit sensor. According to the equation (10.12), all the N radar cross section parameters could be taken into account to detect or recognize the target, so that the diversity gain of transmit side can be obtained as well.

10.3 Increased Range Resolution

The range resolution improvement is one of the important properties of the linear Stepped-Frequency waveforms (LSFWs). The details of the Doppler response and range resolution can be expressed by the Ambiguity Function (AF) of the LSFW [94]. The AF is defined as

$$\widehat{A}(\tau, \upsilon) \equiv |\chi(\tau, \upsilon)| = |\int_{-\infty}^{\infty} u(t)u^*(t+\tau)exp(j2\pi\upsilon t)dt| \tag{10.13}$$

We designate the complex envelope of the Stepped-Frequency pulse train by $u(t)$ given by

$$u(t) = \sum_{m=0}^{M-1} u_1(t - mT_p)e^{j2\pi m\Delta F(t-mT_p)} \tag{10.14}$$

where $u_1(t)$ is a radar pulse waveform. Fig. 10.2 presents a sample AF of a Stepped-Frequency train of unmodulated pulses calculated by using the MATLAB tool.

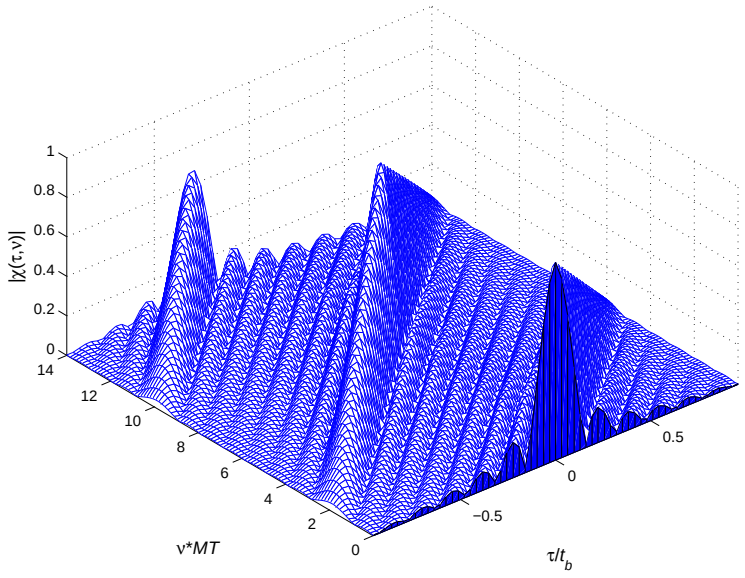

Figure 10.2. Ambiguity function of Stepped-Frequency train of unmodulated pulses.

It is obvious to see that the range resolution of the signal is improved, but there are still prominent sidelobes in delay and ambiguity in Doppler. As a result, LFMs and Stepped-Frequency can be combined to mitigate the raging lobes, i.e. , Stepped-Frequency train of LFM pulses could be used. An example of Stepped-Frequency train of LFM is shown in Fig. 10.3.

We compare the AF of a Stepped-Frequency train of LFM pulses, as shown in Fig. 10.3, with the AF of a Stepped-Frequency train of unmodulated pulses as seen in Fig. 10.2. Clearly, by adding the LFM, the range and the Doppler resolutions are improved by canceling the sidelobes along the delay and Doppler axes. As a result, we choose to use the Stepped-Frequency train of LFM pulses as the transmit waveforms in our model to obtain both the range and Doppler resolution gain.

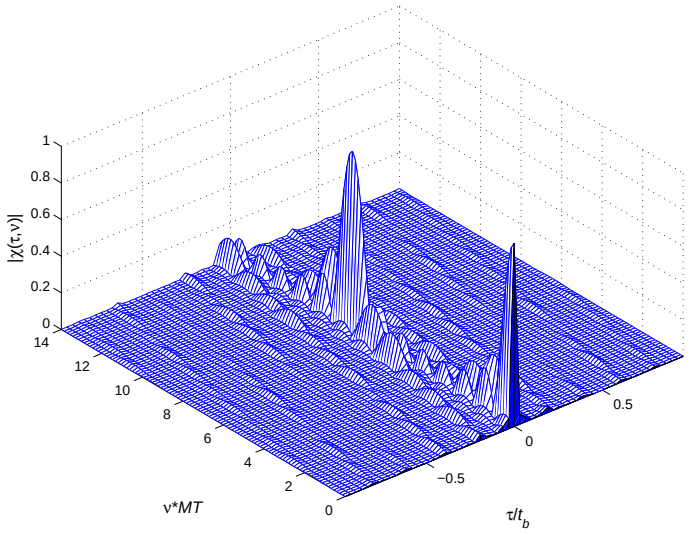

Figure 10.3. Ambiguity function of Stepped-Frequency train of LFM.

10.4 Target RCS Value Estimation

In this section, we use the maximum-likelihood (ML) estimation algorithm to perform target radar cross section (RCS) parameter estimation [108] in the proposed RSN model. For the 'Swerling 2' model, the RCS voltage $|\lambda(u)|$ follows a Rayleigh distribution and the I and Q subchannels of $\lambda(u)$ follow zero-mean complex Gaussian distribution with a variance γ^2 (the RCS average power value)

$$\lambda(u) = \lambda_I(u) + j\lambda_Q(u) \tag{10.15}$$

In addition, $n(u) = n_I(u) + jn_Q(u)$ follows a zero-mean complex Gaussian distribution with a variance σ^2 for each I and Q subchannel. We express equation (10.12) as following

$$\bar{Z}(u) \quad = \quad [\lambda_1(u)E + n'_1(u), \lambda_2(u)E + n'_2(u), ..., \lambda_N(u)E + n'_N(u)]^T \tag{10.16}$$

Here, we let

$$|Z_n(u)| = |\lambda_n(u)E + n'_n(u)| \tag{10.17}$$

Since $\lambda_n(u)$ and $n'_n(u)$ are zero-mean complex Gaussian random variables, $\lambda_n(u) + n'_n(u)$ is zero-mean complex Gaussian random variable with a variance $E^2\gamma^2 + \sigma^2$.

Assuming that $y_n \cong |Z_n(u)|$ follows a Rayleigh distribution:

$$f(y_n) = \frac{y_n}{E^2\gamma^2 + \sigma^2} \exp\left[-\frac{y_n^2}{2(E^2\gamma^2 + \sigma^2)}\right] \tag{10.18}$$

Let $\mathbf{y} = |\bar{Z}(u)|$, $|\bar{Z}(u)| = [|Z_1(u)|, |Z_2(u)|, ..., |Z_N(u)|]$ and $y_n = |Z_n(u)|$, we can obtain that $\mathbf{y} \cong [y_1, y_2, ..., y_N]$. Assuming that y_n are independent of each other, then the P.D.F. of $\mathbf{y}$ is

$$f(\mathbf{y}) = \prod_n^N f(y_n) = \prod_n^N \frac{y_n}{E^2\gamma^2 + \sigma^2} \exp\left[-\frac{y_n^2}{2(E^2\gamma^2 + \sigma^2)}\right] \tag{10.19}$$

If $\theta \cong \gamma^2$, we can express (10.18) as

$$f(y_n) = \frac{y_n}{E^2\theta + \sigma^2} \exp\left[-\frac{y_n^2}{2(E^2\theta + \sigma^2)}\right] \tag{10.20}$$

Therefore, we represent the ML algorithm to estimate the RCS average value θ as

$$\begin{aligned} \widehat{\theta}_{ML}(\mathbf{y}) &= \arg\sup_{\theta \in R^+} f(\mathbf{y}) \\ &= \arg\sup_{\theta \in R^+} \prod_n^N \frac{y_n}{E^2\theta + \sigma^2} \exp\left[-\frac{y_n^2}{2(E^2\theta + \sigma^2)}\right] \end{aligned} \tag{10.21}$$

It is equivalent to maximize $\log f(\mathbf{y})$ (natural logarithm),

$$\log f(\mathbf{y}) = \sum_{n=1}^N \left[\log(\frac{y_n}{E^2\theta + \sigma^2}) - \frac{y_n^2}{2(E^2\theta + \sigma^2)}\right] \tag{10.22}$$

It is a continuous function for $y_n > 0$ and $\theta > 0$, hence, a necessary condition for the ML estimation is

$$\begin{aligned} &\frac{\partial}{\partial\theta} \log f(\mathbf{y})|_{\theta=\widehat{\theta}_{ML}(\mathbf{y})} \\ = \;& \frac{E^2(\sum_{n=1}^N y_n^2 - 2N(E^2\theta + \sigma^2))}{2(E^2\theta + \sigma^2)^2} = 0 \end{aligned} \tag{10.23}$$

Equation (10.24) has the unique solution

$$\widehat{\theta}_{ML}(\mathbf{y}) = \frac{1}{E^2}\left(\frac{\sum_{n=1}^{N} y_n^2}{2N} - \sigma^2\right) \tag{10.24}$$

Since $\theta > 0$,

$$\widehat{\theta}_{ML}(\mathbf{y}) = \max\left[\frac{1}{E^2}(\frac{\sum_{n=1}^{N} y_n^2}{2N} - \sigma^2), 0\right] \tag{10.25}$$

Since

$$\begin{aligned}\frac{\partial^2}{\partial\theta^2}\log f(\mathbf{y})|_{\theta=\widehat{\theta}_{ML}(\mathbf{y})} &= E^4\left(\frac{N}{(E^2\theta+\sigma^2)^2} - \frac{\sum_{n=1}^{N} y_n^2}{(E^2\theta+\sigma^2)^3}\right) \\ &= -\frac{4E^4N^3}{(\sum_{n=1}^{N} y_n^2)^2} \\ &< 0 \end{aligned} \tag{10.26}$$

this solution gives the unique maximum of $\log f(\mathbf{y})$. The expectation of $\widehat{\theta}_{ML}(\mathbf{y})$ is then

$$E_\theta\left[\widehat{\theta}_{ML}(\mathbf{y})\right] = E_\theta\left[\frac{\sum_{n=1}^{N} y_n^2}{2NE^2}\right] - \frac{\sigma^2}{E^2} \tag{10.27}$$

The mean value of y_n is $\sqrt{\pi(E^2\theta+\sigma^2)/2}$, and its variance is $(4-\pi)(E^2\theta+\sigma^2)/2$. Since y_n are independent of each other, it is

$$E_\theta(y_n^2) = 2(E^2\theta+\sigma^2) \tag{10.28}$$

Therefore,

$$\begin{aligned} E_\theta[\widehat{\theta}_{ML}(\mathbf{y})] &= \frac{E_\theta[y_n^2]}{2E^2} - \frac{\sigma^2}{E^2} \\ &= \frac{2(E^2\theta+\sigma^2)}{2E^2} - \frac{\sigma^2}{E^2} \\ &= \theta \end{aligned} \tag{10.29}$$

As a result, it is an unbiased estimator.

Fisher's information [109] in this case can be obtained as

$$\begin{aligned} I_\theta &= -E_\theta \left[\frac{\partial^2}{\partial \theta^2} \log f(\mathbf{y}) \right] \\ &= -E_\theta \left[\frac{N(E^2\theta + \sigma^2) - \sum_{n=1}^{N} y_n^2}{(E^2\theta + \sigma^2)^3} \right] \\ &= \frac{E^4 N}{(E^2\theta + \sigma^2)^3} \left(E_\theta(y_n^2) - (E^2\theta + \sigma^2) \right) \\ &= \frac{E^4 N}{(E^2\theta + \sigma^2)^2}. \end{aligned} \tag{10.30}$$

Taking equation(10.28) into account, we can obtain the Cramer-Rao lower bound (CRLB) [109]

$$\mathrm{Var}_\theta[\widehat{\theta}(\mathbf{y})] \geq \frac{1}{I_\theta} = \frac{(E^2\theta + \sigma^2)^2}{E^4 N} \tag{10.31}$$

From (10.31), we observe that CRLB is inversely proportional to the number of radars N in the RSN, which means that the RSN with large N will have a low CRLB. We draw this conclusion by assuming that the radar pulses are independent (in time and space) and follow a Rayleigh distribution, according to the 'Swerling 2' model.

10.5 Simulation Results

10.5.1 Signal Recovery

In this section, we study the scenario where we have N transmit sensors but only one receiving sensor. We assume that the number of samples is set to 500. We apply the Stepped-Frequency train of LFM pulses as pulse compression codes on the transmit side and use the CS technique in the receiving side. The classical 'Swerling model 2' and Gaussian noise are also considered in the simulation. The reconstructed signal is compared with the original signal by calculating the mean square error (MSE) in order to evaluate the reconstruction ability. The Mean Square Error between the original signal and the reconstructed signal is shown in Figs. 4 and 5 as a function of

different number of measurements M and SNR values. The noise considered here is introduced by the propagation in the air but not by compressing and decompressing process. We use the Monte-Carlo simulation model here and the results are averaged by 10^5 runs/iterations. The cases of $N = 50$ and $N = 100$ where N is the number of transmit sensors are illustrated in Fig. 10.4 and Fig. 10.5 separately.

According to both Figs. 10.4(a) and 10.5(a), MSE is reduced as the number of measurements M is increased. The system can perfectly reconstruct the signal which includes the received signal and the system noise when the number of measurements M is equal to the number of transmit sensors N. In addition, the slope of MSE versus the number of measurements M is almost a consistent for each SNR value. From Figs. 10.4(b) and 10.5(b), we draw the same conclusion that the closer the number of measurements approaches N ($M \leq N$), the better performance of signal recovery is achieved. In addition, we also discover that the MSE does not depend much on the SNR, especially when M is large. As a result, the proposed model can be used under a low SNR if the number of measurements M could be properly chosen according to the number of transmit sensors N.

On the basis of the simulation results, we can draw a brief conclusion that the number of measurements M of our model only depends on the size of RSN even when the number of samples is fixed as large as 500 here. Another important result emerging from the simulations is that the probability of target miss detection is zero no matter how small a number of measurements we use in the recovery process. That is to say, less measurements can be used to detect the target in the system, since a kind of diversity gain is achieved at the output of the matched filters on the receiving sensors.

10.5.2 RCS Parameter Estimation

In this section, we will consider the fluctuating target with an RCS parameter θ (following Rayleigh distribution). We will apply the ML estimation algorithm to estimate the parameter $\widehat{\theta}$. The scenario is similar to the one in the section above, but the number of samples in time domain is reduced to 100 for complexity reasons. We ran Monte Carlo simulations for 10^5 iterations at each SNR value. We have considered the fluctuating target with RCS parameter $\theta = 2$ (Small flighter aircraft or 4 passenger jet) in Fig. 10.6. We plotted the variance of the RCS ML estimator with different number of radars in RSN.

According to Fig. 10.6, the variance of $\widehat{\theta}$ closely approaches the CRLB but doesn't exactly match it. The reason why the variance of $\widehat{\theta}$ is not exactly the same as the CRLB is that the noise power is to some extent increased after processing with the matched filters. We take the noise power in the transmitting signal into account directly, therefore, the value of noise power used in the simulation is not exactly the same as σ^2 in equations 10.27 and 10.31. The power of noise σ^2 reduces so that the calculated CRLB might be lower than the practical CRLB and the obtained variance of $\widehat{\theta}$ becomes larger than the accurate $\widehat{\theta}$. It is also easy to see that the actual variance of $\widehat{\theta}$ reduces as the number of radars increases from $N = 10$ to $N = 20$. Hence, the actual variance of $\widehat{\theta}$ is inversely proportional to N, as we have shown in the theoretical result $\mathrm{Var}_\theta[\widehat{\theta}(\mathbf{y})] \geq \frac{(E^2\theta+\sigma^2)^2}{E^4 N}$.

It is easy to see that the actual variance of $\widehat{\theta}$ and the CRLB do not change much as the SNR increases. Stating differently, our ML estimator performs well even for low SNR ratios. In all, the simulation results validate the theoretical results. The variance of the RCS parameter estimation satisfies the CRLB and our ML estimator on the RCS parameter is an accurate estimator.

10.6 Conclusions

Motivated by the representation of Stepped-Frequency waveforms, we introduced CS to the Radar Sensor Network (RSN) exploiting the pulse compression technique. A set of Stepped-Frequency waveforms were applied as pulse compression codes at the transmit sensors, and the sparse matrix is also constructed based on the same Stepped-Frequency waveforms. We observed that the signal samples along the time domain can be significantly compressed and recovered by using a small number of measurements which depend on the number of transmit sensors. A diversity gain is also achieved after the matched filters in the proposed model, so the probability of target miss detection can be zero even if the signal could not be perfectly recovered. In addition, we propose a ML algorithm to estimate the target RCS parameter and use the CRLB to successfully verify our theoretical result.

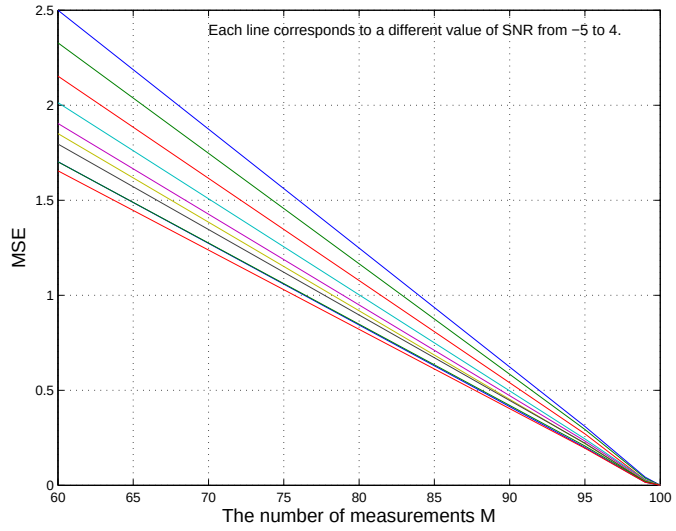

(a)

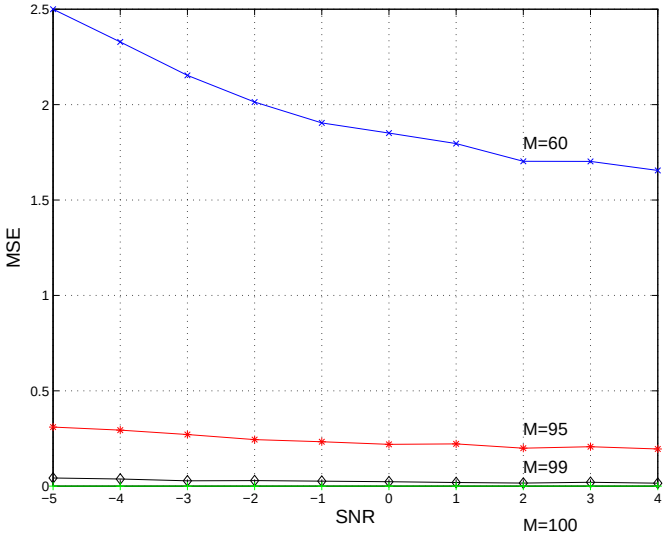

(b)

Figure 10.4. Normalized MSE between reconstructed signal and original signal for fixed $N = 100$: (a) Normalized MSE versus M; (b) Normalized MSE versus SNR.

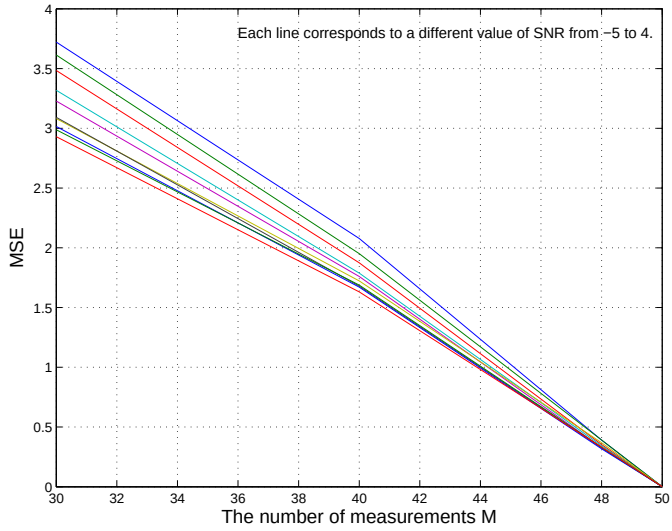

(a)

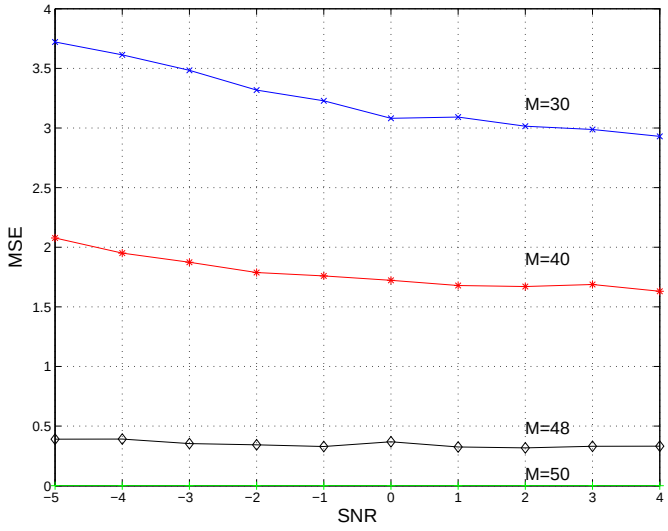

(b)

Figure 10.5. Normalized MSE between reconstructed signal and original signal for fixed $N = 50$: (a) Normalized MSE versus M; (b) Normalized MSE versus SNR.

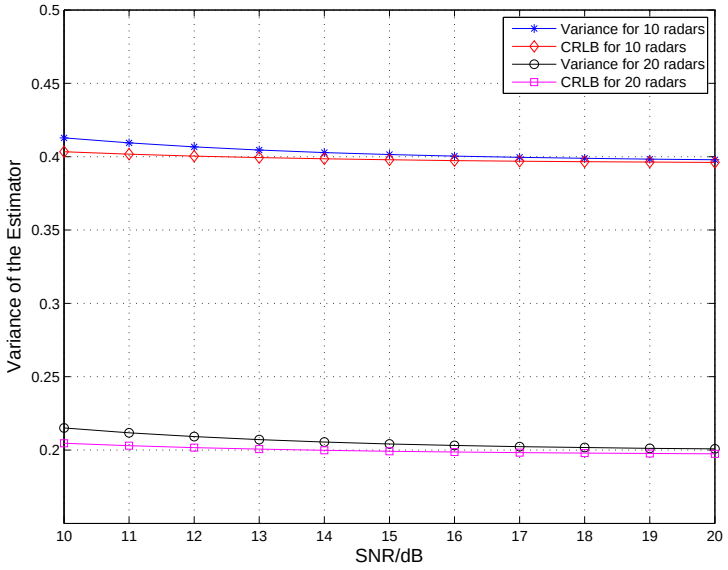

Figure 10.6. Variance of RCS ML estimator with different number of radars in RSN (The actual RCS parameter $\theta = 2$).

CHAPTER 11

CONCLUSIONS

This chapter concludes the whole dissertation. It begins with a summary of the dissertation results and contributions, follows with a discussion of future research directions in further investigation of Compressive Sensing.

11.1 Summary

This dissertation has focused on but not limited to signal processing in radar sensor network. The main work is of the waveform design problem . The contributions of this dissertation are:

- *Optimized Punctured Sequence-Pair Sets and Three Constructing Methods* (Chapter 2 and 3): based on the Zero Correlation Zone concept, we introduced the Optimized Binary Sequence-pair which has high autocorrelation peak and zero autocorrelation sidelobe. Based on the ideal autocorrelation property of the Optimized Binary Sequence-pair, we present and study the Optimized Punctured Binary Sequence-pairs, the LCZ/ZCZ Sequence-pair Sets and the Optimized Punctured LCZ/ZCZ Sequence-pair Sets. We have presented three methods to construct the Optimized Punctured LCZ/ZCZ Sequence-pair sets: using the odd length Optimized Punctured Binary Sequence-pair together with Hadamard matrix to construct an Optimized Punctured ZCZ Sequence-pair set; using the even length Optimized Punctured Binary Sequence-pair together with modified Hadamard matrix to construct an approximately Optimized Punctured LCZ Sequence-pair set and using any length Optimized Punctured Binary Sequence-

pair together with Orthogonal matrix to construct an Optimized Punctured ZCZ Sequence-pair set. According to the property analysis of sample sequence-pair sets constructed by each method, the Optimized Punctured ZCZ Sequence-pair set constructed by the first method have zero autocorrelation sidelobes during the ZCZ but zero cross correlation values during the whole time domain, the approximately Optimized Punctured LCZ Sequence-pair set using the second method have zero autocorrelation sidelobes during the LCZ, a low cross correlation peak value and zero cross correlation sidelobe during the LCZ, and the Optimized Punctured ZCZ Sequence-pair set constructed by the last method have zero autocorrelation sidelobes and zero cross correlation values during the ZCZ. The ambiguity function is also used to study the sequence-pairs under the condition of time delay and Doppler shift. To sum up, these sequence-pair sets, which possess both the good cross correlation between different sequence-pairs of the set and the ideal autocorrelation property of each sequence-pair, could be potent candidates for set of best signals.

- *Radar System Using Optimized Punctured Sequence-pair* (Chapter 4): the significant advantage of the optimized punctured sequence-pair is the considerably reducedn autocorrelation sidelobe. According to the simulation results, the new code can provide better performances than the Barker and P4 codes of corresponding length and be a good alternative for the current used pulse compression codes in radar system.
- *Radar Sensor Network Using Optimized Punctured Sequence-Pair Sets* (Chapter 5): we have studied the phase coded waveforms design for the radar sensor networks (RSN). We provide a new ternary codes–the optimized punctured ZCZPS which could be used as the phase coded waveforms in a RSN. The significant advantage of the optimized punctured ZCZPS is the considerably re-

duced sidelobe as low as zero and zero mutual cross correlation value in the zero correlation zone (ZCZ). Based on the ideal orthogonal property of the proposed codes, they can coexist in the RSN and achieve better detection performance than that of a RSN using other orthogonal codes such as the Gold codes. Consequently, the optimized punctured ZCZPS could be effectively applied to RSN in order to satisfy higher demands criterion for detection accuracy of the RSN in the modern military and security affairs.

- *Sonar Sensor Network Using Optimized Punctured Sequence-Pair Sets* (Chapter 6): we investigate the definition and properties of optimized punctured ZCZPS constructed by one of the three constructing methods. The significant advantage of the optimized punctured ZCZ sequence-pair set is a considerably reduced autocorrelation sidelobe as low as zero and zero mutual cross correlation value within ZCZ. The results show that applying our optimized punctured ZCZPS as a bank of phase coded waveforms to the SSN can effectively satisfy higher demands criterion for detection accuracy in modern military and security affairs.
- *MIMO Radar Sensor Network Using Optimized Punctured Sequence-Pair Sets* (Chapter 7): we present and analyze two MIMO radar system models, in which Beamforming is used to find the direction of the target at receive part. We also apply the proposed codes to the above MIMO radar systems to improve the radar range resolution and direction finding performance. The MIMO radar ambiguity function of the system within phase coded waveforms are investigated and used to study the properties of our proposed codes. Simulation results showed that significant diversity gain could be obtained in both MIMO radar systems using orthogonal phase coded waveforms. In the first MIMO radar system model, the more antennas applied, the better performance obtained only if there are equal number of transmit antennas and receive antennas. In

addition, the direction finding performance could be improved by increasing the number of either transmit antennas or receive antennas for the second MIMO radar system model.

- *Radar Sensor Network from Information Theory Perspective* (Chapter 8): we studied the waveforms design for the measurement of extended radar targets in radar sensor networks (RSN) in the view of information theory. Considering the effect of different channel gains, we investigated the estimation waveforms that maximize the mutual information between a target ensemble and the received signal within additive Gaussian noise given the transmitting signals so that characteristics of the target could be well recgonized. From the study of the maximum mutual information under the constraints of the number of radar sensors, waveform energy and duration, which could be taken into consideration when waveforms are designed for RSN, some useful conclusions for waveforms design in RSN could be drawn. If the channel could be well estimated, the transmitter could allocate more power to the stronger channel to gain better performance. Considering the factors such as the number of radars in RSN N, the signal duration T, and average power P_x, and their relations the corresponding maximum mutual information as a function of them could be used.
- *Compressive Sensing Using Singular Value Decomposition (SVD)* (Chapter 9): motivated by the concept of SVD, we provide a new CS technique-the CS-SVD algorithm in this paper. We propose two methods to implement the CS-SVD algorithm. The theoretical results show that the CS-SVD algorithm requires less measurements than the standard state-of-art compressive sensing techniques and provide a simpler and more efficient recovery scheme. The simulation results demonstrate that both of our two methods provide considerable gains over

convex relaxation algorithm in terms of number of measurements required for stable recovery. And each of them could work well in different cases in which different original signal could be sparsely represented in different sparse basis.

- *Compressive Sensing in Radar Sensor Network* (Chapter 10): motivated by the representation of Stepped-Frequency waveforms, we introduced CS to the Radar Sensor Network (RSN) exploiting the pulse compression technique. A set of Stepped-Frequency waveforms were applied as pulse compression codes at the transmit sensors, and the sparse matrix is also constructed based on the same Stepped-Frequency waveforms. We observed that the signal samples along the time domain can be significantly compressed and recovered by using a small number of measurements which depend on the number of transmit sensors. A diversity gain is also achieved after the matched filters in the proposed model, so the probability of target miss detection can be zero even if the signal could not be perfectly recovered. In addition, we propose a ML algorithm to estimate the target RCS parameter and use the CRLB to successfully verify our theoretical result.

11.2 Future Directions

11.2.1 Extending Compressive Sensing using SVD

In chapter 9, we provided a new CS technique-the CS-SVD algorithm and proposes two methods to implement the CS-SVD algorithm. Both of the theoretical and simulation results show that the CS-SVD algorithm requires less measurements than the standard state-of-art compressive sensing techniques and provide a simpler and more efficient recovery scheme. However, after the original signal has been projected to the sparse matrix, the nonzero values of the sparsed vector have to be continuously

allocated among the beginning part of the vector to comfier the efficiency of the propose algorithm. Due to this restriction, two methods might be taken into account. Firstly, we could further study how to choose the sparse basis and measurements matrix in our scheme, since the sparse representation of the signal has a great effect on the performance of the proposed scheme. Secondly, Compressive Sampling Matching Pursuit (CoSaMP) could be investigated and introduced to CS-SVD so that priory information of positions of non-zero values of sparsed vector could be provided to help improve the restrictions of CS-SVD algorithm.

11.2.2 Compressive Sensing in SAR (Synthetic Aperture Radar)

Synthetic Aperture Radar (SAR) is an active ground imaging system based on coherent processing of multiple radar echoes acquired along the path of a moving platform (aircraft or satellite). Due to the low computational resources of the acquisition platforms and the steadily increasing resolution of SAR systems, the data cannot generally be processed on board and must be stored or transmitted to the ground where the image formation process is performed. The amount of image data produced is now constrained by on board storage capabilities and transmission links.

To address this problem, many techniques have been proposed to compress the raw SAR data [110][111][112]. However, SAR systems in practice mostly use the simplest methods because of their low computational requirements. In this context, an appealing idea is to apply results of the rapidly developing field of compressed sensing. The key idea of compressed sensing is to exploit redundancy in the data modeled as sparsity in an appropriate dictionary.

In the future work, we would like to exploit our study in two directions.

Firstly, in the spotlight mode, SAR data is acquired from a moving platform by emitting at close intervals a bandpass microwave radar signal in direction of a

specific area, or scene, and sampling the signal backscattered by the ground objects. Based on this simple interpretation of SAR data in the Fourier domain (2D Fourier transform of the scene), we could use simulation data of SAR to study the application of compressive sensing matrix to SAR.

Secondly, we have obtained the practical SAR raw data of Greenland icesheet. We could study the redundancy in the SAR raw data modeled as sparsity in an appropriate dictionary to better compress SAR raw data.

APPENDIX A

PUBLICATIONS

[1] L. Xu and Q. Liang, "Zero correlation zone sequence pair sets for MIMO radar", accepted by *IEEE Trans. on Aero. and Elec. Systems.*

[2] L. Xu and Q. Liang, "Radar sensor network using a set of new ternary codes: theory and application", *IEEE Sensors Journal.* vol 11, No. 2, 2011, pp. 439-450.

[3] L. Xu, Q. Liang, X. Wu and B. Zhang, "Phase coded waveform design for sonar sensor network", selected to be included in *Special Issue of ACM/Springer Mobile Networks and Applications (MONET).*

[4] L. Xu and Q. Liang, "Optimized punctured ZCZ sequence-pair set: design, analysis and application to radar system", *EURASIP Journal on Wireless Communications and Networking*, Paper ID: 254837, vol. 2010.

[5] L. Xu, T. Jiang, Z. Zhou, "The research of perfect punctured binary sequence pair in LCZ/ZCZ", *Journal on Communications*, Vol.27, No.10, 2006.

[6] L. Xu and Q. Liang, "Waveform design and optimization in radar sensor network", *IEEE Global Communications Conference, exhibition & Industry Forum 2010 (IEEE Globecom '10)*, Miami, FL, Dec. 2010.

[7] L. Xu and Q. Liang, "Orthogonal pulse compression codes for MIMO radar system", *IEEE Global Communications Conference, exhibition & Industry Forum 2010 (IEEE Globecom '10)*, Miami, FL, Dec. 2010.

[8] L. Xu and Q. Liang, "Compressive sensing using singular value decomposition", *International Conference on Wireless Algorithms, Systems, and Applications 2010 (WASA '10)*, Beijing, China, Aug. 2010.

[9] L. Xu, Q. Liang, T. Jiang, "A ternary pulse compression code: design and application to radar system", *IEEE International Conference on Acoustic, Speech, and Signal Processing 2010 (ICASSP '10)*, Dallas, TX, Mar. 2010.

[10] L. Xu and Q. Liang, "A set of triphase coded waveforms: design and application to radar System", *IEEE Military Communications Conference 2009 (MILCOM '09)*, Boston, MA, Oct 2009.

[11] L. Xu and Q. Liang, "Radar sensor network using a new triphase coded waveform: theory and application", *IEEE International Conference on Communications 2009 (ICC '09)*, Dresden, Germany, Jun. 2009.

[12] L. Xu, Q. Liang, X. Wu and B. Zhang, "Phase coded waveform design for sonar sensor network", *International ICST Conference on Communications and Networking in China 2011 (Chinacom '11)*, Aug., 2011, Harbin, China.

[13] V. Bolar, Q. Liang, L. Xu, X. Wu and B. Zhang, "Performance Analysis of Multiple Antenna Systems within Different Techniques", *International ICST Conference on Communications and Networking in China 2011 (Chinacom '11)*, Aug., 2011, Harbin, China.

[14] T. Jiang, L. Xu, Z. Zhou, "The research on theory and application of the perfect punctured ZCZ sequence pair sets", *International Symposium on Communications and Information Technologies 2006 (ISCIT '06)*, Bangkok, Thailand, Oct. 2006.

[15] T. Jiang, Z. Li, L. Xu, Z. Zhou, "Research on construction of perfect punctured binary sequence pairs and its application in spread frequency telecommunication", *International Symposium on Communications and Information Technologies 2006 (ISCIT '06)*, Bangkok, Thailand, Oct. 2006.

[16] L. Xu and Q. Liang, "Compressive sensing in distributed radar sensor networks using pulse compression waveforms", submitted to *IEEE Trans. Parallel and Distributed Systems.*

[17] L. Xu and Q. Liang, "A triphase coded waveform: design, analysis and application to radar system", submitted to *IET radar sonar & navigation.*

[18] L. Xu and Q. Liang, "Compressive sensing in radar sensor networks for target RCS value estimation", submitted to *IEEE International Conference on Communications 2012 (ICC '12)*.

[19] L. Xu and Q. Liang, "Compressive sensing in radar sensor networks using pulse compression waveforms", submitted to *IEEE International Conference on Communications 2012 (ICC '12)*.

REFERENCES

[1] S. W. Golomb, "Two-valued sequences with perfect autocorrelation," *IEEE Trans. on Aero. and Elec. Systems*, vol. AES-28(2), pp. 382–386, Mar. 1992.

[2] V. P. Ipatov, "Periodic discrete signals with optimal correlation properties," *Radio I Svyaz, Moscow*, 1992.

[3] R. Sato and M. Shinrhu, "Simple mismatched filter for binary pulse compression code with small psl and small s/n loss [radar]," *IEEE Trans. on Aero. and Elec. Systems*, vol. AES-39(2), pp. 711–718, Apr. 2003.

[4] K. Sato, H. Horie, H. Hanado, and H. Kumagai, "A digital-analog hybrid technique for low range sidelobe pulse compression," *IEEE Trans. on Aero. and Elec. Systems*, vol. AES-39(7), pp. 1612–1615, Jul. 2001.

[5] A. Tanner, S. L. Durden, R. Denning, E. Im, F. K. Li, W. Ricketts, and W. Wilson, "Pulse compression with very low sidelobes in an airborne rain mapping radar," *IEEE Trans. on Aero. and Elec. Systems*, vol. AES-32(1), pp. 211–213, Jan. 2004.

[6] L. R. Welch, "Lower bounds on the maximum cross correlation of signals," *IEEE Trans. Inform. Theory*, vol. IT-20(3), pp. 397–399, 1974.

[7] V. M. Sidelnikov, "On mutual correlation of sequences," *Soviet Math doklady*, vol. 12, pp. 197–201, 1971.

[8] D. V. Sarwate and M. B. Pursley, "Crosscorrelation properties of pseudorandom and related sequences," in *Proc.IEEE*, vol. 68, no. 3, 1980, pp. 593–620.

[9] P. G. Boyvalenkov, D. P. Danev, and S. Bumova, "Upper bounds on the minimum distance of spherical codes," *IEEE Trans. on Inform. Theory*, vol. 42(5), pp. 1576–1581, 2002.

[10] P. Z. Fan and M. Darnell, *Sequence Design for Communications Applications*. U.K.: Research Studies: Hertfordshire, 1996.

[11] ——, *On the construction and comparison of period digital sequences sets*. U.K.: Research Studies: Hertfordshire, 1996.

[12] P. Z. Fan, N. Suehiro, N. Kuroyanagi, and X. M. Deng, "A class of binary sequences with zero correlation zone," *Electron. Lett.*, vol. 35, no. 10, pp. 777–779, 1999.

[13] A. M. Boehmer, "Binary pulse compression codes," *IEEE Trans. on Inform. Theory*, vol. 13, pp. 156–167, April 1967.

[14] R. Turyn, "On barker codes of event length," in *Proc.IEEE*, vol. 51, no. 9, Sep. 1963.

[15] U. Somaini, "Bianry sequences with good autocorrelation and cross correlation properties," *IEEE Trans. on Aero. and Elec. Systems*, vol. 11, no. 6, pp. 1226–1231, Nov. 1975.

[16] R. L. Frank, "Polyphase codes with good nonperiodic correlation properties," *IEEE Trans. on Inform. Theory*, no. 9, pp. 43–45, Jan. 1963.

[17] B. L. Lewis and F. F. Kretschuner, "A new class of polyphase pulse compression codes and techniques," *IEEE Trans. on Aero. and Elec. Systems*, vol. 17, pp. 364–372, May 1981.

[18] ——, "Linear frequency modulation derived polyphase pulse compression codes," *IEEE Trans. on Aero. and Elec. Systems*, vol. 18, pp. 637–641, Sep. 1982.

[19] S. Ariyavisitakul, N. Sollenberger, and L. Greenstein, *Introduction to Radar System.* New York, NY: Tata McGraw-Hill, 2001.

[20] M. R. Bell, "Information theory and radar waveform design," *IEEE Trans. on Inform. Theory*, vol. 39, no. 5, pp. 1578–1597, June 1993.

[21] S. Sowelam and A. Tewfik, "Waveform selection in radar target classification," *IEEE Trans. on Inform. Theory*, vol. 46, no. 3, pp. 1014–1029, 2000.

[22] Q. Liang, "Waveform design and diversity in radar sensor networks: Theoretical analysis and application to automatic target recognition," in *Sensor and Ad Hoc Communications and Networks*, vol. 2, no. 28, Sep. 2006, pp. 684–689.

[23] ——, in *Radar Sensor Networks for Automatic Target Recognition with Delay-Doppler Uncertainty*, vol. 23-25. Military Communications Conference, 2006. MILCOM 2006, 2006, pp. 1–7.

[24] J. Liang and Q. Liang, "Orthogonal waveform design and performance analysis in radar sensor networks," in *Military Communications Conference*, no. 23-25, Oct. 2006, pp. 1–6.

[25] P. F. Worcester, B. D. Cornuelle, and R. C. Spindel, "A review of ocean acoustic tomography: 1987-1990," *Re. Geophys.*, vol. suppl., pp. 557–570, 1991.

[26] D. Behringer, T. Birdsall, M. Brown, B. Cornuelle, R. Heinmiller, R. Knox, K. Metzger, W. Munk, J. Spiesberger, R. Spindel, D. Webb, and P. Worcester, "A demonstration of ocean acoustic tomography," *Nature*, vol. 299, pp. 121–125, Sep. 1982.

[27] A. Baggeroer and W. Munk, "The heard island feasibility test," *Phys. Today*, pp. 22–30, Sep. 1982.

[28] J. L. Spiesberger and K. Metzger, "Basin-scale tomography: A new tool for studying weather and climate," *J. Geophys. Res.*, vol. 96, pp. 4869–4889, Mar. 1991.

[29] B. C. et al., "Tomographic maps of the ocean mesoscale-1: Pure acoustics," *J. Phys. Oceanogr.*, vol. 15, pp. 133–152, Feb. 1985.

[30] T. G. Birdsall and J. K. Metzger, "Factor inverse matched filtering," *J. Acoust. Soc. Amer.*, vol. 79, pp. 91–99, 1986.

[31] P. Z. Fan, N. Suehiro, N. Kuroyanagi, and X. M. Deng, "A class of binary sequences with zero correlation zone," *IEE Electron.Letter*, vol. 35, pp. 777–779, 1999.

[32] P. F. Sammartino, C. J. Baker, H. D. Griffiths, and M. Rangaswamy, "Decentralized detection in radar networks," in *IET RADAR 2007*, Edinburgh, UK, Oct. 2007.

[33] P. F. Sammartino, C. J. Baker, and H. D. Griffiths, "A comparison of algorithms for mimo and netted radar system," in *2nd International Waveform Diversity and Design Conference*, Lihue, HI, Jan. 2006.

[34] ——, "Target model effects on mimo radar performance," in *IEEE International Conference on Acoustic, Speech and Signal Processing*, Toulouse, Fr, May 2006.

[35] L. B. White and P. S. Ray, "Signal design for mimo diversity system," in *Conference Record of the 38th Asilomar Conference on Signal, Systems and Computers*, Nov. 2004.

[36] P. Stoica, J. Li, and Y. Xie, "On probing signal design for mimo radar," *IEEE Trans. on Signal Proce.*, vol. 55, pp. 4151–4161, Aug. 2007.

[37] J. Li, P. Stoica, and X. Zhu, "Mimo radar waveform synthesis," in *IEEE Radar Conference*, May 2008, pp. 1–6.

[38] G. S. Antonio, D. R. Furhrmann, and C. R. Frank, "Mimo radar ambiguity functions," *IEEE Journal of Selected Topics in Signal Processing*, vol. 1, no. 1, pp. 167–177, 2007.

[39] G. S. Antonio and D. R. Furhrmann, "Beampattern synthesis for wideband mimo radar systems," in *2005 1st IEEE International Workshop on Computational Advances in Multi-Sensor Adaptive Processing*, Dec. 2005, pp. 105–108.

[40] D. R. Furhrmann and G. S. Antonio, "Transmit beamforming for mimo radar systems using partial signal correlation," in *the 38th Asilomar Conference on Signal, Systems and Computers*, Nov. 2004, pp. 295–299.

[41] L. Xu, J. Li, and P. Stoica, "Target detection and parameter estimation for mimo radar systems," *IEEE Trans. on Aero. and Elec. Systems*, vol. 44, no. 3, pp. 927–939, July 2008.

[42] A. Dogandzic and A. Nehorai, "Cramer-rrao bounds for estimating range, velocity ,and direction with an active array," *IEEE Trans. on Signal Proce.*, vol. 49, no. 6, pp. 1122–1137, June 2001.

[43] S. Pasupathy and A. N. Venetsanopoulos, "Optimum active array processing structure and space-time factorability," *IEEE Trans. Aerosp. and Elec. syst.*, vol. 10, pp. 770–778, 1974.

[44] S. Haykin, J. Litva, and T. J. Shepherd, *Radar Array Processing.* New York, NY: Springer-Verlag, 1993.

[45] P. Woodward and I. Davis, "A theory of radar information," *Phil. Mag.*, vol. 41, pp. 1101–1117, October 1951.

[46] I. Davis, in *On determining the presence of signals in noise*, vol. 99. Proc. IEE, 1952, pp. 45–51.

[47] P. Woodward, *Probability and Information Theory with Applications to Radars.* London: England: Pergamon, 1953.

[48] R. Blahut, W. Miller, and C. Wilcox, *Radar and Sonar.* New York: Springer-Verlag, 1991.

[49] H. Naparst, "Dense target signal processing," *IEEE Trans. on Inform, Theory*, vol. IT-37, pp. 317–327, March 1991.

[50] M. Bell, "Information theory and radar: Mutual information and the design and analysis of radar waveforms and systems," *Ph.D. Dissertation, California Inst. Technol.*, 1988.

[51] E. Candès, J. Romberg, and T. Tao, "Robust uncertainty principles: exact signal reconstruction from highly incomplete frequency information," *IEEE Trans. on Inform. Theory*, vol. 50, pp. 489–509, Feb. 2006.

[52] E. Candès and T. Tao, "Near-optimal signal recovery from random projections: universal encoding strategies," *IEEE Trans. on Inform. Theory*, pp. 5406–5425, Dec. 2006.

[53] R. Baraniuk and P. Steeghs, "Compressive radar imaging," *Proc. Radar Conference*, pp. 128–133, Agu. 2007.

[54] A. C. Gurbuz, J. H. McClellan, and W. R. Scott, "Compressive sensing for gpr imaging," in *Proc. 41th Asilomar Conf. Signals, Syst. Comput.*, Pacofoc Grove, CA, Nov. 2007, pp. 2223–2227.

[55] ——, "A compressive sensing data acqisition and imaging method for stepped frequency gprs," *IEEE Trans. on Signal Proce.*, vol. 57, pp. 2640–2650, Jul. 2009.

[56] S. Shah, Y. Yu, and A. Petropulu, "Step-frequency radar with compressive sampling (sfr-cs)," in *Acoustics Speech and Signal Processing (ICASSP), 2010 IEEE International Conference on*, 2010, pp. 1686–1689.

[57] Y. Yu, A. Petropulu, and H. Poor, "Mimo radar using compressive sampling," *Selected Topics in Signal Processing, IEEE Journal of*, vol. 4(1), pp. 146–163, Feb. 2010.

[58] ——, "Range estimation for mimo step-frequency radar with compressive sensing," in *Communications, Control and Signal Processing (ISCCSP), 2010 4th International Symposium on*, May 2010.

[59] S. Gogineni and A. Nehorai, "Adaptive design for distributed mimo radar using sparse modeling," in *Waveform Diversity and Design Conference (WDD), 2010 International*, Aug 2010.

[60] D. Donoho, "Compressed sensing," *IEEE Trans. on Inform. Theory*, vol. 6, pp. 1289–1306, Apr. 2006.

[61] E. Candès, "Compressive sampling," *Int. Congress of Mathematics*, vol. 3, pp. 489–509., 2006.

[62] S. S. Chen, D. L. Donoho, and M. A. Saunders, "Atomic decomposition by basis pursuit," *SIAM J. Sci. Comput.*, vol. 20, pp. 33–61., 1999.

[63] J. Tropp and D. Needell, "Cosamp: Iterative signal recovery from incomplete and inaccurate samples," *Appl. Comput. Harmon. Anal.*, p. 30., 2008.

[64] J. A. Tropp, "Greed is good: Algorithmic results for sparse approximation," *IEEE Trans. on Inform. Theory*, vol. 50, pp. 2231–2242., 2004.

[65] S. Mukhopadhyay, C. Schurgers, D. Panigrahi, and S. Dey, "Model-based techniques for data reliability in wireless sensor networks," *IEEE Trans. on Mobile Computing*, vol. 8, pp. 528–543, Sep. 2008.

[66] T. Onel, C. Ersoy, and H. Delic, "Information content-based sensor selection and transmission power adjustment for collaborative target tracking," *IEEE Trans. on Mobile Computing*, vol. 8, pp. 1103–1116, April 2009.

[67] J. Liang and Q. Liang, "Design and analysis of distributed radar sensor networks," *Parallel and Distributed Systems, IEEE Transactions on*, Jan 2011.

[68] H. Deng, "Synthesis of binary sequences with good correlation and cross-correlation properties by simulated annealing," *IEEE Trans. on Aero. and Elec. systems*, vol. 8, pp. 684–689, Agu. 2009.

[69] M. A. Richards, *Fundamentals of Radar Signal Processing.* New York, NY: McGraw-Hill, 2005.

[70] E. Candès and M. Wakin, "An introduction to compressive sampling," *IEEE Signal Processing Magazine*, vol. 25, pp. 21–30, Mar. 2008.

[71] M. A. Herman and T. Strohmer, "High-resolution radar via compressed sensing," *IEEE Trans. on Signal Proce.*, vol. 57(6), pp. 2275–2284, May 2009.

[72] Y. X. Yang, *Best Signal Theory and Design.* Beijing: Posts and Telecom Press, 1996.

[73] Y. X. Zhong, *Pseudonoise Coded Communication.* Beijing: Posts and Telecom Press, 1979.

[74] T. Jiang, "Research on quasi-perfect binary signal pair and perfect punctured binary signal pair theory," Ph.D. dissertation, Yanshan University, Qing Huangdao, 2003.

[75] L. Xu, T. Jiang, and Z. Zhou, "The research on applying optimzed punctured binary sequence-pair in zcz/lcz," *Journal on Communications*, vol. 27, no. 10, 2006.

[76] P. Z. Fan and L. Hao, "Generalized orthogonal sequences and their applications in synchronous cdma systems," *IEICE Trans. Fundamentals*, vol. 11, pp. 1–16, 2000.

[77] P. Z. Fan, "New direction in spreading sequence design and the related theoretical bounds," in *International Conference of Communications,Circuits and Systems*, PRC, June 2002.

[78] J. R. Klauder, A. C. Price, S. Darlington, and W. J. Albersheim, "The theory and design of chirp radars," *Bell System Technical Journal*, vol. 39, 1960.

[79] C. E. Cook and M. Bernfeld, *Radar Signals, an Introduction to Theory and Application*. New York, NY: Academic Press, 1967.

[80] J. W. Arthur, "Saw pulse compression in modern multi-channel radar applications," *Microwave Journal*, pp. 159–169, 1986.

[81] M.B.N.Butler, "Radar applications of saw dispersive filters," in *IEE Proceedings*, vol. 127, no. 2, April 1980.

[82] J. L. Eaves and E. K. Reedy, *Principles of Modern Radar*. Van Nostrand Reinhold, 1987.

[83] L. Bomer and M. Antweiler, "Polyphase barker sequences," in *Electronics Letters*, Dec. 1989, pp. 159–169.

[84] M. I. Skolnik, *Radar Handbook*. New York, NY: McGraw-Hill, 1970.

[85] P. Z. Fan and L. Hao, "Generalized orthogonal sequences and their applications in synchronous cdma systems," *IEICE Trans. Fund.*, vol. 2, pp. 82–85, Nov. 2000.

[86] X. Tang, "Zcz sequences construction from perfect sequences based on interleave technique," in *Proc. IWSDA05*, vol. E83-A, no. 11, Oct. 2005, pp. 2054–2069.

[87] P. Z. Fan, "Spreading sequence design and theoretical limits for quasisynchronous cdma systems," *EURASIP J. Wireless Commun. Netw.*, vol. 1, pp. 19–31, Nov. 2004.

[88] H. Torii, M. Nakamura, and N. Suehiro, "A new class of zero correlation zone sequences," *IEICE Trans. Fund.*, vol. E88-A, pp. 1987–1994, Jul. 2005.

[89] T. Hayashi and S. Matsufuji, "On optimal construction of two classes of zcz codes," *IEICE Trans. Fund.*, vol. E88-A, pp. 2345–2350, Sep. 2006.

[90] E. Fishler, A. Haimovich, R. S. Blum, L. J. Cimini, D. Chizhik, and R. A. Valenzuela, "Spatial diversity in radars-models and detection performance," *IEEE Trans. on Signal Proce.*, vol. 54, no. 3, pp. 823–838, 2006.

[91] B. Friedlander, "Adaptive waveform design for a multi-antenna radar system," in *Proceedings of the Asilomar Conference on Sginal, Systems and Computers*, Pacific Grove, CA, Nct.29-Nov.1 2006, pp. 105–108.

[92] ——, "Waveform design for mimo radars," *IEEE Trans. on Aero. Elec. Systems*, Oct. 2007.

[93] ——, "On data-adaptive waveform desgin for mimo radar," in *Proceedings of the Asilomar Conference on Sginal, Systems and Computers*, Pacific Grove, CA, Nov. 2007.

[94] N. Levanon and E. Mozeson, *Radar Signals*. New York, NY: Wiley-IEEE Press, 2004.

[95] N. Lehmann, E. Fishler, and A. Haimovich, "Transmit-receive beamforming for mimo radar," *IEEE Trans. on Signal Proce.*, vol. 55, no. 5, May 2007.

[96] D. Bliss and K. Forsythe, "Multiple-input multiple-output (mimo) radar and imaging: Degrees of freedom and resolution," in *Proc. 37th Asilomar Conf. Signals, Systems, Computers, Pacific Grove*, vol. 1, Nov. 2003.

[97] C. Y. Chen and P. Vaidyanathan, "Mimo radar ambiguity properties and optimization using frequency-hopping waveforms," *IEEE Trans. on Signal Proce.*, vol. 56, no. 12, Dec 2008.

[98] R. Gold, "Optimal binary sequences for spread specturm multiplexing," *IEEE Trans. on Inform. Theory*, vol. IT-13, pp. 619–621, 1967.

[99] T. Kasami, "Weight distribution formula for some class of cyclic codes," in *Report 0475236 at Coordinated Science Lab, University of Illinois at Urbama*, Apr. 1967.

[100] P. Kumar and O. Moreno, "Prime-phase sequences with periodic correlation properties better than binary sequences," *IEEE Trans. on Inform. Theory*, vol. 37, no. 3, pp. 603–616, Mar. 1991.

[101] A. Papoulis, *Probability, Random Variables, and Stochastic Processes*. New York: McGraw-Hill, 1965.

[102] T. Cover and J. Thomas, *Elements of Information Theory*. 2nd ed. John Wiley & Sons, Inc, 2006.

[103] F. Hildebrand, *Advanced Calculus for Applications*. NJ: Prentice-Hall: 2nd ed. Englewood Cliffs, 1976.

[104] R. Gallager, *Information Theory and Reliable Communication*. New York: Wiley, 1968.

[105] F. Santosa and W. W. Symes, "Linear inversion of band-limited reflection seismograms," *SIAM J. Sci. Statist. Comput.*, vol. 7, pp. 1307–1330, 1986.

[106] G.H.Golub and C. Loan, *Matrix Computations*. Wiley, New York: John Hopkins University Press, Maryland, 1996.

[107] P. Swerling, "Probability of detection for fluctuating targets," *IRE Trans. on Inform. Theory*, vol. 6, pp. 269–308, April 1960.

[108] Q. Liang and X. Cheng, "Kups: Knowledge-based ubiquitous and persistent sensor networks for threat assessment," *IEEE Trans. on Aero. and Elec. System*, vol. 44(3), Jul. 2008.

[109] J. M. Mendel, *Lessons in Estimation Theory for Signal Processing, Communications, and Control*. NJ: Prentice-Hall, 1995.

[110] R. Kwok and W. Johnson, "Block adaptive quantization of magellan sar data," *IEEE Trans. on Geosc. and Remote Sensing*, vol. 27(4), pp. 375–83, Jul. 1989.

[111] U. Benz, K. Strodl, and A. Moreira, "A comparison of several algorithms for sar raw data compression," *IEEE Trans. on Geosc. and Remote Sensing*, vol. 33(5), pp. 1266–276, Sep. 1995.

[112] V. Pascazio and G. Schirinzi, "Sar raw data compression by subband coding," *IEEE Trans. on Geosc. and Remote Sensing*, vol. 41(5), pp. 964–76, May. 2003.

BIOGRAPHICAL STATEMENT

Lei Xu received her B.S. and M.S. degree from Beijing University of Posts and Telecommunications, China, in 2004 and 2007, respectively, both in Electrical Engineering. From 2008 to now, she is a Ph.D student in the Wireless Communication Network Lab of Electrical Engineering Department at the University of Texas at Arlington. Her current research interest include in the area of waveform design, radar system, radar sensor network, MIMO, compressive sensing, information theory and wireless communications.